Dissertation zur Erlangung des Doktorgrades
der Fakultät für Chemie und Pharmazie
der Ludwig-Maximilians-Universität München

Investigation of self-assembling machinery in cell shape formation

Nirakar Basnet

Kathmandu, Nepal

2019

Erklärung:

Diese Dissertation wurde im Sinne von § 7 der Promotionsordnung vom 28 November 2011 von Frau Prof. Elena Conti betreut.

Eidesstattliche Versicherung:

Diese Dissertation wurde selbstständig, ohne unerlaubte Hilfe erarbeitet.

München den 13.11.2019

_____

Nirakar Basnet

Dissertation eingereicht am: 26.11.2019

1. Gutachterin / 1. Gutachter: Prof. Dr. Elena Conti, PhD

2. Gutachterin / 2. Gutachter: Prof. Dr. Karl-Peter Hopfner

Mündliche Prüfung am: 9.1.2020

Table of Contents

Summary

Microtubules, dynamic polymers of tubulin heterodimers, are one of the three major cytoskeletal components along with actin and intermediate filaments in eukaryotic cells (Pollard and Goldman, 2018). Microtubules play an important role in various cellular processes such as intracellular trafficking, organization, cell division, polarization and migration. Not only eukaryotes but many prokaryotes also have at least one protein that is homologous to tubulin. The most common of them is the FtsZ protein in *Archaea* and bacteria, which can also assemble into polymers and play a role in cell division in prokaryotes (Pollard and Goldman, 2018). Microtubules are long, stiff polymers but its special property, the "dynamic instability", takes the centre stage while controlling most of the fundamental microtubule-based processes.

In cells, generally microtubules are nucleated from a special machinery called "Microtubule-Organizing Centres (MTOCs)" such as centrosomes or spindle pole bodies (Goodson and Jonasson, 2018). One end of the microtubules which are embedded to these MTOCs is known as minus end and microtubules grow outwards radially by adding GTP-tubulin dimers to the other end known as growing end or plus end (Akhmanova and Steinmetz, 2019; Goodson and Jonasson, 2018). Most of the time these microtubules undergo stochastic transitions between the growth and shortening, known as "dynamic instability" (Mitchison and Kirschner, 1984). This dynamic nature can be harnessed by the cells for various processes like polarization, migration, segregation of chromosomes and also allows cell to adapt to changes in environment and cell shape (Goodson and Jonasson, 2018).

The change in cell shape is critical for various physiological processes such as cell division, polarization, migration and dynamic microtubules are at the heart of these processes. It is thought that, MTOCs like centrosomes are the sole source for microtubules inside the cells. However, microtubules can also dissociate or get severed by severing proteins and transported to other cellular locations where they are needed by molecular motors. Although this kind of transport of microtubules is possible in certain cell types, local microtubule nucleation and local remodelling of microtubules takes place at locations independent of centrosomes (Ishihara et al., 2014; Meunier and Vernos, 2016; Petry and Vale, 2015). The fact that microtubules can nucleate from the Golgi apparatus (Chabin-Brion et al., 2001), nuclear envelope (Tassin et al., 1985), kinetochore (Maiato et al., 2004), pre-existing microtubules (Murata et al., 2005; Petry et al., 2013) and plasma membrane (Mogensen and Tucker, 1987) suggests that the local nucleation and remodelling of microtubules plays an important role in maintaining the cellular microtubule architecture and in turn cell shape and morphology.

Among many different cells, neurons are specialized cells with a complex morphology. They have a long axon protruding out of the cell body and stretching over long distances. Axons form a branch like formation along the shaft and the tips of the branched axons form synapse with the dendrites of their neighbouring neurons, resulting in the basis of the formation of the intricate communication network of nervous system. This complex network is central to basic brain functions like memory, sensory perception, learning, cognition and motor behaviour (Kalil and Dent, 2014). During neural development, branches come out from specific locations in axons as dynamic protrusions that can extend and retract. Some of these protrusions later on stabilize into branches and then connect to its synaptic targets (Kalil and Dent, 2014).

Microtubules are major cytoskeletal elements in neurons and they control various fundamental neuronal processes such as migration, polarity formation and differentiation (Kapitein and Hoogenraad, 2015). They act as structural elements for neurons to maintain their polarized morphology and for long distance intracellular transport of signalling vesicle from soma to synapse and vice versa. Hence, the proper maintenance and control of various microtubule properties like number, length, distribution, orientation and bundling is critical for proper functioning of neurons (Kapitein and Hoogenraad, 2015). Several human neurodevelopmental disorders such as lissencephaly, perry syndrome, hereditary spastic paraplegia have been linked to the genes of microtubule-related proteins reflecting the importance of microtubules in neuronal development (Kapitein and Hoogenraad, 2015) (Franker and Hoogenraad, 2013; Reiner and Sapir, 2013).

Microtubules are central for different stages of axon development from axon initiation to elongation and axon branch formation and for all these processes the microtubule architecture has to undergo various types of remodelling and reorganization. In axons, microtubules are bundled parallelly with uniform orientation of growing ends outward whereas microtubules bundles are composed of mixed orientation in dendrites. During the elongation of axons at the growth cone, microtubules display a complex set of organizations like splaying, looping, bending and bundling(Conde and Cáceres, 2009). Similarly, to generate branch points, it is necessary for microtubules to undergo remodelling such that cytoskeletal paths split into separate branches. As centrosomes are not required for the development of axon and axon branching, microtubule remodelling must be regulated locally at branch points (Stiess et al., 2010) (Yu et al., 2008). Current models for axon branching involve the microtubule nucleators augmin and γ-tubulin, which allow microtubules to grow out from nucleation points that attach to the outside of pre-existing microtubules (Sànchez-Huertas et al., 2019)**.** But the exact mechanism how microtubules are remodelled at branching points is still not known. Microtubule-severing proteins like spastin and katanin play an active role in axon branching (Yu et al., 2008), but how severed

microtubules are remodelled at a branch point is still an enigma. Until now, there was no evidence of other proteins that could remodel microtubules at axon branches or that could directly remodel microtubules into branched structures.

In our study, we found the novel microtubule-remodelling factor SSNA1, also known as NA14 or DIP13, which remodels microtubules into a branched structure. SSNA1 was found to be localized at centrosomes, basal bodies and at midbodies during cytokinesis (Lai et al., 2011; Pfannenschmid et al., 2003). Apart from these known MTOCs, recently, SSNA1 was also reported to be present in neurons and promote axon elongation and branching (Goyal et al., 2014).

In vitro reconstitution showed that SSNA1 mediates microtubule nucleation and further induces formation of branched microtubules, where new daughter microtubules directly branch out from existing microtubules. Cryo-EM analysis revealed that SSNA1 co-polymerizes together with tubulins by attaching along single protofilaments, guiding them to grow away from a mother microtubule, further to split and create a branched microtubule. The branching activity of SSNA1 relies on its ability to self-assemble into fibrils in a head-to-tail fashion and mutating residues essential for the self-assembly of the protein lead to abrogation of branching in-vitro. It was found that SSNA1 localizes at axon branching sites in primary neurons and it has a key role in neuronal development. SSNA1 mutants that abolish microtubule branching in vitro also fail to promote axon development and axon branching, showing a correlation of SSNA1's microtubule-remodelling activity and axon branching. We have therefore discovered a novel mechanism for microtubule-branching, in which microtubules are directly remodelled into branched structures and we identified its implication in neuronal development.

Preface

The work presented in this thesis was performed at the laboratory of Dr. Naoko Mizuno at Max Planck Institute of Biochemistry, Martinsried, Germany. The thesis mainly comprises two topics: 1) Direct induction of microtubule branching by microtubule nucleation factor SSNA1 and 2) Structural insights into the cooperative remodelling of membranes by amphiphysin/BIN1. Therefore, this thesis is presented in a cumulative manner. Chapter 1 includes introduction which gives a general view about microtubule dynamics, its importance in the cell as a structural and functional component and how its dynamics inside the cell is controlled either via various microtubule binding proteins or fine-tuned via various post-translational modifications. The introduction also includes the neuronal cytoskeleton and how microtubule is essential for various processes of neuronal development. Chapter 2 presents the result section which consists of the published research articles divided into two sub-chapters. The first sub-chapter 2.1 presents the research article first topic: Direct induction of microtubule branching by microtubule nucleation factor SSNA1 followed by second sub-chapter 2.2 which includes the research article: Structural insights into the cooperative remodelling of membranes by amphiphysin/BIN1. Finally, the chapter 3 includes extended discussion, the relevance of findings and the last chapter 4 includes the outlook and future directions of the first topic.

List of Publications

1) **Basnet, N**., Nedozralova, H., Crevenna, A.H., Bodakuntla, S., Schlichthaerle, T., Taschner, M., Cardone, G., Janke, C., Jungmann, R., Magiera, M.M., et al. (2018). Direct induction of microtubule branching by microtubule nucleation factor SSNA1. Nature Cell Biology *20*, 1172–1180.

2) Adam, J., **Basnet, N**., and Mizuno, N. (2015). Structural insights into the cooperative remodeling of membranes by amphiphysin/BIN1. Srep *5*, 15452.

1. Introduction

1.1. Microtubules and tubulin

Microtubules are long, ~25 nm hollow cylindrical polymers assembled from heterodimers of α- and β-tubulin, which are normally referred as αβ-tubulin or tubulin (Figure 1A). The structural subunit, tubulin heterodimer consists of very compact globular "body" and can be divided into three distinct functional regions: N-terminal (N-terminal) containing nucleotide-binding region, intermediate region containing taxol-binding site and a negatively charged, disordered C-terminal tail (Nogales et al., 1998c). Each tubulin monomer binds a single molecule of GTP nucleotide. The GTP nucleotide bound to α-tubulin at N-site is not hydrolyzable and only the GTP bound to β-tubulin at E-site is hydrolyzed to GDP during microtubule polymerization (Nogales et al., 1998c). The α-and β-tubulin "body" structure is highly similar with roughly 80-95% sequence identity and the most isoform sequence variation and posttranslational modifications are concentrated on the C-terminal tails (50% sequence identity between the tails tubulin) (Roll-Mecak, 2015).

In cells, microtubules are typically composed of 13 linear protofilaments (pf) connecting with each other laterally, to form a closed tubular polymer (Figure 1B and D). Although in most of the cells microtubules have 13 pf, pf numbers ranging from 8-20 have been observed both in-vitro and in-vivo conditions with 14 pf being the majority in in-vitro conditions (Chrétien and Wade, 1991). Microtubules are polar structures with a fast growing plus end exposed with β-tubulin and a slow growing minus end exposed with α-tubulin. Microtubules grow by the addition of tubulin dimers at the growing end whereas in most of the cases slow growing end is connected to microtubule-organizing center (MTOC) (Goodson and Jonasson, 2018).

During the polymerization of a typical 13 pf microtubule, the main body of microtubule is composed of B-lattice where α-subunits of a protofilament is next to the α -subunit of neighboring protofilament (α-α) and β-tubulin next to the β-tubulin(β-β), except at the boundary where it closes. This boundary is referred to as a "seam" of the microtubule, where the α-tubulin of a protofilament is next to the β-tubulin of next protofilament (α-β), forming a B lattice (Figure 1C-D) (Chrétien and Wade, 1991). Due to slight shift of protofilaments in main body with respect to its neighbouring protofilament there is an offset of 1.5 dimers at the seam for 13 pf resulting a 3 start helix. Changing the number of the protofilaments changes the offset, so the microtubules with 15 pf and 16 pf have a shift of 2 dimers resulting in 4-start helix (Goodson and Jonasson, 2018; Hunyadi et al., 2007). Due to the presence of

the seam microtubules cannot be described as a true helix but a pseudo-helical structure (Zhang and Nogales, 2015).

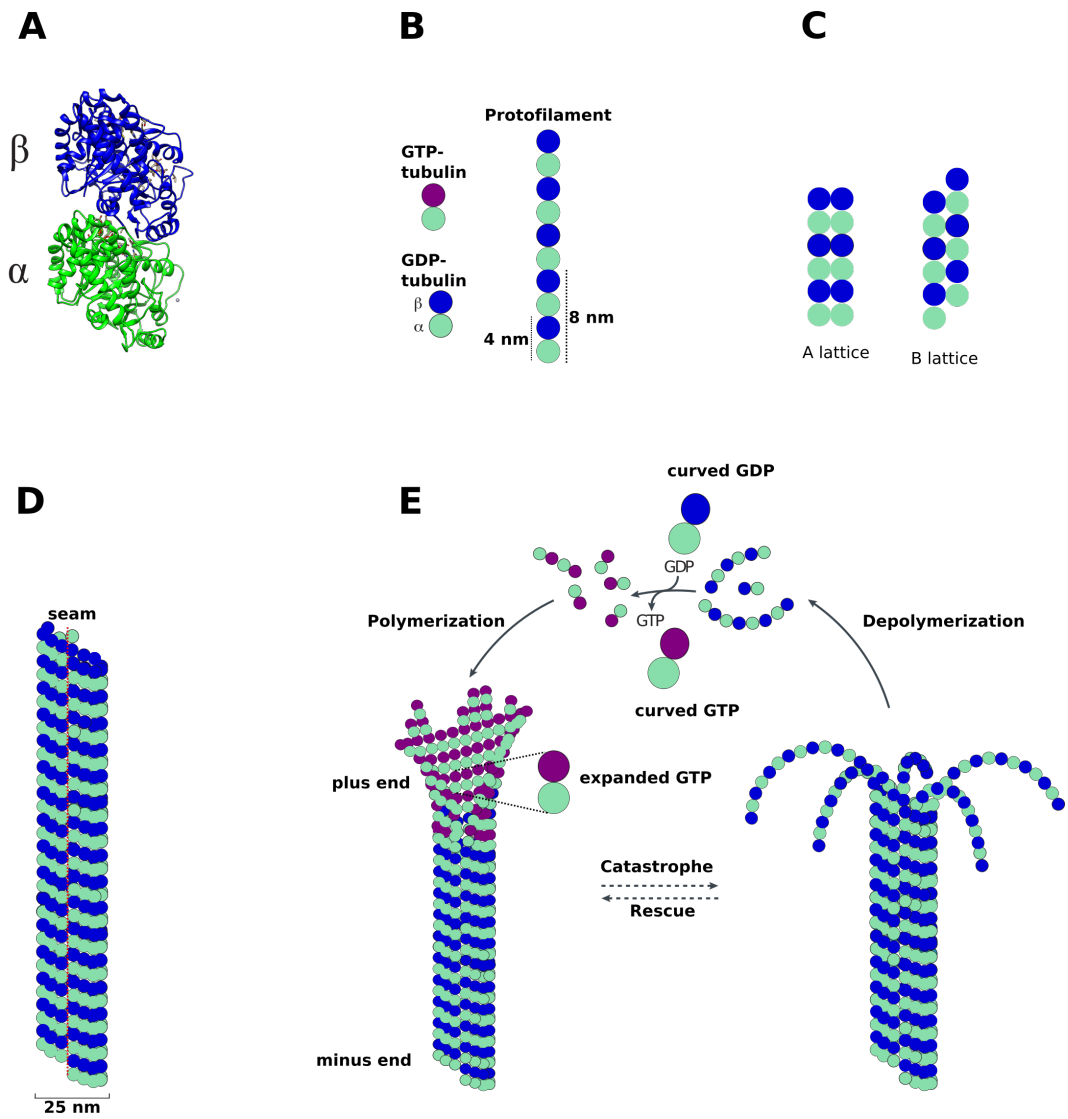

Figure 1.Microtubule structure and dynamic instability. (A, B) Tubulin structure (PDB: 1jFF) and microtubule protofilament. (C) A and B type lattice seen in microtubule body. (D) 13pf microtubule with seam marked with red. (E) Microtubule "dynamic instability" model.

The presence of seam has an important implication in high resolution microtubule structure determination (Zhang and Nogales, 2015). Due to high similarity between α- and β-tubulin at low resolution, which usually drives the image alignment, it is important to determine seam location for each microtubule segment in order to obtain true structure of microtubule (Zhang and Nogales, 2015). Different method has been used recently to address this issue. One of the strategy that have been frequently used was to decorate microtubule with kinesin motor which acts as a low-resolution marker for tubulin dimer(Sindelar and Downing, 2007) (Alushin et al., 2014). In this method, the seam location

was determined by a reference-based analysis where cross-correlation values between the raw images and projection of reference model decorated with kinesin was calculated. Although with this method, the seam location for majority of well decorated microtubules were accurately determined, it was still limited, in case of situations where kinesin decoration was less or the protein markers were relatively small for example doublecortin or EB3 (Zhang and Nogales, 2015). Due to the small size of the protein or sparse decoration, it was hard to determine the clear cross-correlation peak values resulting in failure of correct seam determination for the given microtubule segments (Zhang and Nogales, 2015). Recently with improved data quality obtained from the direct detector and combining with the improved data processing algorithm, Rui Zhang and colleagues have been able to obtain high resolution cryo-EM reconstruction of naked or undecorated microtubule at 3.5 Å resolution. This development has helped us to understand different aspects of microtubules such as nucleotide binding site and different nucleotide state of the microtubule (GTP-microtubule or GDP-microtubule) (Zhang et al., 2015).

Another important aspect of the microtubule structure is that it is highly negatively charged at the outer surface due to the disordered C-terminal tail of tubulin. These C-terminal tails, which are also known as E-hooks due to the presence of multiple glutamate residues, play an important role for the interaction with many microtubule-binding proteins (MTBPs). The tubulin tail acts as a hotspot for different post-translational modifications (PTMs) such as phosphorylation, detyrosination, glutamylation and glycylation and could affect the recruitment and interaction of various MTBPs (Roll-Mecak, 2015). Different studies have shown that the C-terminal tail also plays a critical role in microtubule polymerization. Subtilisin treated tubulin where C-terminal tails were removed, have a significantly lower critical concentration at which microtubule polymers will form (Bhattacharyya et al., 1985). Even the shielding of the negative charge by the CAP-Gly domain of MTBPs such as p150 glued leads to the neutralization of charge on the surface, resulting in promoting microtubule polymerization (Wang et al., 2014b).

Another structurally relevant aspect of the microtubules which is relatively under studied is the inner-lumen space. Cryo-electron microscopic images of microtubules in neurons, platelets and insect sperms tails have shown the closely packed electron density at inner-lumen of microtubules (Garvalov et al., 2006). Cryo-EM images have also shown inner-luminal particle in flagellar microtubules (Ichikawa et al., 2017; Nicastro et al., 2006). One of the possible candidate for the inter-luminal particle is tubulin acetyltransferase TAT which acetylates the Lys40 of α-tubulin located at the flexible internal loop of microtubule (Akella et al., 2010; L'Hernault and Rosenbaum, 2002).

Microtubules are structurally very rigid, with a Young's modulus of 1-2 GPa in-vitro, which is comparable to the stiffness of a pexi-glass and exhibits the persistence length of ~5000 μm which is comparable to the dimension of a cell (Goodson and Jonasson, 2018; Sui and Downing, 2010). Although being very rigid, microtubules are very dynamic undergoing phases of growth and shrinkage due to addition and removal of tubulin dimers at their end. This property of microtubule is also known as "dynamic instability". Interestingly, microtubules are also found to be highly curved in vivo, in contrast to the view of highly rigid polymers. This curvedness of microtubules is suggested to be the result of force exerted by the motor proteins or due to its interaction with other cytoskeleton proteins (Goodson and Jonasson, 2018) and also there is a possibility of lattice defects, when a tubulin dimer is either missing or wrongly incorporated into the microtubule lattice (Schaedel et al., 2019).

1.2. Tubulin isoforms and post-translational modification

The α- and β- subunits of microtubules have a compactly folded body, which has a very high sequence similarity (about 95 %). The most isoform sequence variation and posttranslational modification is concentrated at the disordered C-terminal tail of the tubulin dimer (Figure 2A) (Janke, 2014; Roll-Mecak, 2015). The changes in the C-terminal tail could possibly effect the behavior of microtubules and their interactions with various MTBPs. In human, nine genes of α-tubulin and nine β-tubulin genes has been reported (Gadadhar et al., 2017) (Figure 2B) Many tubulin isoforms are present in a given cell type although it was thought that a single isoform will form a single type of microtubule with specialized functions like in neuronal microtubules or microtubules at the marginal band of platelets and cilia which is composed of high amount of specific β-tubulin isoform (Janke, 2014). It appears that the microtubule polymers can be formed from the complex pool of different tubulin isoforms resulting in the formation of heterogeneous microtubules (Gadadhar et al., 2017). But it is still not clear how the different level of tubulin isoforms could control or fine tune microtubule dynamics inside the cell (Gadadhar et al., 2017; Janke, 2014). Recently a large number of mutations in single tubulin isoforms have been shown connected to the various pathologies like blood clotting and neurological disorders, which in turn is providing us with insights on possible functions of these isoforms (Fiore et al., 2017; Tischfield et al., 2011).

The C-terminal tail of tubulin can also undergo different kinds of post translational modifications like detyrosination/tyrosination (addition or removal of C-terminal tyrosine), polyglutamylation (addition of free glutamates to the side chain of glutamates), polyglycalation (addition of glycine to side chain of glutamates and acetylation of the lysine 40 of α-tubulin (Figure 2A). Apart from these well studied posttranslational modifications, there are others which have been discovered recently; phosphorylation, polyamination, methylation, palmitoylation, arginylation, ubiquitylation,

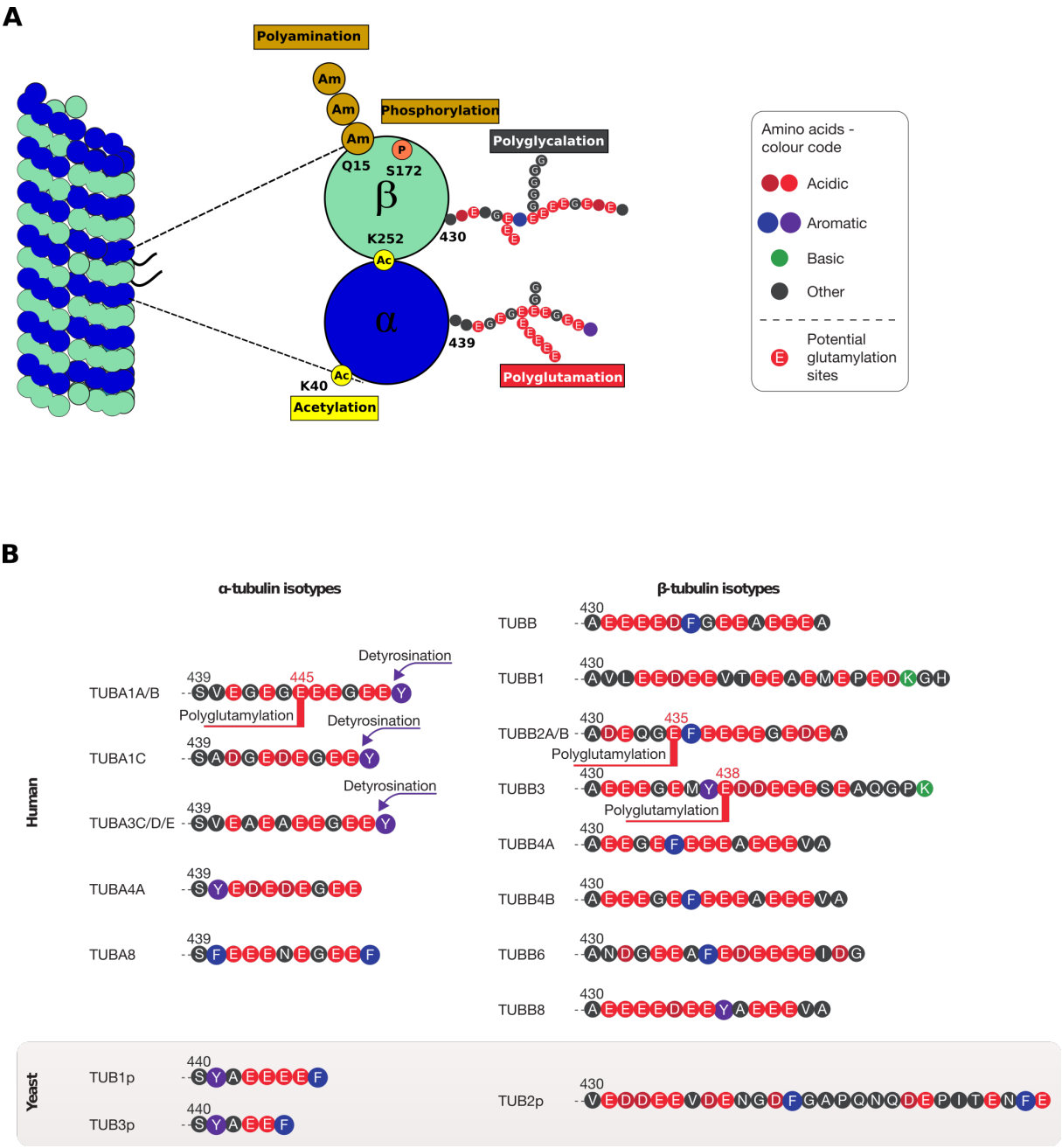

Figure 2. Tubulin isoforms and PTMs (A) Schematic representation of the PTM distribution in tubulin. (B) Tubulin C-terminal sequences from human and yeast α and β tubulin isoforms. Source:(Wehenkel and Janke, 2014).

glycosylation and sumoylation (Gadadhar et al., 2017). Among these only few of the PTMs have been well studied so far. Phosphorylation of serine 172 of β-tubulin by cyclin dependent kinase-1 cdk1 has been shown to affect microtubule dynamics during cell division (Fourest-Lieuvin et al., 2006). The methylation of K40 in α-tubulin seems to compete with the acetylation of same residues (Park et al., 2016) and polyamination seems to add positive charge to glutamate residues and is involved in stabilization of microtubules (Song et al., 2013).

1.2.1. Detyrosination/Tyrosination

Tyrosination is a reversible, ATP dependent and tRNA-independent addition of free tyrosine to the absolute C-terminal glutamate of α-tubulin via α-linked peptide bond (Gadadhar et al., 2017; Roll-Mecak, 2015). The enzyme responsible for the tyrosination is known as tubulin tyrosine ligase (TTL) (Janke, 2014), which is also the first enzyme discovered that modifies tubulin. After being elusive for 40 years since the discovery of tyrosination, the enzyme responsible for detyrosination, vasohibins has been recently discovered (Aillaud et al., 2017; Nieuwenhuis et al., 2017). The tyrosination/detyrosination cycle acts as ON/OFF signal for the recruitment of MTBPS at the growing end of the microtubules (Roll-Mecak, 2015). The proteins like p150 subunit of dynactin, cytoplasmic linker protein CLIP170 are recruited to the growing end of the microtubule via the short GEEY/F motif at the C-terminal of α-tubulin (Peris et al., 2006). The tyrosination can also act as an OFF signal, in case of kinesin-1 which prefers binding to the detryrosinated axonal microtubules in comparison to the tyrosinated microtubules at the dendrites (Konishi and Setou, 2009). Freshly incorporated tubulin at the growing end of microtubules is highly tyrosinated whereas detyrosination occurs only at tubulin units in polymerized microtubules. This generates a gradient of tyrosination from freshly polymerized growing end, to the older part of microtubule where the degree of tyrosination is less (Roll-Mecak, 2015). This gradient is thought to play an important role in localizing certain MTBPs to the growing end of microtubule. The plus end or growing end tracking protein, end binding protein (EBs) specifically follows the growing end of protein through its interaction with tyrosinated microtubules. The EBs then acts as a platform to recruit number of other MTBPs to the growing end of the microtubule. These set of proteins which bind to the growing end are also known as +TIPs and the process of tyrosination/detyrosination is important for their interaction with microtubules (Akhmanova and Steinmetz, 2008; 2015).

1.2.2. Polyglutamylation, Polyglycalation and K40 acetylation

Polyglutamylation and polyglycalation is an enzymatic addition of one or more glutamate or glycine residues to γ-carboxyl group of one of the internal glutamate residues of α-or β-tubulin resulting in a branched peptide structure (Figure 2A). After the formation of branch structure glutamate and glycine residues can be added to make a chain structure containing up to 21 glutamates and 34 glycines (Roll-Mecak, 2015). Polyglutamylation and polyglycalation is mediated by the enzymes glutamylases and glycylases, which are the members of the TTL-like family(TTLL) family. Each enzyme from this family has a substrate and a reaction preference, so different enzymes that either initiate the branch formation or elongate the chain with preference for either α-tubulin or β-tubulin exits. Some enzymes are found to be highly substrate specific, whereas some catalyzes a range of substrate (Janke, 2014).

Tubulin polyglutamylation is a reversible process and the enzymes or deglutamylases which catalyzed the reverse reaction belongs to the family of tubulin carboxypeptidases(CCP). CCP1, 4 and 6 remove long polyglutamate chains and CCP5 shows preference for removing of branched polyglutamate chains (Rogowski et al., 2010).

Polyglutamylation has been shown to play a role in regulating microtubules and their interactions with various MTBPs. Addition or removal of glutamate and glycated residues could either increase or decrease the net negative charge of the C-terminal tail respectively. Considering most of the MTBPs and motor protein's microtubule-binding sites have a patch of positive charge, these polyglutamate residues could act as a fine tuner for this charge based interaction between the microtubule and MTBPs (Roll-Mecak, 2015). Blot-overlay assays have shown that tau, MAP2, MAP1B and kinesin-1 preferentially interacts with microtubules that have up to three glutamates while MAP1A shows preference towards microtubules with up to 6 glutamates (Roll-Mecak, 2015). The tubulin purified from the brain tissues have in average 3 to 6 glutamates and maximum up to 11 glutamates (Roll-Mecak, 2015). The longest chain of glutamate was found in cilia where up to 21 glutamates has been observed (Roll-Mecak, 2015). Polyglutamylation in cilia regulates the dynein motors which alters the ciliary beating and movement (Gadadhar et al., 2017). In neurons, it was shown that the polyglutamylation influences microtubule dynamics by regulating the activity of the microtubule-severing enzyme spastin (Valenstein and Roll-Mecak, 2016). In neurons, polyglutamylation has also an important role in differentiation and survival (Janke, 2014).

So far, it is still not known how polyglycylation controls microtubule dynamics but glycylating enzymes were found in all organisms and depletion of the glycases leads to ciliary disassembly and ciliary defects (Janke, 2014). In mammals, TTLL3 and TTLL8 initiates the glycylation which is then elongated by another enzyme TTLL10 whereas in *Drosophila melanogaster* a single glycase TTLL3 can do both initiation and elongation (Rogowski et al., 2009). Similar to the glycylation, the mechanism by which acetylation of K40 control the microtubule dynamics is unclear (Gadadhar et al., 2017). Microtubules of cilia and flagella and long-lived cytoplasmic microtubules are highly acetylated and loss of TAT leads to neurodegeneration and defect in axonal morphology in *C. elegans* and abnormalities in sperm in mice (Roll-Mecak, 2015)**.** Since acetylation is mostly found in stable microtubule it has become marker for the stable microtubule (Roll-Mecak, 2015). This selectivity must be the consequences of TAT's preference for polymerized microtubule compare to free tubulin (Roll-Mecak, 2015). Since K40 is present at the inner-lumen side, it is thought that, it is necessary for regulating the interaction of microtubules with microtubule inner-lumen proteins(MIPs) (Janke, 2014).

1.2.3. Tubulin code

Apart from the genetic isoform, the C-terminal tail of tubulin can also undergo various posttranslational modifications. There is a plethora of different combination of these modifications possible, which could give rise to a chemically diverse and complex signaling platform on the microtubule surface, which is now referred to as "Tubulin code" (Janke, 2014; Verhey and Gaertig, 2007). This is analogous to the "histone code", where various posttranslational modification and sequence variability is concentrated at the N-terminal tail (Jenuwein and Allis, 2001). Recent discoveries in isoform specific tubulin mutations and its involvement in range of human pathologies is shedding some light in its importance on various cellular processes (Gadadhar et al., 2017; Janke, 2014). To summarize, the ''Tubulin code" plays a key role in the control of microtubule dynamics and the production of tubulin with controlled posttranslational modification in order to study its role in microtubule dynamics in-vitro will give us important information about biological function.

1.2.4. Other tubulin isoforms (γ-, δ-, ε-, ζ- and η-tubulin)

γ- tubulin is a member of tubulin gene family which is important for the microtubule nucleation and determination of polarity. In centrosomes or spindle bodies it is a part of a machinery γ-tubulin ring complex(γ-TURC) (Kollman et al., 2011). It is well characterized in vertebrates but γ-TURC dependent nucleation seems to be conserved across the eukaryotes as it has been found in all non-parasitic eukaryotic organisms (Findeisen et al., 2014a; 2014b; Gull, 2001; Kollman et al., 2011). δ-, ε-, ζ- and η-tubulin was found in cilia/flagella and basal bodies and was proposed to be connected to triplet microtubules. Although δ-, ε- and ζ-tubulins was identified in all major eukaryotic kingdom it is not ubiquitous as α-β-and γ -tubulin, suggesting they might not perform important function in cells. Other tubulin isoforms such as η-tubulin is restricted to certain lineages of protists (Findeisen et al., 2014a).

1.3. Microtubule assembly and dynamic instability

Although the immunofluorescence images of microtubules give a very "static" image about its nature, but in reality, microtubules are very dynamic structure. The microtubules can nucleate spontaneously when the αβ-tubulin dimers exceeds a certain critical concentration in a solution. The growth occurs by addition of GTP-tubulin at the microtubule end, which is also known as growing end. The polymerization or addition of GTP-tubulin to microtubule is a spontaneous process driven by the hydrophobic effect (Vulevic and Correia, 1997). After the GTP-tubulin is added, it forms a stabilizing cap (GTP-tubulin cap) at the growing end of the microtubule (Figure 1E). The region below the cap mainly consists of tubulin in GDP bound state, as a result of GTPase activity of the incoming tubulin

dimer (Figure 1E) (Nogales et al., 1998a). When this stabilizing cap composed of the GTP-tubulin is lost, the microtubule undergoes an event known as “catastrophe” where the microtubule shrinks rapidly. This catastrophe can be rescued stochastically and after rescue the microtubule switches from catastrophe back to growth (Figure 1E) (Mitchison and Kirschner, 1984).

This behavior of microtubules, where their ends transit between the phase of growth and shrinkage is known as “Dynamic Instability”. The process of shrinkage or depolymerization is driven by the energy from GTP hydrolysis as microtubules, which are polymerized in the presence of the slowly hydrolysable GTP analogue GMPCPP, could polymerize but fail to disassemble (Hyman et al., 1992).

1.3.1. Molecular view of microtubule dynamics

The mechanism of dynamic instability has been elusive since its discovery by Mitchinson and Kirschner in 1984 (Mitchison and Kirschner, 1984). Recent development in single-molecule microscopy (Brouhard and Rice, 2018) and high resolution cryo-EM structure (Alushin et al., 2014; Zhang et al., 2015) has provided new insights into the microtubule assembly process. Both α- and β-tubulin bind GTP nucleotide at their N-site and E- site respectively (Löwe et al., 2001).The GTP bound to α-tubulin is not hydrolysable but the β-tubulin bound GTP undergoes hydrolysis due to GTPase activity of incoming tubulin (Nogales et al., 1998a). Recent high-resolution cryo-EM structures of microtubules (Alushin et al., 2014; Zhang et al., 2015) and crystal structures (Ravelli et al., 2004) has shown that α- and β-tubulin undergo at least three different conformation changes during the microtubule growth and shrinkage cycle. These conformations are described as curved, expanded and compact conformations. Free GTP-tubulin dimers have a curved conformation characterized by ~12° kink at the intra-dimer space (Brouhard and Rice, 2018). After binding to the growing end, tubulin dimers straighten into expanded conformation. This change in conformation introduces strain to the lateral lattice as the microtubule lattice holds tubulin dimers in an unfavorable conformation. After GTP bound to β-tubulin is hydrolyzed, the dimers undergo another structural change to compaction, which results in shortening of the microtubule lattice by 2 Å (Alushin et al., 2014). When the stabilizing GTP cap is present, the relatively strong lateral bond holds the polymer structure resulting in continued polymerization but when the GTP cap is lost, GDP-tubulin relaxes and adopt their preferred curved confirmation, releasing the stored strain energy in dimer and peeling outward forming a curved structure (also known as ram’s horns)(Figure 1E) (Brouhard and Rice, 2018; Nawrotek et al., 2011; Ravelli et al., 2004; Rice et al., 2008; Rubén M Buey et al., 2006).

The GDP lattice under the stable cap stores the energy from GTP hydrolysis which is then used for the microtubule depolymerization. Although the model is able to answer a lot of question pertaining microtubule dynamic instability, there are still many questions yet to be answered. The compaction microtubule lattice on GTP hydrolysis was observed in mammalian microtubule but similar compaction was not observed in yeast microtubule (Howes et al., 2017). The minus end or slow growing end of the microtubule is also undergoing the dynamic instability but the exact mechanism of dynamic instability at minus end and how it differs from the growing end is still not known.

1.3.2. Microtubule dynamics in cells

In cells, there is a constant turnover of microtubules due to dynamic instability, but what could be the biological implication of such an energy consuming process? The dynamic microtubules allow cells to undergo morphological changes in response to the various internal and external signals like specific polarized organization of microtubules and signaling molecules inside cell during migration (Kaverina and Straube, 2011). The growing and shrinking microtubule generates pushing and pulling force respectively. This generated pushing force is important for localizing or centering the cellular structures like nuclei (Tran et al., 2001) and mitotic spindles during cell division (Tolić-Nørrelykke et al., 2004). Similarly, the pulling force is important for moving the segregated chromosome to opposite end during division (Coue et al., 1991). One of the important functions of microtubules is to act like “tracks” on which various cargo like vesicles, organelles, chromosome are transported across the cell with the help of various motors (Sweeney and Holzbaur, 2018). The dynamic instability also allows microtubules to explore the cellular space and bring microtubules close to various cellular structures, a process which is also known as “search-capture” (Goodson and Jonasson, 2018).

1.4. Microtubule nucleation in vitro and in cells

In in-vitro conditions spontaneous polymerization of microtubules is rare unless the tubulin concentration exceeds the critical concentration. This process is known as nucleation and is an energetically unfavorable process that does not occur until a critical nucleus is formed (Voter and Erickson, 1984). Cells go through this unfavorable condition through a specialized machinery γ-TURC (Kollman et al., 2011) or newly severed microtubule (Lindeboom et al., 2013). γ-TURC is a nucleation machinery associated with γ-tubulin and the nucleation involving these components is one of the well-studied mechanism in-vivo (Goodson and Jonasson, 2018). γ-TURC is a ‘lock washer shaped structure’ which not only provides template for the nucleation but also caps the minus end (Figure 5A). These nucleators play an important role in the spatio-temporal control of microtubule nucleation inside the cell and in generating different kinds of microtubule arrays (Akhmanova and Steinmetz, 2019).

Although γ-tubulin based nucleation is well characterized, other mechanism of nucleation also exists inside cells. An example is the nucleation of microtubules from katanin-severed microtubule fragments at cortical arrays of higher plants (Lindeboom et al., 2013) (Figure 5C). Many microtubule-stabilizing proteins have microtubule nucleation activity in vitro, but weather they also nucleate microtubules in vivo or only stabilize them is not clear (Goodson and Jonasson, 2018). Different MTBPs like XMAP215, targeting protein for Xklp2 (TPX2) and neuronal migration protein doublecortin (DCX) promote nucleation in-vitro. They recognize the curved confirmation of αβ-tubulin at the microtubule tip and either accelerate αβ-tubulin additions (XMPA215) or stabilize tubulin-tubulin interaction interface (TPX2 and DCX (Figure 4C). Petry et al. also showed that augumin can nucleate microtubule from pre-existing microtubule in γ-tubulin dependent mechanism and it has been shown to play a role for the function of the mitotic spindle and neuron axonal development (Petry et al., 2013; Sànchez-Huertas et al., 2019). Microtubule-severing proteins like spastin or katanin contribute to microtubule nucleation by increasing microtubule numbers by breaking existing microtubule. On the one hand, these breakages increase the pool of free tubulin, thus initiating nucleation and on the other hand, broken microtubules can act as templates for nucleation (Ehrhardt and Shaw, 2006; Lindeboom et al., 2013).

1.5. Microtubule-binding proteins (MTBPs)

In order to perform various cellular functions, the spatio-temporal dynamics of microtubules in the cell has to be controlled precisely. In order to achieve this, there exists a set of special regulatory proteins, which can interact with microtubules and change its dynamics in response to the various environmental cues. These proteins are known as microtubule-binding proteins or MTBPs and they share some common elements, like motifs, domains, mechanism and cellular process they control, with each other and can be grouped together according to these common elements or properties. MTBPs consist of large variety of proteins that have been shown to bind microtubules experimentally and another term, microtubule-associated proteins (MAPs) is used to denote a subset of MTBPs which can co-sediment with microtubules through multiple rounds of polymerization and depolymerization and proteins like MAP2 and tau belongs to this class of proteins (Goodson and Jonasson, 2018).

In general, the MTBPs can classify into different groups, either according to their functions like stabilizer, destabilizer, bundlers/cross-linkers and capping or where they localize or bind on microtubule surface like, +TIP binding proteins (recruited to the growing end), minus end binding proteins (recruited to the minus ends) and lattice binding proteins (associate with microtubules along the length) (Figure 3)**.** Other MTBPs proteins include motor proteins which use microtubules for intracellular trafficking and cytoplasmic linker proteins(CLIPs) which is responsible to maintain the cellular organization by anchoring with organelles and fixing its position (Goodson and Jonasson,

2018). There are also a set of MTBPs which links microtubules with other component of cytoskeletons like actin and are known as cytoskeletal integrators (Goodson and Jonasson, 2018).

1.5.1. MTBPs category according to the function

1.5.1.1. Stabilizers

Stabilizers are set of proteins, which either promote polymerization or slows down the depolymerization or catastrophe. Although proteins falling into this group are quite diverse they can be grouped into one or another sub-group according to some similarities in motif, domain or their behaviors. Some of these proteins also contain a conserved domain which are sometimes found to be repeated in their structure. One example is protein XMAP215, a member of cytoplasmic linker associated proteins (CLASP) family proteins which suppresses the microtubule catastrophe and promotes rescue, contains multiple conserved TOG domain (Al-Bassam and Chang, 2011). Calponin-homology domain (CH-domain) containing proteins like EB1 and kinetochore-microtubule linker NDC80 and CAP-GLY containing proteins like CLIP170 and p150glued show microtubule-stabilizing activity and consists a conserved domain. Some stabilizers such as MAP2 and tau, belonging to MAP2/tau family, are only expressed specifically in certain cell types. These proteins also contain, a conserved C-terminal microtubule-binding repeat and are expressed specifically in neurons (Dehmelt and Halpain, 2004). Similarly, the doublecortin family of proteins comprises another set of stabilizers important for neuronal development (Fourniol et al., 2013).

The exact mechanism of how all these stabilizers work has not been elucidated yet, but the presence of multiple conserved domains in these stabilizers indicates that the mode of interaction is most likely conserved among these proteins and occurs through specific binding domains. Some of these proteins seems to act also as a cross-linker and are stabilizing protofilaments both, laterally and longitudinally (Brouhard and Rice, 2018). The neuronal migration protein doublecortin (DCX) recognizes the partially curved structure of $\alpha\beta$-tubulin and bind at the vertex of four $\alpha\beta$-tubulins (Fourniol et al., 2010) (Figure 4C). Another protein TPX2 also binds preferentially to the slightly curved tubulin dimers at growing end and binds at both longitudinal and lateral interface of $\alpha\beta$-tubulin (Brouhard and Rice, 2018; Roostalu et al., 2015a) (Figure 4C). These two completely unrelated proteins seem to suppress catastrophe by same general mechanism that is by stabilizing tubulin-tubulin dimer interface (Brouhard and Rice, 2018).

XMAP215 family proteins recognize the curved tubulin dimers at the growing end and accelerate microtubule polymerization by the addition of the $\alpha\beta$-tubulin dimers (Brouhard and Rice, 2018;

Brouhard et al., 2008) (Figure 4C). But another TOG domain containing family protein CLASP seems to stabilize microtubules in a different way compare to XMAP215. The TOG domains in CLASP seems to recognize a different confirmation compare to the curved confirmation recognized by TOG domain of XMAP215 (Leano et al., 2013). The TOG domain of CLASP seems to recognize a specific tubulin confirmation that occurs during protofilament peeling and initiate microtubule rescue but the exact mechanism is still not known (Brouhard and Rice, 2018). Apart from working alone, recent studies have shown that many different proteins can act synergistically to stabilize microtubules, for example +TIP network protein (Akhmanova and Steinmetz, 2015).

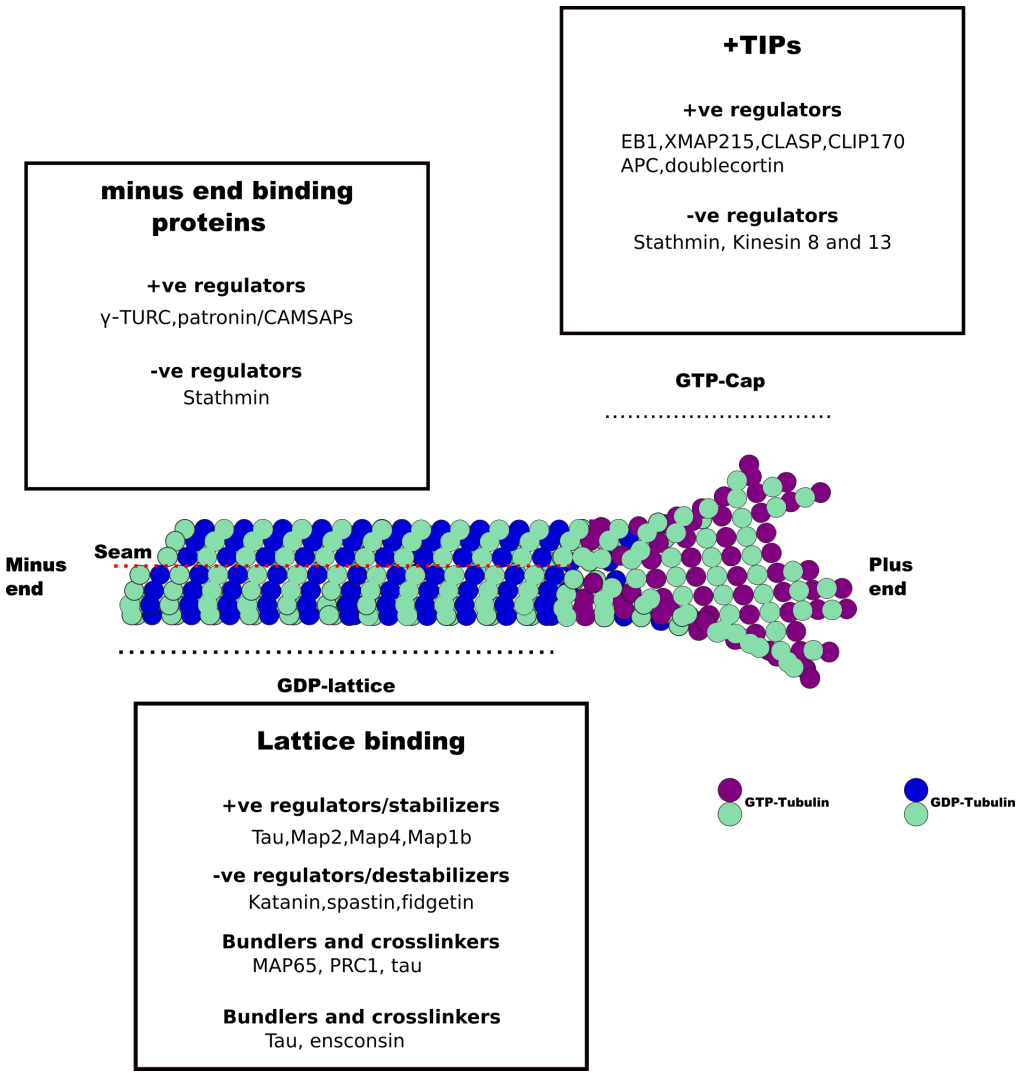

Figure 3. Microtubule-binding proteins can be grouped according to where they localize at microtubule lattice or according to their function.

1.5.1.2. Destabilizers

Destabilizers are a set of MTBPs, which either induce catastrophe by binding to microtubule or sequester the pool of free tubulin, inhibiting the growth or polymerization or even breaking and severing stable microtubules. So, in general they increase the pool free tubulins through one or another mechanism (Goodson and Jonasson, 2018). The protein like stathmin induces the depolymerization by sequestering the free tubulin. When stathmin binds to the tubulin dimers in a curved confirmation, it cannot be incorporated into the microtubule lattice (Cassimeris, 2002). Microtubule-severing proteins like spastin, katanin and fidgetin use the energy from ATP hydrolysis to extract tubulin dimers from the microtubule lattice. This action destabilizes the lattice and results in rapid microtubule depolymerization or catastrophe (Roll-Mecak and McNally, 2010; Sharp and Ross, 2012).

There are also set of destabilizers which can directly attack the growing end of microtubule. The microtubule depolymerase of kinesin-13 family binds specifically to the curved $\alpha\beta$-tubulin and use ATP hydrolysis to induce the outward curvature in filaments resulting catastrophe (Mulder et al., 2009). The mitotic centromere associated kinesin (MCAK) is one of the example of kinesin belonging to this family (Figure 4C). Similarly, another kinesin fold containing protein called Kip3 from kinesin 8 family also binds preferentially to the curved $\alpha\beta$-tubulin dimers and induces the depolymerization (Arellano-Santoyo et al., 2017).

1.5.1.3. Cross-linkers and bundles

During mitotic spindle formation in cell division, microtubule's growing ends arrange themselves to form a bundle of antiparallel microtubule filaments. This organization of microtubules is critical for both segregation of chromosome and cytokinesis (Walczak and Shaw, 2010). The protein regulator of cytokinesis 1 (PRC1) cross-links dynamic microtubules that interact in anti-parallel fashion and also co-operates with kinesin motor proteins, kinesin-4 and kinesin-5, to control the dynamics and size of bundled region (Walczak and Shaw, 2010). The bundling of microtubules is not only seen during cell division but also in other stages of the cell cycle. The microtubule cross-linking factor 1 (MTCL1) cross-links microtubules in post-mitotic cells via its N-terminal microtubule-binding domain (Kader et al., 2017). Microtubule bundling is also very important for the axon development in neurons. Tau and MAP2 are known to bundle microtubules inside axons and dendrites, respectively (Dehmelt and Halpain, 2004). In vitro experiment has also shown that shielding or neutralizing the negative charge

produced by acidic C-terminal tail by CAP-GLY domain could result in bundling of microtubule and promotion of polymerization of microtubule (Wang et al., 2014b).

1.5.1.4. Capping proteins

Several proteins can bind to the growing plus end or minus end in order to stop either tubulin dimer association or dissociation. One of the most characterized capping protein is γ-TURC and γ-TUSC complex which nucleates microtubules and also caps the minus end of microtubules. At the growing end, some evidence shows that stathmin can cap PFs and stop tubulin dimer addition (Gupta et al., 2013). Although the minus end tracking proteins such as CAMSAP and patronin are also suggested to be minus end capping protein and suggested to suppress dissociation, they do not bind to microtubules as γ-TURC complex but binds laterally to the microtubule lattice at minus end (Jiang et al., 2014).

1.5.1.5. Cytoskeletal integrators

The interaction of microtubule with other cytoskeletal components like actin is very important for proper functioning of processes such as cytokinesis, cell polarity, migration and neuronal development (Dent et al., 2011; Rodriguez et al., 2003). The actin nucleating protein formin (Bartolini et al., 2008), myosin10 (Weber et al., 2004) and also microtubule associated protein like tau has been reported as integrators that bind both actin and microtubule (Gallo, 2007). Even large scaffolding proteins like cancer associated protein (APC) and plakin family protein seems to act as integrator (Suozzi et al., 2012). Although we know there exists communications between various cytoskeletal element such as actin and these interactions are important for various fundamental cellular process, the mechanisms are still poorly understood (Goodson and Jonasson, 2018).

1.5.1.6. Other microtubule-binding proteins

There are various other proteins that do not fall in the above-mentioned categories but still play important roles in microtubule-related processes in the cell. Microtubule motors like kinesin, dynein and their accessory proteins such as the dynactin complex play an important role in intracellular transport in the cell (Sweeney and Holzbaur, 2018). There are also a set of proteins like ensconcin (Barlan et al., 2013) and tau (Dixit et al., 2003), which alter the behavior of motor proteins when bound to the microtubule lattice. There is also a membrane-microtubule linker like the cytoskeleton-linking membrane protein CLIMP63, which links the endoplasmic reticulum membrane to microtubules (Gurel et al., 2019).

1.5.2. MTBPs category according to its localization

1.5.2.1. Plus-end tracking protein

The plus end tracking proteins (+TIPs) include a broad group of structurally and functionally diverse set of proteins which have an ability to concentrate at the growing end of the microtubule. +TIPs can further sub-divided into two groups, “autonomous tip trackers”, which can recognize microtubule growing end independent of any other factor and “hitchhikers”, which have some affinity for microtubule but mainly concentrates at the growing end by interacting with other autonomous tip tracker (Akhmanova and Steinmetz, 2015) (Figure 4A). The +TIPs can also be distinguished into different groups according to the conserved structural elements which enable them to interact with microtubule or each other forming a synergistic +TIP network (Akhmanova and Steinmetz, 2015).

EBs (End-binding proteins)

End-binding (EB) family proteins are a small number of +TIPs which are known for their ability to track growing ends preferentially to the stable GTP cap (Maurer et al., 2012) (Zanic et al., 2009). The end binding proteins contain conserved N-terminal calponin homology (CH) domain, which binds at the vertex of four $\alpha\beta$-tubulin dimers (Figure 4B). The EB binding protein is also known as “Master TIP” since other proteins localize to +TIP by binding to EB1 (Akhmanova and Steinmetz, 2015). The CH domain is followed by coil-coil structure mediating the homo or hetero-dimerization of EB proteins. The coil-coil domain extends to four helical bundles followed by a disordered C-terminal EEY/F motif, which mimics the C-terminal tail of tubulin (De Groot et al., 2010). The four-helix bundle along with some part of C-terminal tail form EB homology domain (EBH domain). Through the EEY/F motif, EB protein interacts with various CAP-Gly proteins like p150glued and CLIP170. Also, the EBH domain contain a hydrophobic pocket which binds the SxIP motif of EB1-binding proteins like APC, MCAK, melanophilin and STIM1 (Akhmanova and Steinmetz, 2008).

CAP-Gly (Cytoskeleton-associated protein Gly-rich) proteins

The cytoskeleton-associated protein glycine-rich (CAP-Gly) domain is a globular module which specifically recognizes the C-terminal EEY/F motif of the tubulin tail or EB family proteins. This domain contains a conserved hydrophobic cavity and several characteristic glycine residues which enables it to interact with C-terminal tail of both microtubule and EB proteins. The most notable examples are CLIP proteins and largest subunit of the dynactin complex p150 glued (Weisbrich et al., 2007).

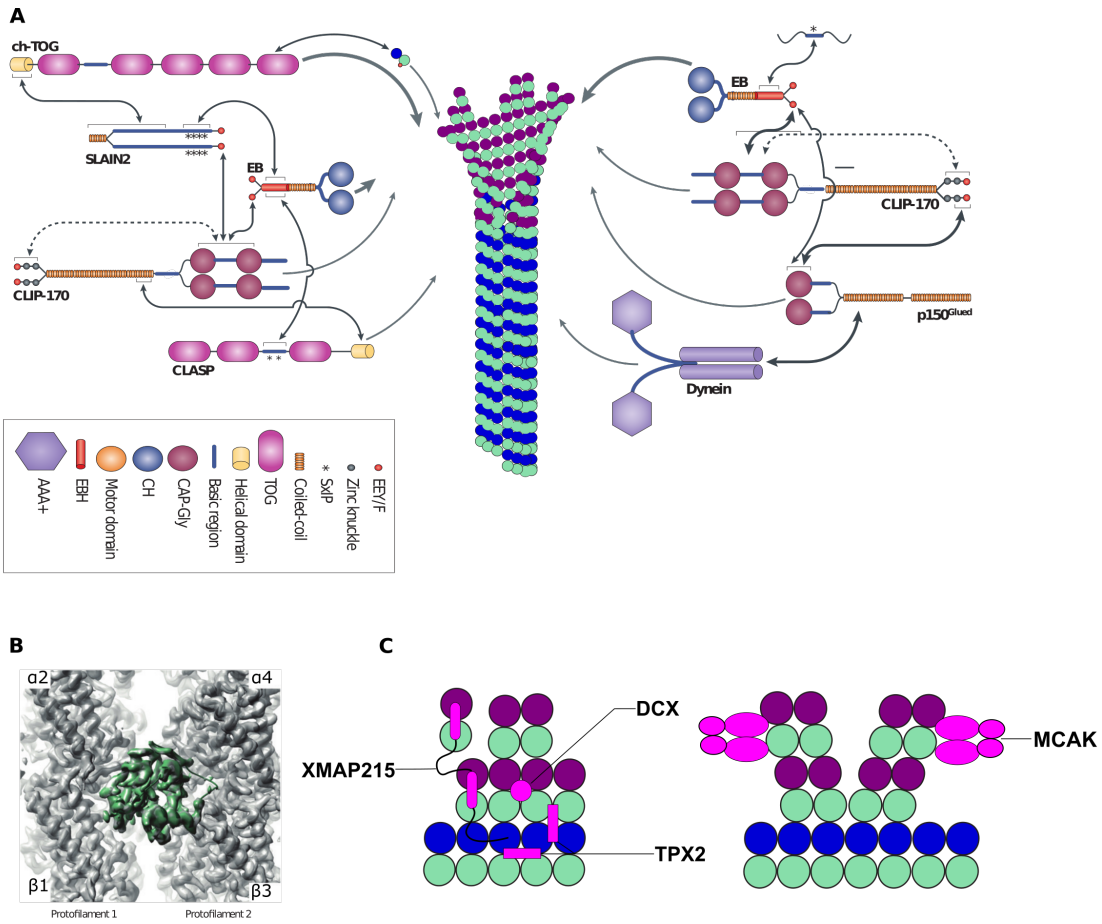

Figure 4. Microtubule plus end binding protein. (A) +TIP network. Schematic illustration of plus end binding protein and their interaction network. The plus end proteins are often composed of structurally conserved domains illustrated in the box. In case of ch-TOG, the TOG domains are repeating and tandemly arranged. EB protein acts as a "Master Tip". Through its CH domain EB protein binds to the microtubule surface and via its C terminal EBH domain and EEY motif it can recruit other proteins like CLIP-170, p150glued, APC, MCAK, CLASP etc. to the microtubule surface. Figure adapted from (Akhmanova and Steinmetz, 2015). (B) EB protein CH domain binds to microtubule at the vertex of four αβ-tubulin dimers (Akhmanova and Steinmetz, 2015) (C) +TIPs like XMAP215, tPX2 and DCX recognizes the curved tubulin and promotes nucleation whereas MCAK stabilizes the curved tubulin confirmation and promotes catastrophe**.**

SxIP motif containing protein

The large number of plus end tracking proteins include large, complex and often multi-domain proteins that contain short Ser-x-Ile-Pro (SxIP) polypeptide motif (Akhmanova and Steinmetz, 2015). This polypeptide motif is localized in low-complexity sequence region of protein that is rich in basic serine and proline residues (Kumar and Wittmann, 2012)**.** This SxIP motif enables these proteins to interact with EBH domain of EB proteins at the +TIP end of microtubule. Some notable examples of the protein

belonging to this family are adenomatous polyposis coil (APC) tumor suppressor, the microtubule-actin crosslinking factor (MCAF) and the mitotic centromere associated kinesin (MCAK) (Figure 4A) (Kumar and Wittmann, 2012).

TOG domain containing proteins

The protein family that contains multiple TOG domains, which include XMAP215 and CLASPS family proteins, are another group of proteins which can autonomously track the +TIP of microtubule (Akhmanova and Steinmetz, 2015) (Figure 4C)**.** TOG domains are arranged tandemly and are responsible for the binding to tubulin (Al-Bassam et al., 2007; Slep, 2009)**.** The TOG domain preferentially binds to the curved $\alpha\beta$-tubulin dimer and increases the rate of microtubule polymerization by increasing the concentration of unpolymerized tubulin near the growing microtubule end (Figure 4C) (Geyer et al., 2015).

Most of the +TIP proteins can bind to each other, which could result in forming a network or web of interacting proteins that work together and the synergistic interaction between these protein is very important to regulate the microtubule dynamics and link it to various other cellular activities (Akhmanova and Steinmetz, 2008; 2015) **(**Figure 4A)**.** This network at +TIP is very dynamic and involves only limited number of protein modules and linear sequence motifs such as CH, EBH and CAP-Gly domain and EEY/F and SxIP motifs.

1.5.2.2. Minus end tracking proteins(-TIP)

One of the most studied minus end protein is γ-TURC complex which caps and blocks the exchange of tubulin dimers at the minus end of the microtubule (Wiese and Zheng, 2000). Apart from the capping function, γ-TURC also acts as a template for the nucleation of the microtubule (Kollman et al., 2011) (Figure 5A). The eight subunits protein augmin (HAUS in mammals) is a γ-TURC interacting protein and mediates the nucleation from the lateral surface of pre-existing microtubule (Petry et al., 2013). In cells, the minus end protein plays important role in determine the geometry of the microtubule as they are stably anchored to the place where they nucleate (Akhmanova and Steinmetz, 2015; 2019). Recently it is becoming clearer that minus end proteins include the structurally and functionally diverse group of proteins and they play an important role in controlling microtubule organization inside the cells (Akhmanova and Steinmetz, 2019) (Figure 5B)

Apart from γ-TURC complex, recently characterized set of proteins, calmodulin-regulated spectrin-associated protein (CAMSAP or patronin in invertebrates) family proteins are found to play an

important role at microtubule minus end (Akhmanova and Hoogenraad, 2015). CAMSAP consists of an N-terminal CH domain followed by a coil-coil region and a conserved C-terminal CKK motif (Baines et al.) (Figure 5B). CAMPSAP protein can track minus end protein, bind to it and inhibit their growth. They interact with the microtubules by laterally binding to the microtubule minus ends (Jiang et al., 2014), unlike the conventional cap like interaction seen in γ-TURC-microtubules. Other proteins that interact with the microtubule minus end are abnormal spindle-like microcephaly-associated protein (ASPM), which inhibit their growth after localizing at the minus end and components of interphase chromatin-associated protein complex (KANSL) that contain KAT8 regulatory NSL complex subunits 1 and 3

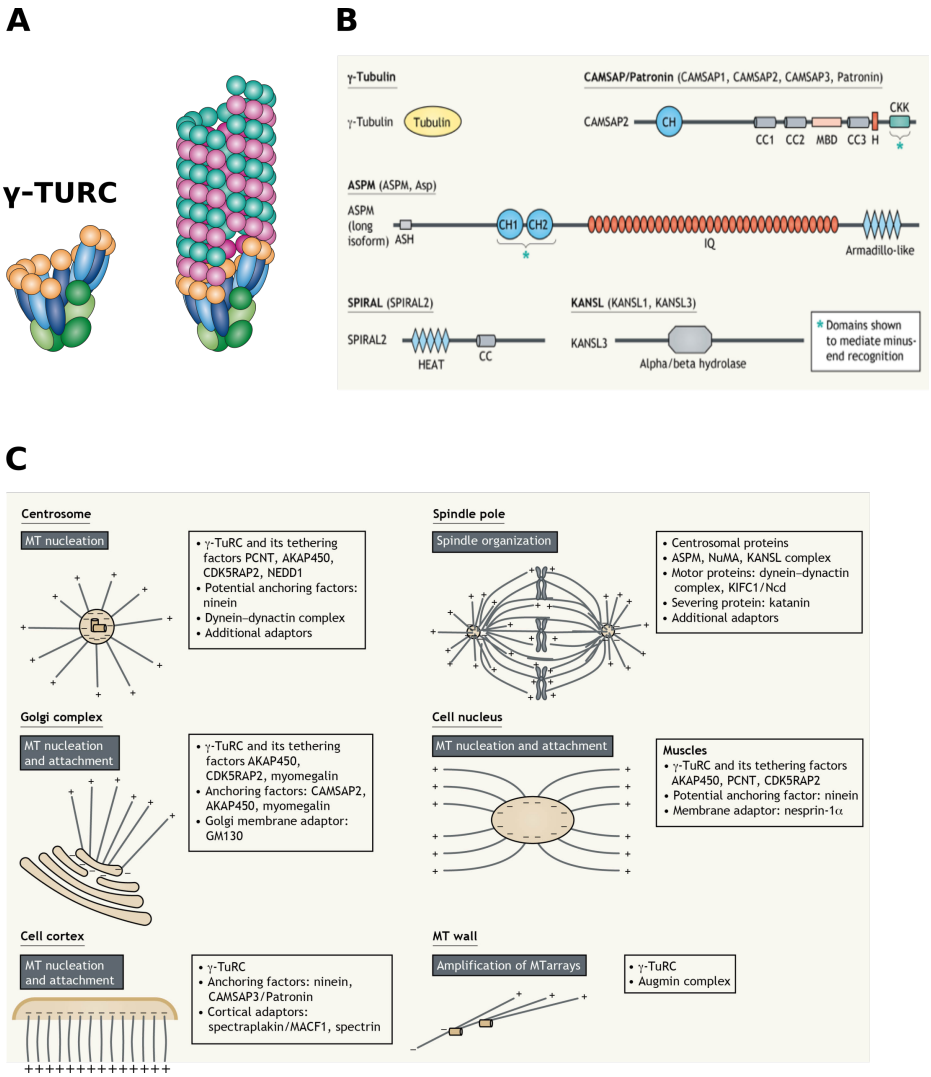

Figure 5. Microtubule minus end protein and microtubule organizing centers in the cell. (A) γ-TURC complex and microtubule nucleation from γ-TURC complex 1(Kollman et al., 2011). (B) Schematic representation of minus end protein (Akhmanova and Steinmetz, 2019). (C) Microtubule organizing center. Apart from centrosome, microtubules can nucleate from various other cellular structures like Golgi complex, chromosome and pre-existing microtubules. Minus end proteins play important role in organizing microtubule organization inside the cell (Akhmanova and Steinmetz, 2019).

(KANSL1 and KANSL3)(Meunier et al., 2015) (Fig. 5B).

1.5.2.3. Lattice binding proteins

Lattice binding proteins include all the proteins that bind to microtubule surface and do not interact with either plus or minus ends of the microtubule (Figure 3). The classical lattice binding proteins are MAP2, tau and MAP4. MAP2 and tau are specifically expressed in neurons and bind to microtubule at dendrites and axon respectively, whereas, MAP4 is expressed in most of other tissues (Dehmelt and Halpain, 2004). Microtubule destabilizers proteins such as spastin and katanin also interacts with microtubule lattice and extracts the $\alpha\beta$-tubulin dimers inducing depolymerization (Roll-Mecak and McNally, 2010). Other microtubule lattice binding protein includes motor regulators such as esconsin (or MAP7) which on binding to microtubule surface regulates motor kinesin-1 activity (Barlan et al., 2013).

1.6. Microtubule based patterns and structures in the cell

One of the most important functions of the microtubule is to maintain cellular architecture and morphology. We can view microtubules as a very dynamic self-organized machinery which undergoes considerable amount of remodeling during various cellular processes. During the cell division, it makes a mitotic spindle making sure the chromosomes are segregated to opposite end, during cytokinesis it forms major component of midbody, during interphase it forms an array which gives cell a certain architecture and microtubule based cilia and flagella plays an important role in motility in various organisms.

1.6.1. The microtubule array during interphase

The microtubule array during interphase plays an important role in maintaining cell shape, organization of cellular organelles like nuclei and also act as a "track" for intracellular transport. In many cell types, the minus end is attached to a microtubule organizing center (MTOC) and the growing ends (+TIP) are grown radially outwards towards the cell boundary (Figure 6A) (Dogterom and Surrey, 2013). Although the radial organization of the microtubule is common in most of the cell types, it is not universal (Figure 6B, D-E). For example, the microtubule array in polarized epithelial cells of vertebrates is parallel with growing end located at the base of cell and minus end at the apical side (Figure 6E) (Bartolini and Gundersen, 2006). In plant like *Arabidopsis,* the cortical parallel bundles of microtubules with mixed polarity are oriented perpendicular to the axis of cell elongation (Ehrhardt and Shaw, 2006) (Figure 6D). Similar mixed polarity and parallel bundles of microtubules is also present in dendrites of neurons but in the axon of neurons microtubules are observed as parallel bundles with

uniform polarity (Conde and Cáceres, 2009; Kapitein and Hoogenraad, 2015) (Figure 7). Also during the elongation of neuron, the parallel bundles of microtubules from axon enters into the growth cone and gets reorganized into various structures like splayed, bend and looped structure (Conde and Cáceres, 2009) (Figure 6B and 7).

During cell migration, the microtubules are organized in a polarized manner, with more microtubules at the cell-front than the rear resulting in an asymmetric distribution. This asymmetric or polarized organization of microtubules results in overall asymmetry in cellular activities which gives direction to the cell migration (Etienne-Manneville, 2013; Garcin and Straube, 2019). This polarity is necessary for the cell to get direction during migration. It was reported that many animal cells can migrate without microtubules but they lose the directionality (Ganguly et al., 2012).

1.6.2. Microtubule organizing centers (MTOC): Centrosomes and spindle pole bodies

A structure which acts as localized foci, from which microtubules nucleate inside the cell is known as the microtubule organizing center (MTOC) and this generally includes centrosomes in animal and spindle pole bodies in fungi such as budding yeast *Saccharomyces cerevisiae* and fission yeast *Schizo-saccharomyces pombe* (Goodson and Jonasson, 2018) (Figure 5c). MTOC contains a specialized nucleating machinery composed of γ-tubulin and γ-TURC, and generally considered as major component of MTOC (Goodson and Jonasson, 2018). Similarly, in the budding yeast *Saccharomyces cerevisiae* MTOC consists of nucleation machinery composed of γ-tubulin small complex (γ-TUSC) and γ-tubulin (Kollman et al., 2011). Apart from these two nucleating components, MTOC also contains complex array of the other regulatory proteins, motors, +TIPs and in most of the case also contains centrioles (Goodson and Jonasson, 2018; Petry and Vale, 2015; Wu and Akhmanova, 2017). Although centrioles were thought to be the important part of centrosome activity it was found to be not necessarily needed, as fly mutant lacking centrioles develop normally (Basto et al., 2006) and many organisms (e.g. higher plants) also lack centrioles (Goodson and Jonasson, 2018).

Although γ-tubulin and γ-TURC complex is consider to be the major components for microtubule nucleation machinery in cells, in flies the depletion of γ-tubulin did not affect the steady state microtubule at interphase and generation and arrangement of microtubules are independent of centrioles (Rogers et al., 2008). Similarly, depletion of γ-tubulin in *C.elegans* suggested that γ-tubulin is required for centrosomal aster formation but was not necessary for nucleation and stabilization of cytoplasmic microtubules (Hannak et al., 2002; Strome et al., 2001). It suggests that there is a possibility of alternative γ-tubulin independent microtubule assembly pathway or presence of other

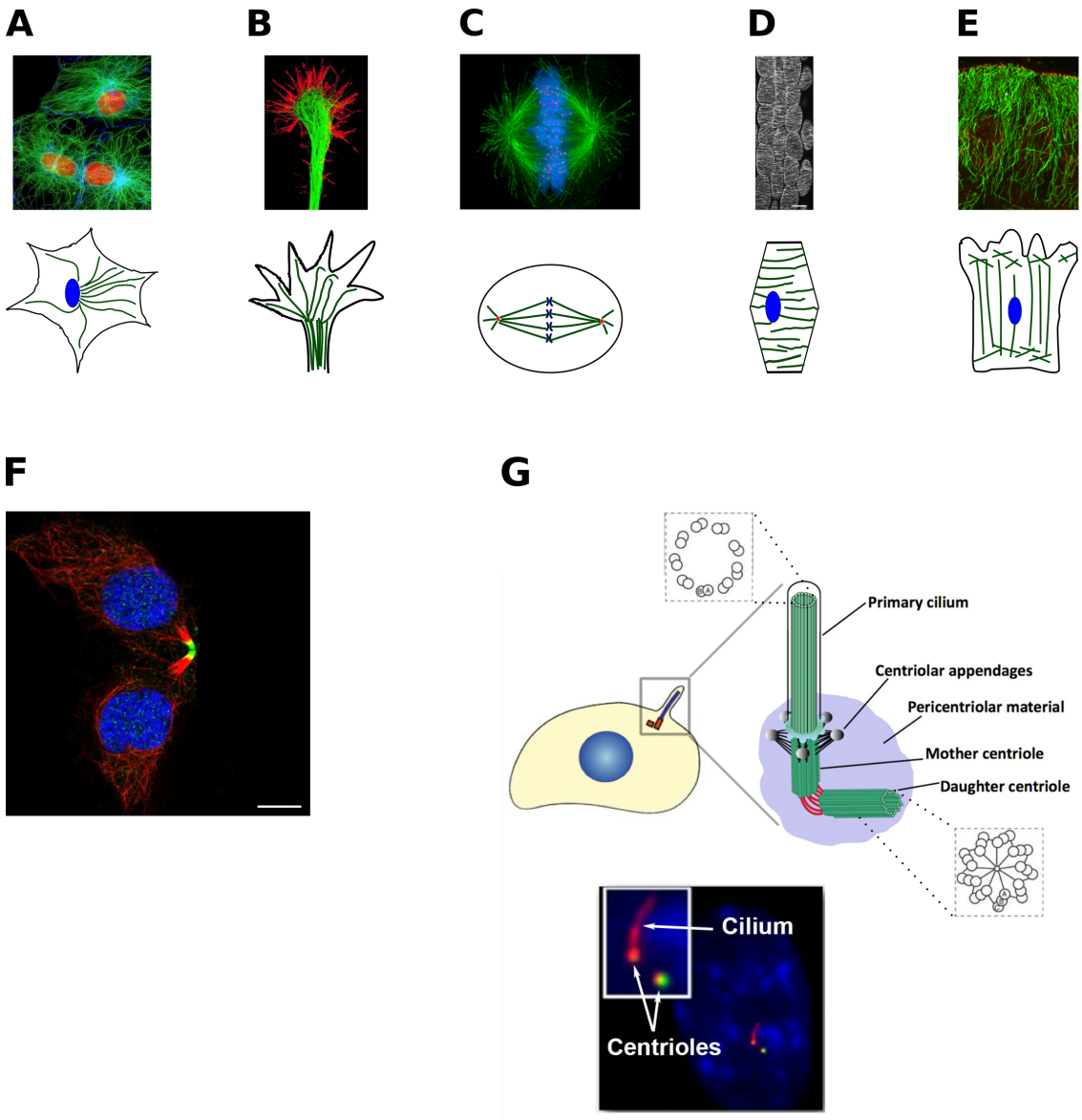

Figure 6. **Microtubule based structures and patterns**. (A) Radial organization of the microtubule array at interphase of fibroblast**)**. Microtubule shown in green and nucleus in red (B) Neuronal growth cone where microtubule shown in green and actin in red (C) Metaphase mitotic spindle during cell division with microtubule in green and DNA in blue and kinetochore in red (D) Cortical array of microtubule from epidermal hypocotyl cells (GFP-tubulin) in plant cells (Elliott and Shaw, 2018) (E) Parallel microtubule array in polarized epithelia cells of vertebrates with microtubule shown in green (F) Midbody formation during cytokinesis in human U-2 OS cells. Microtubule is shown is red and midbody localizing protein LBX2 in green (G) Centrosome is generally composed of pericentriolar material and centrioles. Centrioles generally contain one older "Mother centriole" and younger "daughter centriole". Centrioles at the base of cilia and flagella is known as basal bodies. In centrioles, nine triplet microtubules are arranged in a cartwheel assembly whereas in the primary cilium has nine double microtubules surrounding two central pair of microtubules in a "9+2" arrangements.

[Figure sources: A) *https://pixels.com/featured/1-fibroblast-cells-dr-jan-schmoranzerscience-photo-library.html* B) *https://en.wikipedia.org/wiki/File:Growthcone.jpg* C) *Source: https://commons.wikimedia.org/wiki/File:Kinetochore.jpg E) Source: https://www.bdr.riken.jp/en/research/labs/takeichi-m/index.html* F) *https://www.proteinatlas.org/learn/dictionary/cell/cytokinetic+bridge+4 G)* https://cpb-us-w2.wpmucdn.com/sites.wustl.edu/dist/8/1090/files/2017/11/Anatomy-of-the-centrosome-cilium-complex-12yuinl.jpg]

MTBPs with nucleation activity like TPX2 (Petry et al., 2013) and ch-TOG (Roostalu et al., 2015b) which could rescue the nucleation and centrosome function.

Apart from centrosomes other cellular components can also acts as a MTOC center, nucleating microtubule locally and manipulating the local organization of microtubule architecture (Petry and Vale, 2015; Wu and Akhmanova, 2017). The Golgi-apparatus represents major alternative MTOC in mammalian cells (Wu and Akhmanova, 2017) especially in some special retinal pigment epithelium cells [RPE1 cells] where nearly half of the microtubule initiate from the Golgi apparatus (Efimov et al., 2007).In muscle cells and plant cells microtubule minus end are organized at the nuclear envelope (Masoud et al., 2013; Petry and Vale, 2015; Wu and Akhmanova, 2017).
Microtubule local nucleation in cells not only occur at the intracellular membranes but could also occur independent of it. During mitosis microtubule nucleation can occur around chromatin and kinetochore and plant cells do not contain any centrosome where most of the microtubules are nucleated at cell cortex from older microtubule or at nucleus envelope (Wu and Akhmanova, 2017). The eight subunits protein augmin (HAUS in mammals) is a γ-TURC interacting protein and mediates the nucleation form the lateral surface if pre-existing microtubule (Petry et al., 2013).

1.6.3. Centrioles and basal body

The centrosome generally contains two centrioles, the older “mother centriole” and the younger “daughter centriole”. Centrioles have a symmetrical cartwheel like structure, which typically consists of nine sets of triplet microtubule and two set of appendages at the distal end of the “mother centrioles” (Figure 6G) (Vertii et al., 2016). The cartwheel like structure serves as a platform for microtubule triplets in organized nine-fold symmetry. Apart from centrosomes, centrioles are also found in base of flagella and cilia where they are known as basal-bodies. The centrioles/centrosomes duplicate once per cycle in a highly regulated manner and is directly coupled with the cell division cycle (Wang et al., 2014a).

1.6.4. Cilia and flagella

Cilia and flagella are highly conserved organelle made up of highly organized microtubule based structure, motors and various other proteins (Figure 6G) (Goodson and Jonasson, 2018). They are required for cell signaling and motility in various organisms (Viswanadha et al., 2017). Motile cilia typically contain a single axoneme with nine outer doublet microtubules and two central pair of microtubules in "9+2" arrangement. The cilia and flagella are anchored at the cell membrane by another microtubule based structure called basal bodies (Goodson and Jonasson, 2018). Although the core structure of cilia and flagella is highly conserved, various genomic and functional studies have shown variation in their architecture, function and biogenesis (Carvalho-Santos et al., 2011).

1.6.4.1. Mitotic spindle

The mitotic spindle is a complex, enigmatic self-assembled microtubule based structure formed during cell division and organizes the duplicated DNA so that each copy is attached to each end of the spindle (Figure 6C). It's a bipolar machine mainly composed of dynamic microtubule, various motor and other regulatory proteins. The spindle starts to form at the end of prophase before dispersion of nuclear envelope (McIntosh, 2016). In cells with centrosome, the dynamic microtubules grow radially from the centrosome at the opposite poles, forming the spindle. Microtubules for spindle formation are not only nucleated from centrosome but also from chromatin and microtubule based nucleation pathways (Petry and Vale, 2015; Prosser and Pelletier, 2017). In cells from higher plants which lack centrosomes, a sheath of microtubule is formed around prophase nucleus. As the sheath disperses, the region lying just outside the nucleus at both ends becomes the microtubule nucleation sites, which then enters the nucleus as the nuclear envelope disappears (McIntosh, 2016).

1.6.5. Midbody

The midbody is a transient structure formed during cytokinesis and is localized at the point of abscission or separation of two daughter cells. After the replication of genetic material, at the last step of cell division, the mother cell divides by the formation of cleavage furrow and during the formation of cleavage furrow the microtubule from central spindle gets compacted to form midbody (Dionne et al., 2015). Although it was thought to act as a diffusion barrier that limits the cytoplasmic exchange during telophase, recent studies have shown that post-mitotic midbody acts as a signaling platform regulating stem cell fate and proliferation. It can also serve as extracellular and intracellular polarity

cues during early embryogenesis and during neuron and epithelial cells polarization (Dionne et al., 2015; Goodson and Jonasson, 2018).

1.7. Microtubule dynamics and neuron development

Neurons are highly polarized cells with a single long, thin axon and multiple short dendrites emerging from the cell body. Interestingly, the polarization is not only limited to the morphology but also to its function. The long axon transmits signal and sends information over the long distances whereas the dendrites are specialized in receiving signal. The ability of the neurons to polarize is very crucial to form a complex nervous system. Over the period of development, neuron undergoes various morphological changes like migration, development of axon and dendrites, axon branching and establishment of synaptic connections (Kapitein and Hoogenraad, 2015). Along with actin, structural organization and dynamic remodeling of microtubules is essential for completing these morphological changes (Conde and Cáceres, 2009; Kapitein and Hoogenraad, 2015). Recent studies have shown that, microtubule defects caused by mutations in genes of microtubule binding proteins is related to various neurological disorders and neurodevelopment problems (Kapitein and Hoogenraad, 2015). Also, various genetic studies are able to identify mutation in tubulin family members which are involved in neurodegenerative diseases (Franker and Hoogenraad, 2013; Kapitein and Hoogenraad, 2015; Tischfield et al., 2011).

1.7.1. Neuronal microtubule cytoskeleton

Neuronal microtubules form densely packed parallel arrays in dendrites and axons which are required for both growth and maintenance of the neurons (Conde and Cáceres, 2009). It has two major functions inside the neurons, the first one of which is to guide the intracellular transport of the various neuronal cargos like organelles, synaptic vesicle precursors, adhesion molecules, signaling molecules, mRNAs and neuro transmitter receptors (Hirokawa et al., 2010) and the other is to induce morphological changes during various stages of neuro-development and synapse formation (Conde and Cáceres, 2009).

1.7.2. Microtubule and neuron morphology

Microtubule along with actin plays a very important role in various phases of neuronal development like neurite initiation, growth cone formation, axon branching, synapse formation and migration (Lewis et al., 2013). Microtubules contribute to these processes either by acting as a structural element or by providing mechanical forces or by being the medium for intracellular transport and also acting as a signaling platform (Kapitein and Hoogenraad, 2015). Various pharmacological studies have shown that

microtubule depolymerizing drugs inhibit the growth of neurites and causes their retraction (Daniels, 1973; Yamada et al., 1970). Microtubule organization in neuron differs in both axon and dendrites in terms of the orientation and the microtubule associated protein (MAP) they contain. The microtubules are organized in uniform plus end out oriented parallel bundles in axons whereas dendrites contain the microtubule bundles of mixed polarity (Figure 7). Similarly, the axon mainly contains the protein tau whereas dendrites are rich in MAP2(Conde and Cáceres, 2009; Kapitein and Hoogenraad, 2015).

One of the most important function of the microtubules in neurons is to transport diverse cargoes and maintain robust signalling pathways from synapse to soma and vice versa. Various neurodevelopmental and neurodegenerative diseases have been associated with mutations in the axonal transport machinery (Maday et al., 2014). Since intracellular transport plays crucial roles in the development and maintenance of axonal, dendritic and synaptic processes, cells employ a set of mechanisms to ensure that cargo is delivered to the right destination (Maday et al., 2014). Neurons show polarization in terms of cargo transportation to axon or dendrites, with specific motors targeting either one of them (Kapitein and Hoogenraad, 2011; Kapitein et al., 2010). Although the exact mechanism for this polarized transport remains unclear, recent studies have shown that the specific organization of microtubules in terms of orientation in dendrites and axon provides the selective transport routes for the sorting of cargoes (Kapitein and Hoogenraad, 2011; Rolls, 2011). Microtubule minus end directed motor protein dynein selectively transports the cargoes in dendrites (Kapitein et al., 2010) whereas the plus end directed kinesin family member protein such as kinesin-1 seems to be selectively transporting cargoes into axons despite the presence of plus end out microtubules in dendrites (Nakata and Hirokawa, 2003). Non-polarized targeting in both axon and dendrites when treated with microtubule stabilizing agent taxol shows that there is also some interconnection between microtubule stability and polarized transport (Kapitein et al., 2010).

1.7.3. Neuron initiation and axon specification

Axon specification, how the newborn neuronal cells decides which minor extension to choose from the many available to form a single axon, is a longstanding question in the field of neuroscience. Axon specification is the first step towards the neuron polarization and development (Conde and Cáceres, 2009; Kapitein and Hoogenraad, 2015; Rao and Baas, 2018). The major cytoskeleton components, actin and microtubules, play a major role in neuronal polarization and development. Various studies have shown that the actin and microtubule provide mechanical force of pull and push which contribute to the formation membrane protrusion (Dent et al., 2011; 2007). Various ultrastructural and immunofluorescence studies have shown that the neuronal microtubules are composed of two distinct population, in terms of stability. There is a distinct stable microtubule domain which is enriched in

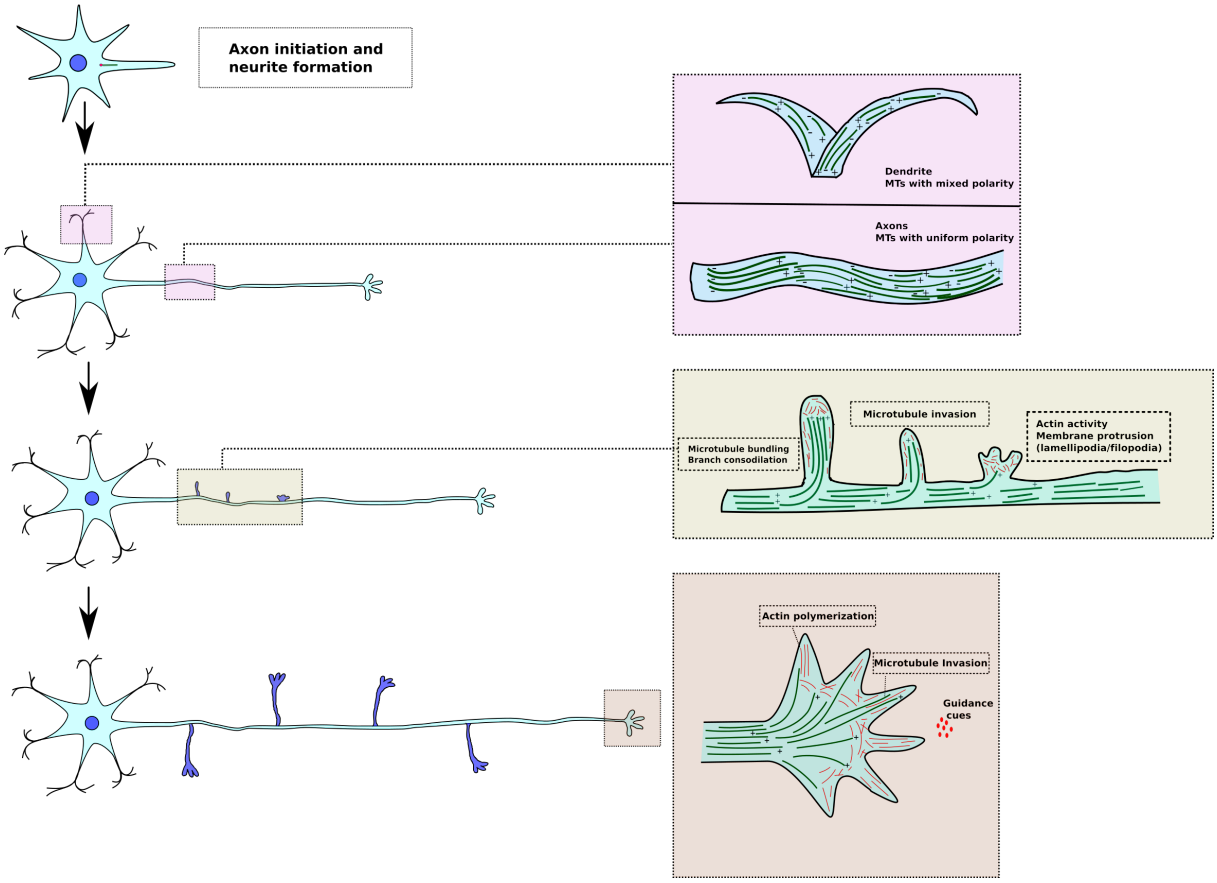

Figure 7 Role of microtubule in neuron initiation and elongation. Axon initiation is the first step towards neuron elongation and development and microtubule stabilization is central to this process. After the axon initiation, the axon growth cone leads the axon elongation process. The axon contains uniformly oriented microtubules with growing end out parallelly bundled together whereas the dendrites contain microtubules with mixed orientation. During axon elongation, the dynamic microtubules play important role as the polymerizing microtubules gives the pushing force needed and whereas the retrograde flow of actin provides the pulling force. During the axon growth, the collateral branches can appear at various region on axonal shaft. Axon branch can form either by bifurcation of the growth cone or via interstitial mode of branching. For branch formation, the dynamic actin leads to the formation of membrane protrusions knowns as lamellopodia or filopodia which is then stabilized by the invasion of the microtubules. The invading microtubules then bundle resulting in elongation and stabilization of the branch.

acetylated and de-tyrosinated tubulin and is resistant to nocadazole treatment with long half-life ($t_{1/2}$ > 2hr). The other domain consists of tyrosinated tubulin rich region with a short half-life ($t_{1/2}$ < 5 min) and depolymerizes rapidly on treatment of nocadazole (Conde and Cáceres, 2009). The tyrosinated tubulin rich region which consists of dynamic microtubule was found to be assembled from the plus

end of stable microtubules and are highly concentrated at the tip of neurites whereas the stable microtubules are present more at the proximal axon (Baas et al., 1993; Brown, 1992).

The stability of microtubules plays a critical role in axon differentiation. When the neurons were treated with low amount of microtubule stabilizing drug taxol, the extended neurites showed high acetylated to tyrosinated microtubule ratio, proximo-distal tau protein distribution and no MAP2 was present in these extensions. All of the extended neurites were showing similar microtubule organization and MAP distribution compare to the axons in neurons (Witte et al., 2008). Similarly, selective stabilization of the microtubules in one of the neurites using caged photoactivable taxol resulted in the formation of axon and this local stabilization of microtubules did not interfere with neither normal axon elongation nor the growth cone dynamics (Witte et al., 2008).

Microtubule stabilization is at the center of axon initiation, it could act as a seed for dynamic microtubule assembly which generates the required mechanical force during axon elongation (Conde and Cáceres, 2009). They also provide tracks for special motor proteins in order to transport several macromolecular complexes and membrane bound organelles to various locations in axons. A motor protein kinesin-1 binds to acetylated or stable microtubule with higher affinity and this lead to an axon specific polarized trafficking(Reed et al., 2006) (Nakata and Hirokawa, 2003; Nakata et al., 2011). The kinesin-1 motor domains when overexpressed, starts accumulating at the future axon even before the polarization process has actually started (Jacobson et al., 2006).

1.7.4. Axon elongation and growth cone

Axon determination is followed by axon elongation and growth with an axon growth cone leading the elongation process. Axon elongation through the growth cone is a result of coordinated action of actin and microtubule dynamics, with microtubule polymerization providing the pushing force and retrograde transport of actin providing the pulling force (Kapitein and Hoogenraad, 2015a; Lewis et al., 2013). Along with microtubule polymerization, translocation of whole microtubule bundle also drives the growth cone forward. This translocation presumably occurs due to the microtubules sliding on each other as a result of pulling and pushing force generated by the molecular motors (Lu et al., 2013; Roossien et al., 2014; Suter and Miller, 2011).

Unlike the process of axon determination where stable microtubule formation is pivotal to the process, dynamic microtubules function in growth cone formation and elongation. When the low dose of vinblastine, a drug which slows down the microtubule dynamics by inhibiting microtubule assembly, was applied on neurons, it resulted in the growth cone wandering (lateral movements rather than

forward) and axonal elongation was abolished. This process was reversible as when vinblastine was washed out, the neuron presumed its normal growth (Tanaka, 1995). Microtubules not only provide mechanical force at growth cone but also participates in various functional interactions with other important cellular components such as actin, cell cortex, organelles, cargos and adhesion complexes. These functional interactions are regulated by various +TIPs and MTBPs that interact with microtubules (Kapitein and Hoogenraad, 2015; Prokop et al., 2013). It has been reported that the β3-tubulin could directly interact with the membrane protein netrin receptor DCC at the cortex which couples axon guiding cue Netrin-1 directly to the microtubule dynamics during axon growth and elongation (Qu et al., 2013). Microtubules along with being a structural element also acts as a signaling hub that regulates various aspect of neuronal polarization and growth (Conde and Cáceres, 2009; Kapitein and Hoogenraad, 2015).

1.7.5. Axon branch formation

The axon during neuronal development not only elongates but also forms many collateral branches in order to connect with multiple postsynaptic targets. It is a fundamental mechanism for the connectivity in central nervous system and can occur through two distinct mechanisms: splitting or bifurcation of growth cone and interstitial mode of branching (Lewis et al., 2013; Portera-Cailliau et al., 2005). In splitting or bifurcation, the growth cone splits into two of roughly equal sizes during the elongation and enables one single neuron to reach two targets which are far away from each other with a single axon (Lewis et al., 2013). This mechanism of branching is reported to be promoted by guidance cues such as Netrin-1 and is independent of the axon growth (Tang, 2005). The growth cones of the dorsal root ganglion neuron (DRG) neuron splits into two daughter branches and make connection to the target site through these collaterals (Le Ma and Tessier-Lavigne, 2007; Schmidt et al., 2007).

In the interstitial branching mode, the branches are directly formed orthogonally from the axonal shaft days after the growth cone have bypassed the target area (Kalil and Dent, 2014). In the axons of corticospinal neurons, the growth cone first bypasses the basilar pons and only after a delay they form dynamic-finger-like actin rich filopodia which develops into stable branches and arborizes the pons (Bastmeyer and OLeary, 1996). This mode of branching was also observed in callosal axons which connects the two-cerebral hemisphere (Norris and Kalil, 1991), in retinal ganglion cell axons of retinotectal system (SIMON and OLeary, 1990) and in neocortex neurons (Portera-Cailliau et al., 2005). In both thalamocortical neurons and cajal-retzius axons of the neocortex, interstitial branching is the dominant form of branching (Portera-Cailliau et al., 2005). In cortical neurons, the branching occurs at the region where the growth cone pauses shortly before the continuing (Györgyi Szebenyi et al., 1998).

This pause of the growth cone was thought to leave a 'mark' which could determine the future axon branching sites (Kalil et al., 2000).

Neuronal axon branching is critical for the formation of complex neural circuitry by connecting one single neuronal cells to the various synaptic targets. Regardless of type of branching, the cytoskeletal reorganization and dynamics during the formation of branches remain the same. First the actin filaments undergo the reorganization through the cycle of polymerization and depolymerization, giving rise to a membrane protrusion (filopodia, lamellopodia), followed by the invasion of microtubule which then consolidates otherwise transient structure. After the invasion, the branch starts to mature and elongate through microtubule bundling (Ketschek and Gallo, 2010; Lewis et al., 2013) (Figure 7). In sensory neurons, the actin filaments transiently accumulate to form an actin patch at the axon membrane protrusions, which gives rise to filopodia and lamellipodia (Ketschek and Gallo, 2010; Spillane et al., 2011). Actin dynamics is highly regulated in neurons by an array of actin-associated proteins during branch formation. Enable/vasodilator-stimulated phosphoprotein (ENA/VASP) that binds at the barb end of actin and promotes actin polymerization plays an important role in filopodial dynamics. It remodels the actin network in response to the guidance cues and when the amount of ENA/VASP was reduced by sequestering it to the mitochondria, it resulted in fewer filopodia formation in hippocampal neurons (Lebrand et al., 2004) Other actin nucleator proteins such as formin/mDia2 (Dent et al., 2007), cordon-bleu (Ahuja et al., 2007) and actin-related protein 2/3 (ARP2/3) function in neurite initiation and axon branching (Dent et al., 2011). Not only nucleators, but also actin severing proteins play a role in filopodial dynamics and subsequent axon branching. An actin severing protein gelsolin when depleted in hippocampal neurons, promotes filopodia formation through reduced retraction (Lu et al., 1997). Another actin severing protein, actin depolymerizing factor (ADF)/cofilin, promotes actin polymerization by increasing the pool of free actin and generating free barbed ends, which are important for filopodial dynamics in retinal growth cones (Chen et al., 2005).

The dynamic instability property of microtubules enables it to reorganize, explore and extend into the filopodia and stabilize the branches which is otherwise a transient structure(Kalil and Dent, 2014). The microtubules in the axons are parallelly bundled so the first step during filopodia invasion is unbundling or splaying of the microtubules, then the local fragmentation occurs at the branch points and then these fragmented short microtubules enters into the filopodia(Kalil and Dent, 2014; Lewis et al., 2013).The invasion of filopodia is very important process during the axon branching as the time-lapse imaging shows that only those filopodia containing microtubules were developed into branches (Dent et al., 1999). Similar to actin, various MTBPs such as bundlers, stabilizers, severing proteins, +TIPS and various motor proteins bind to microtubule and regulate its dynamics during branch formation.

Overexpression of microtubule severing proteins such as spastin and katanin in hippocampal neurons increase the axon branching whereas the depletion of these proteins results in reduction of axon branches (Yu et al., 2008). Also, the tau protein, which stabilizes and protects the microtubule from severing by katanin, when depleted increased the axon branching, most likely due to more activity of katanin (Qiang, 2006). Similarly, other MTBPs like the family of plus end tracking proteins such as EB1 and APC, which regulate microtubule at growing end also contributes to axon outgrowth and microtubule elongation via nerve growth factor(NGF) signaling (Zhou et al., 2004).

During axon branch formation both actin and microtubules play critical, interconnected roles. During neuritogenesis the interaction between F-actin-binding protein debrin and EB3 at the base of filopodia is important for the exploration by microtubules (Geraldo et al., 2008). ADF/cofilin, an actin severing protein, when genetically ablated in cortical and hippocampal neurons, results in failure of neuritogenesis. The ablation leads to actin disorganization due to blockade of actin retrograde flow and impairs microtubule bundling (Flynn et al., 2012). Combined action of two interacting septin protein SEP6 and SEP7 provides a coordinating mechanism for the axon branching. SEP6 when localizes to the axonal patches of F-actin, increases the recruitment of a ARP2/3 regulator cortactin and triggers the formation of filopodia. SEPT7 on the other hand promotes the microtubule entry of axonal microtubules in filopodia leading a formation of collateral branches (Hu et al., 2012). It is getting clearer and clearer that similar to the growth cone, the interconnection interactions between actin and microtubules are important for axon branching.

1.7.6. Formation of neuronal microtubules

In a newly polarized neuron, γ-tubulin rich centrosomes act as an active microtubule organizing center (MTOC) nucleating microtubule. It was thought that the microtubule nucleated at centrosomes are released by microtubule severing protein katanin and this short segment of microtubules was then moved along the axon with motor proteins (Conde and Cáceres, 2009). But over time during development the activity of centrosome loses its function as MTOC and then acentrosomal mode of nucleation plays an important role in axon development (Ori-McKenney et al., 2012; Stiess et al., 2010). During the course of development it was found that the amount of γ–tubulin along with other pericentrioler material like pericentrin is reduced in the centrosome and were delocalized to both axon and dendrites (Nguyen et al., 2011; Stiess et al., 2010). When the microtubules in neurons were depolymerized with nocodazole and microtubule nucleation was visualized after the washout of the drug, acentrosomal nucleation of microtubule in the soma of young neurons and random nucleation all over the whole cell of mature neuron was visualized (Stiess et al., 2010).

Various different type of organelles have been described as MTOC for non-centrosomal nucleation in non-neuronal cells, such as Golgi apparatus, melanosomes in melanophores, plasma membrane of polarized epithelial cells, and nuclear envelope in myotubues (Kuijpers and Hoogenraad, 2011). Similar alternative non-centrosomal mode of nucleation through different nucleation center could also exists in neurons to establish a polarized microtubule network. One of the nucleation center that could play was thought to be Golgi apparatus. In mammals and *Dorsophilla* neuron the Golgi apparatus appears as a stack in soma and as an outpost in dendrites. It was reported that this Golgi outposts along with γ-tubulin and CP309, a Dorsophilla homologue of AKAP450, can act as a nucleation center in dendrites (Ori-McKenney et al., 2012). However later Ngyuen et al. confirmed the importance of γ-tubulin in local nucleation in dendrites but did not support the idea of Golgi outposts housing the microtubule nucleation sites. When an activated kinesin dragged the Golgi out of the dendrites γ-tubulin remained in dendrites and resulted in only small changes in microtubule polarity in dendrites (Nguyen et al., 2014).

An alternative way of acentrosomal nucleation which is independent of any membrane structure was reported, where new microtubules can be generated from the lattice of pre-existing microtubules. In this mechanism an hetero-octameric protein complex called augmin or HAUS is recruited to the lattice of old microtubule which then recruits γ-Turc module and promotes the nucleation (Sànchez-Huertas et al., 2019). More recent study also showed that HAUS complexes are distributed all over the neurons and colocalize with γ-turc and locally regulating microtubule nucleation for proper neuronal development (Cunha-Ferreira et al., 2018). Similar mechanism of branched microtubule nucleation with same components was also reported in dividing cells (Petry et al., 2013). Other mechanism to increase the microtubule number in the cell would be cutting pre-existing microtubules by severing enzymes such as spastin, katanin and fidgetin (Roll-Mecak and McNally, 2010). Microtubule severing by katanin and spastin are important for proper axon branch formation and dendrite development. Depletion of spastin from cultured neuron reduces the axonal branch frequency whereas overexpression resulted into enhanced branch formation (Yu et al., 2008)**,** but the mechanism how these severed microtubules are remodeled into branch structure still remains elusive.

1.8. SSNA1/NA14 (Sjögren's Syndrome nuclear antigen 1/Nuclear Antigen of 14kDa)

SSNA1/NA14 (Sjögren's Syndrome nuclear antigen 1/Nuclear Antigen of 14kDa) is a small coil-coil protein, originally identified as an autoantigen recognized by the serum of a patient with Sjögren's syndrome, localizes at microtubule organizing centers like centrosomes and basal bodies (Andersen et al., 2003; Pfannenschmid et al., 2003). The *Chlamydomonas reinhardtii* homologue of SSNA1 (CrSSNA1)

localizes to the microtubule based structures like basal bodies, flagellar axonemes and also cytoplasmic microtubules. Both human and *Chlamydomonas* protein share around 60% amino-acid sequence similarities with each other and have very similar structural features (Pfannenschmid et al., 2003). SSNA1 is not only conserved in human and algae but the homologous sequence of SSNA1 is found in several other species of fish, insects and protozoan parasites like trypanosoma and trematode (Figure 8B) (Pfannenschmid et al., 2003; Price et al., 2012).

SSNA1 have a relative molecular mass of 14,000 Da and is predicted to adopt a tropomyosin-like single coiled-coil configuration. SSNA1 is predicted to be largely α-helical parallel 2-strand coiled-coiled protein with short disordered C-terminus region (K105-S119)(Rodríguez-Rodríguez et al.) (Figure 8A-B). The N-terminal region of SSNA1 contains a leucine zipper motif from amino-acids 8-22 followed by the region rich in negatively charged residues between amino acids 6-80 and C-terminal region with positively charged residues. SSNA1 seems to make oligomers through head to tail interaction, a property which seems to be conserved across the species(Pfannenschmid et al., 2003; Price et al., 2012; Rodríguez-Rodríguez et al.). The amino acids residues 14-104 was reported to be important for the self-association of SSNA1 by forming parallel coil-coil structure and it was hypothesized that residues Leu 83 and Leu 93 mediate interactions among SSNA1, spastin and microtubule (Rodríguez-Rodríguez et al.).

SSNA1 is a microtubule binding protein and reduction of CrSSNA1 in *Chlamydomonas* with RNAi resulted in multinucleated and multiflagellated cells due to the interference in cell division (Pfannenschmid et al., 2003). Not only in *Chlamydomonas* cells, knockdown of SSNA1 in mammalian cell also affected cell division specially cytokinesis (Goyal et al., 2014). It was reported to interact with spastin and was also proposed as an adaptor to target spastin to centrosome and trigger microtubule severing (Errico et al.). Spastin and SSNA1 also interact with each other at the midbody and plays an important role in cytokinesis(Errico et al.; Goyal et al., 2014). SSNA1 was also reported to be expressed in neurons and overexpression of SSNA1 in primary neurons resulted into the promotion of axon branching and enhanced axonal development.

Apart from this, SSNA1 was also reported to be involved in transport of orphan receptor TPRA40/GPR175 which has been shown to be essential for the regulation of cell division and the interaction with SSNA1 was important for its function of regulating cell division in mouse embryos (Aki et al., 2008). These accumulations of the evidences altogether suggest that SSNA1 is a microtubule binding protein, which is involved in various microtubule related cell processes like cytokinesis,

neuronal development and transport but the exact molecular mechanism the SSNA1 interacts with microtubule and how it modulates its dynamics is still not known.

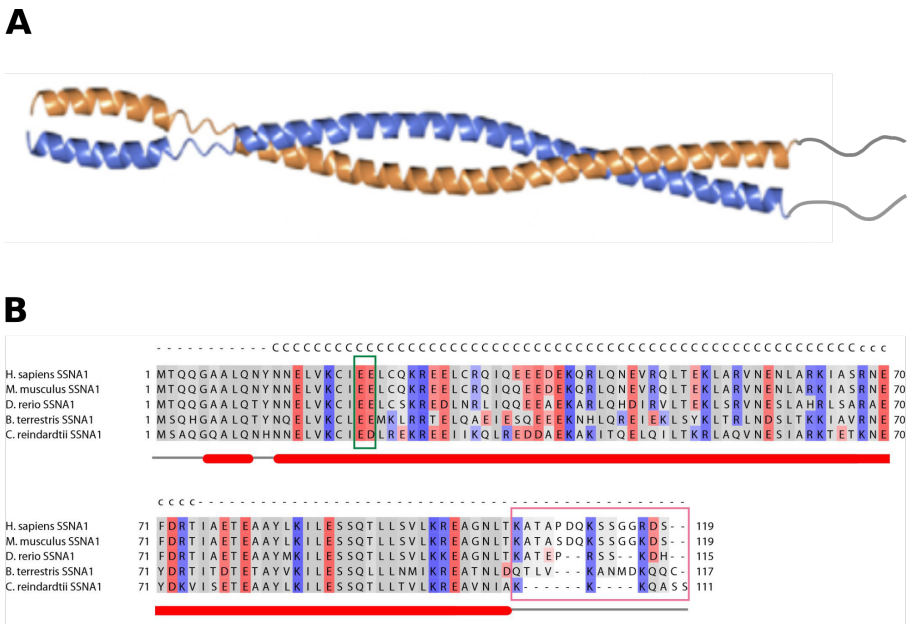

Figure 8. Predicted SSNA1 coil-coil structure and sequence alignment. A) Predicted SSNA1 coil-coil structure. B) The sequence based alignment of SSNA1 proteins. The secondary structure was based on PHYRE2 prediction depicted below the sequence with red bars for α-helices. Coil-coil prediction based on Marcoil is shown above the sequences. The positively charged amino acids are colored in blue, red for negatively charged residues. The red box highlights the variable unstructured region present at the C-terminal.

1.9. Self-assembly in biological system

Self-assembly of small monomers or units into a complex biological macromolecular assembly is crucial to the function of cell. The self-assembly of tubulin and actin monomers into microfilaments such as microtubule and actin is essential for several cellular processes and is tightly controlled inside the cell. Other self-assemblies such as 2D bacterial surface layers (S-layers) and 3D virus capsids plays important roles in other living systems (Yang et al., 2016). Self-assembly does not always involve only protein as a building block but protein could also self-assemble with various other biological components like DNA, RNA and lipids to form a complex structure such as chromatin, ribosomes and coated vesicles. Understanding the self-assembly is very important not only to get insights into the biological mechanism of self-assembled macromolecules but also to understand the mechanism of various pathological diseases triggered due to self-assembly. Some examples include fibrillization of amyloid β-protein(Aβ) in Alzheimer's disease, polymerization of hemoglobin due to single-point mutation in

sickle-cell anemia and aggregation and fibrillization of α-synuclein in Parkinson disease. (McManus et al., 2016; Uversky and Eliezer, 2009).

Self-assembly of protein on membrane surface is critical for the remodeling of membrane for the curvature formation. Remodeling of biological membrane is essential for various biological process such as vesicle trafficking, polarization or migration of cells, cell division and formation of organelles. Various membrane shapes are formed from flat membrane surfaces in coordination of various proteins where protein molecules self-assemble on the membrane surface and drives formation of various kinds of membrane shapes such as flat, tubular, spherical and saddle-like. The non-vaginated plasma membrane shows a flat shape, T-tubules in muscle shows tubular shape, transport vesicles show spherical shape and invaginated vesicle which are not completely developed and emerging from the membranes shows saddle-like shape. The formation of this different shapes and the degree of deformation is controlled by both lipid composition and protein types involved.

Formation of T-tubules is crucial for the excitation-contraction coupling machinery in striated muscles, as *Dorsophilla* amphiphysin mutants are flightless due to disorganized T-tubule network (Razzaq et al., 2001). Amphiphysin2/BIN1 is a crescent shape N-BAR protein which is involved in the formation of these deeply invaginated T-tubules in muscles (Lee et al., 2002). The amphiphysin2 is a special group of membrane curving proteins belonging to the BAR(Bin/Amphiphysin/Rvs) domain superfamily. Numerous proteins of these superfamily play important role in sensing, inducing, binding and stabilizing membrane curvature during cell development and cellular processes (Frost et al., 2009). The amphiphysin structure contains four distinct regions: N-terminal amphipathic helix H0, a BAR domain followed by central region and an C-terminal SH3(Src Homology 3) domain. The highly conserved BAR domain form variably shaped dimers which are used to deform cell membrane into various shapes via electrostatic interactions between the positive charges on its curved surface and negative charges of the membrane headgroups (Peter et al., 2004). The SH3 domain is thought to be involve in downstream interaction partner dynamin (Lee et al., 2002). Amphiphysin2/BIN1 stabilizes the tubular membrane structure in contrast to other N-Bar proteins which are involved in dynamic membrane scission in clathrin-mediated endocytosis (Takei et al., 1999) and it is still not known the structural organization of Amphiphysin/BIN1, how it self-assembles on the lipid surface, how this self-assembly remodel the membrane into tubular structure and its implication on T-tubule formation.

Aim of the thesis

Along with other cytoskeletal components like actin and intermediate filaments, microtubule is essential in order to maintain cell shape and morphology. Change in cell shape, morphology or polarization is very important for various cellular processes. Inside the cell microtubule organizing centres (MTOCs) like centrosome were thought to be only source for microtubule nucleation and organization inside the cell. But recent studies have shown that apart for these known MTOCs there are other components present inside the cell that could nucleate and organize the microtubule architecture locally at the various regions inside the cell and this local organization is critical for cellular processes such as cell division. Specially in a very polarized cell like neurons, where the MTOCs like centrosome loses its activity over the course of development, local nucleation and reorganization is essential for neuronal process like axon elongation and branching.

The microtubule binding protein SSNA1 is known to localize at the microtubule organizing centres like centrioles, basal-bodies and microtubule based structures like mid-body and axoneme. It was reported that this protein could interact with microtubule severing protein spastin and plays important role during cytokinesis in cell division. The knock-down of this protein using RNAi method resulted in multinucleated cell in mammalian cell lines and multi-flagellated cells in green algae. When over-expressed in neuron, it resulted in elongation and hyper-branching of the axons. This phenotypes in different cells shows that this protein is capable of modulating several microtubules based processes inside the cell, but the exact information how it interacts with the microtubule, what it does with microtubule or how it controls the microtubule dynamics inside the cell was not clear. The aim of the thesis is to address these questions, to biochemically and structurally characterize its interaction with the microtubule and the implication of this interaction in neuron axonal branching.

1. Results

1.1. Direct induction of microtubule branching by microtubule nucleation factor SSNA1

Basnet, N., Nedozralova, H., Crevenna, A.H., Bodakuntla, S., Schlichthaerle, T., Taschner, M., Cardone, G., Janke, C., Jungmann, R., Magiera, M.M., et al. (2018). Nature Cell Biology *20*, 1172–1180.

This study shows that SSNA1 can nucleate and induce the remodelling of microtubule into a branched structure where a new microtubule directly branches out from the existing old microtubule. The remodelling or branching property of SSNA1 is related to its ability of self-assembly and the mutants which abrogates the self-assembly of SSNA1 also abolishes microtubule branching. These SSNA1 mutants that abolish microtubule branching in-vitro also fail to promote axon branching when overexpressed in neurons.

This study was conducted under the supervision of Dr.Naoko Mizuno. For this study, I performed biochemical and in-vitro experiments including cloning, design of mutant constructs, data acquisition and analysis for electron and light microscopy (in vitro as well as cellular) experiments. Neuron preparation and super resolution experiments were performed by collaborators. Detailed author contributions are included in the attached article.

ARTICLES
https://doi.org/10.1038/s41556-018-0199-8
nature cell biology

Direct induction of microtubule branching by microtubule nucleation factor SSNA1

Nirakar Basnet[1], Hana Nedozralova[1], Alvaro H. Crevenna[2], Satish Bodakuntla[3,4], Thomas Schlichthaerle[1,5,6], Michael Taschner[1,7], Giovanni Cardone[1], Carsten Janke[3,4], Ralf Jungmann[1,5], Maria M. Magiera[3,4], Christian Biertümpfel[1] and Naoko Mizuno[1*]

Microtubules are central elements of the eukaryotic cytoskeleton that often function as part of branched networks. Current models for branching include nucleation of new microtubules from severed microtubule seeds or from γ-tubulin recruited to the side of a pre-existing microtubule. Here, we found that microtubules can be directly remodelled into branched structures by the microtubule-remodelling factor SSNA1 (also known as NA14 or DIP13). The branching activity of SSNA1 relies on its ability to self-assemble into fibrils in a head-to-tail fashion. SSNA1 fibrils guide protofilaments of a microtubule to split apart to form daughter microtubules. We further found that SSNA1 localizes at axon branching sites and has a key role in neuronal development. SSNA1 mutants that abolish microtubule branching in vitro also fail to promote axon development and branching when overexpressed in neurons. We have, therefore, discovered a mechanism for microtubule branching and implicated its role in neuronal development.

Cell-shape control is critical in a number of physiological processes. Microtubules, the major cytoskeletal component determining cell shape, are mostly nucleated at the centrosome in proliferating cells. During specialized cell-shaping events, such as mitosis or cell polarization, cytoskeletal remodelling is thought to be driven by local nucleation of microtubules using a centrosome-independent mechanism[1–3].

Neuronal cells are a distinctive example of cells with highly complex morphologies. Neurons are shaped in an extremely polarized fashion with a unique-shaped axon protruding from the cell body and stretching over long distances. Individual cells develop branch points from their axons to connect to neighbouring cells, creating an intricate communication network in the nervous system. As the shape of axons is determined by microtubules, these branch points require remodelling of microtubules to split the cytoskeletal path into separate branches[1–5]. As the centrosome is not necessary for the morphological development of the axon[6], it is possible that axonal transformation occurs in a locally regulated manner within the axon. At axon branching points, the local destabilization and fragmentation of microtubules is mediated by the microtubule-severing enzyme spastin, which leads to the emergence of short microtubules[7]. However, the process of splitting the microtubule networks and, specifically, how the local rearrangement of spastin-processed tubulin oligomers or short microtubule fragments occurs has been enigmatic.

Due to its importance in various cell activities, the microtubule cytoskeleton has been well characterized in vitro. In the classical view, microtubules are considered as cylindrical polymers made of ~13 protofilaments. However, in living cells, it has been suggested that microtubules form higher-order branched networks to regulate their distribution within complex cytoskeletal networks[1,8,9]. The branched networks could be envisioned either through the attachment of new microtubule modules onto the side of an existing microtubule, or through direct branching of microtubules. So far, only one example of branching microtubule network has been shown, involving the microtubule nucleators augmin and γ-tubulin, which allow microtubules to grow out from nucleation points that attach to the side of existing microtubules[8,10–13]. There was, however, no evidence that protofilaments in a single microtubule can split apart to form a branched structure. Particularly at axon branch sites, augmin is less likely to be involved in generating branched microtubule networks, but has rather been implicated in determining microtubule orientation by crosslinking adjacent microtubules within an axon[14].

Here we focused on the protein SSNA1, a microtubule-binding protein implicated in the dynamic assembly of microtubules. SSNA1 is found at centrosomes or basal bodies in sperm cells[15,16], and at the midbody in dividing cells[17]. A recent study reported that SSNA1 accelerates neuronal development by promoting axon elongation and branch formation[17]. These observations collectively suggest a versatile role for SSNA1 in microtubule remodelling. However, the nature of its activity in controlling microtubule dynamics is unclear.

We now demonstrate that SSNA1 is a powerful microtubule-nucleating and -branching factor. In vitro reconstitution of SSNA1-mediated microtubule nucleation showed an induction of branched microtubules, where new daughter microtubules directly branch out from existing microtubules. SSNA1 attaches along single protofilaments, guiding them to grow away from a microtubule and template a branched microtubule. Mutation of residues essential for the oligomerization and the microtubule-branching activity of SSNA1, which we designed by structure-guided in vitro experiments, leads to defective axonal branching in primary neurons, showing that the

[1]Max Planck Institute of Biochemistry, Martinsried, Germany. [2]Biomolecular Self-Organization, Instituto de Tecnologia Química e Biológica António Xavier, Universidade Nova de Lisboa, Oeiras, Portugal. [3]Institut Curie, PSL Research University, CNRS, Orsay, France. [4]Universite Paris Sud, Universite Paris-Saclay, Orsay, France. [5]Department of Physics and Center for Nanoscience, Ludwig Maximilian University, Munich, Germany. [6]Graduate School of Quantitative Biosciences Munich (QBM), Ludwig Maximilian University, Munich, Germany. [7]Present address: Department of Fundamental Microbiology, University of Lausanne, Lausanne, Switzerland. *e-mail: mizuno@biochem.mpg.de

simple scaffolding mechanism of SSNA1 can lead to vast morphological changes in neurons.

Results

SSNA1 localizes at axon branching sites in primary neurons. A previous study implicated SSNA1 in the promotion of axon branching[17], but the underlying mechanism remained elusive. To investigate how SSNA1 plays a role in neuron development, we transduced wild-type murine primary hippocampal neurons with lentiviral particles encoding GFP-2A-mouse_SSNA1. Overexpression of SSNA1 led to the promotion of axon outgrowth (Fig. 1a,c), in agreement with a previous report[17]. In addition, we found a striking accumulation of SSNA1 at axon branches (Fig. 1b and Supplementary Fig. 1), which was also observed at secondary branch sites that emanate from an already existing axon branch (Fig. 1b, panel 4, and Supplementary Fig. 1). In agreement with its localization, SSNA1 overexpression led to increased and more complex branching as characterized by the Strahler number (Fig. 1d). Since SSNA1 localizes at the cytosolic compartments where microtubule are dynamic[15–17], we hypothesized that clusters of SSNA1 at branching sites in neurons might facilitate local microtubule nucleation.

SSNA1 induces direct microtubule branching. To assess the influence of SSNA1 on microtubules, we prepared recombinant SSNA1 (from *Chlamydomonas reinhardtii*, CrSSNA1, Supplementary Fig. 2A–C) and tested its interaction using cryo-electron microscopy (cryo-EM; Fig. 2a and Supplementary Fig. 2D). CrSSNA1 induced a formation of direct microtubule branches that split from a single microtubule (Fig. 2a, arrowheads), in contrast to an attachment of a second microtubule on the microtubule surface. Branching occurs by splitting the lattice of the microtubule, and protofilaments of mother microtubules directly continue into the outer surface of the branched microtubule. The bending angle was variable (Fig. 2b,c, 47° ± 15°, and Supplementary Fig. 2D,E), which suggests a rather flexible junction, in contrast to the more rigid, 70° Arp2/3-mediated actin branching[18,19]. Moreover, microtubules occasionally formed fork-like structures with several branches or junctions (Fig. 2b and Supplementary Fig. 2D). This has so far not been observed in any other system, and further underpins the uniqueness of SSNA1-mediated microtubule branching.

Cryo-ET shows diverging microtubules with a break in the microtubule lattice. To further understand the organization of microtubule branches, we performed cryo-electron tomography (cryo-ET) on branched microtubules (Fig. 3 and Supplementary Fig. 2F). Even though SSNA1 itself was not detectable due to the resolution limit of tomographic reconstructions, the microtubule lattice was clearly visible (Fig. 3a,b) and facilitated a tracing of individual protofilaments at the branch (Fig. 3c–e). The tracing showed that two branching microtubules shared a subset of protofilaments with their mother microtubule. In addition, we traced newly assembled protofilaments that were not connected to the mother microtubule (Fig. 3d), as the number of protofilaments doubles compared to the mother microtubule. This shows a discontinuity in the microtubule lattice at the splitting point of the branch.

SSNA1 self-clusters and nucleates microtubules. To explore the dynamic behaviour of SSNA1 causing this unique action in microtubules, we tested the interaction of SSNA1 with unpolymerized tubulin using fluorescence microscopy (Fig. 4a). Considering the average cellular concentration of SSNA1 of 187 nM[20], we mixed 200 nM CrSSNA1 and 8 µM tubulin in the presence of polyethylene glycol (PEG)[21]. Above a concentration of 5% PEG (Fig. 4b), we observed condensates of CrSSNA1 clustering with tubulin (Fig. 4a–c). Interestingly, several microtubules emerged from these CrSSNA1–tubulin clusters (Fig. 4a,b), reminiscent of aster

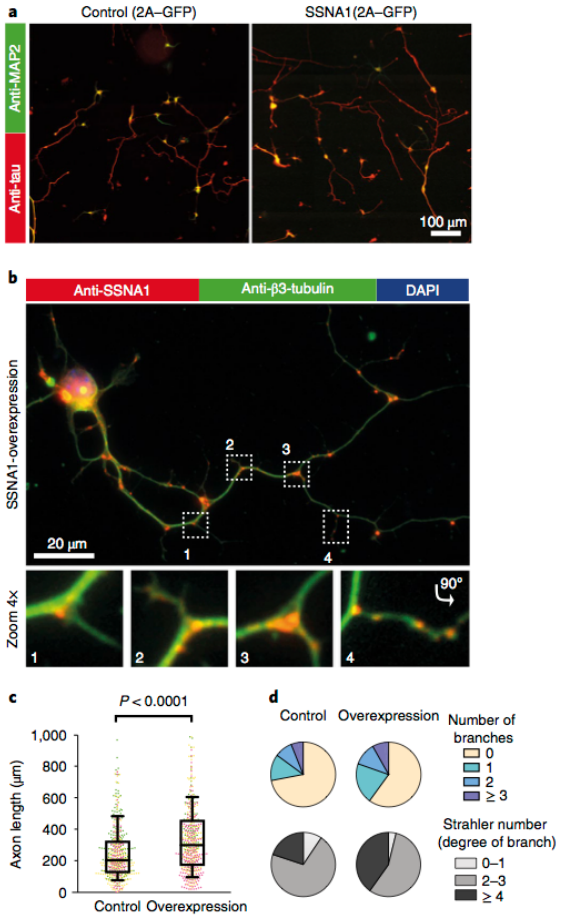

Fig. 1 | The effect of SSNA1 overexpression on primary hippocampal neurons. a, Immunostaining of MAP2 (green) and Tau (red) in control (GFP overexpression) and SSNA1-wild-type overexpression. **b**, Immunostaining of SSNA1 (red) and βIII-tubulin (green) in neurons overexpressing SSNA1 wild type shows the localization of SSNA1 at axon branch sites. **c**, Scatter dot plots of axon length under overexpression of SSNA1. The longest protrusion from the soma was defined as the axon, and cells with very short protrusions were also included in the counting, so that underdeveloped neurons could be assessed as well. The promotion of axon development occurs only in overexpression of wild-type SSNA1. Experiments were performed in triplicates, shown in magenta, green and yellow. Every cell is represented by a single point: control ($n = 505$ cells), wild type ($n = 499$ cells), pooled from 3 independent experiments, and the overlaid box-and-whisker plots cover 50% (boxes) and 90% (whiskers) of the entire population, with median values indicated as lines within the boxes. The results show statistical significance ($P < 0.0001$) as tested using the Kruskal–Wallis test, followed by Dunn's multiple comparison post hoc test. **d**, Pie graphs showing the distribution of the number of branches under overexpression conditions (control ($n = 496$ cells), wild type ($n = 490$ cells) pooled from 3 independent experiments) and Strahler number (degree of sub-branch formations on the existing branches; control ($n = 266$ cells), wild type ($n = 289$ cells) pooled from 3 independent experiments). Distributions of the branches and the Strahler number in SSNA1-expressing neurons differ significantly from the control (GFP overexpression) according to χ^2 two-sample test ($\chi^2 = 20.7$, $P < 0.01$ and 18.6, $P < 0.005$, respectively). See Supplementary Table 3 for source data.

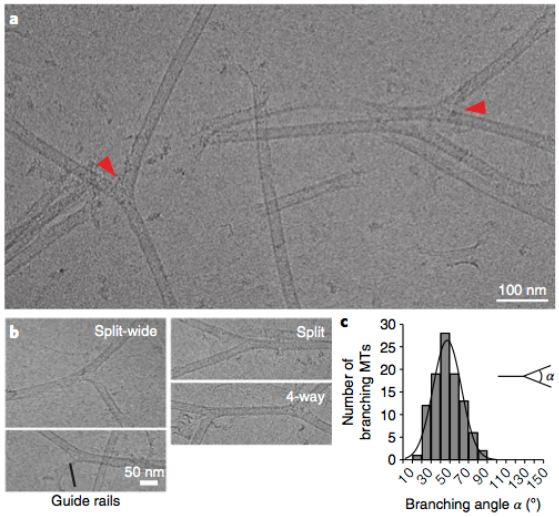

Fig. 2 | Characterization of in vitro-reconstituted microtubule branching. **a**, A cryo-EM image of branched microtubules. The arrowheads show examples of branching points. Microtubules were stabilized with 1 mM GMPCPP. **b**, Snapshots of branching microtubules. The 'guide rail' depicts thin lines of density often seen at the split of the branch point. **c**, Distribution of branching angles (47 ± 15°, $n = 99$ branch points). These experiments were performed three independent times.

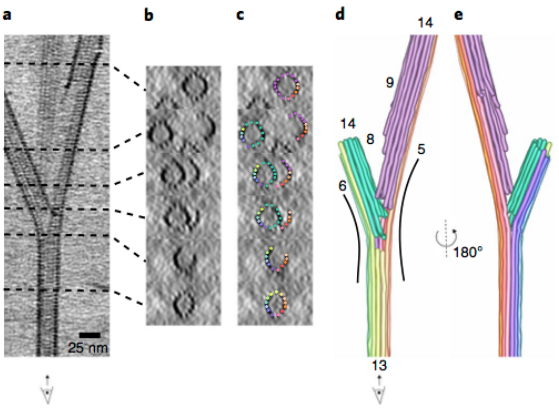

Fig. 3 | The cryo-ET reconstruction of SSNA1-mediated microtubule branching. **a**, A 25-nm slice of a tomographic reconstruction highlighting a branching point of a microtubule. With this view, individual protofilaments and tubulin units are visible, but the SSNA1 density is too thin to be visualized. **b**, Cross-sections of the branched microtubules in **a**. **c**, Individual protofilaments are overlaid with colour represented in the segmentation in **d**. **d**, Tracing of protofilaments in the 3D density map in **a**. Individual protofilaments are coloured in rainbow-colour coding. The newly formed protofilaments from the branched microtubules are coloured in green (left) and in pink (right). The number of protofilaments in this particular branched microtubule is counted to be 13 (mother microtubule), 14 (left branched microtubule) and 14 (right, branched microtubule). Thirteen mother protofilaments are split to 6 to the left and 5 to the right side of branched microtubules. **e**, 180°-rotated segmentation of the branched microtubule.

formation seen during microtubule nucleation[1,22], and thus indicating that CrSSNA1 nucleates microtubules. This process was effective at a CrSSNA1 concentration of as little as 50 nM (Fig. 4d,e). Nucleation events were confined to the local condensates of CrSSNA1 and tubulin did not polymerize without CrSSNA1, highlighting the effect of the SSNA1 condensates and the requirement of a high local concentration. The number of growing asters and microtubules (Fig. 4d,e) correlated well with the concentration of CrSSNA1. We also observed new microtubules emerging from already formed microtubules (Supplementary Videos 1 and 2).

SSNA1 induces microtubule nucleation from mother microtubules. To understand and assess SSNA1-mediated nucleation from template microtubules, we mixed (3 or 30 μM) CrSSNA1 with tubulin in the presence of GTP with GMPCPP-stabilized microtubule seeds[23]. Several microtubules were able to grow out from the ends or the wall of pre-existing microtubules (Fig. 4f,g, Supplementary Fig. 3A,B and Supplementary Videos 3 and 4), agreeing with the cryo-EM observation (Fig. 2a). By differentially labelling pre-existing microtubules (red) and newly polymerized dynamic microtubules (green), we could categorize the branching events into: 'splitting', in which newly formed microtubules split from the end of a pre-formed microtubule; 'end-joining', showing three pre-existing microtubules connected through newly formed tubulin oligomers; 'side branching', seen as new microtubules coming out from the side of pre-existing microtubules; and 'dynamic branching', in which newly generated dynamic microtubules form a branch. The 'side branching' is reminiscent of local microtubule nucleation mediated by augmin and γ-tubulin in cell extracts[8,13]. However, in contrast to the augmin-mediated mechanism, the formation of CrSSNA1-mediated branching did not require γ-tubulin, indicating that SSNA1 works by a novel mode of action.

SSNA1 forms a fibril-like assembly on the surface of the microtubule with 11-nm periodicity. Although cryo-ET did not visualize the decoration of SSNA1 on microtubules, we observed that the free ends of microtubules are often extended with thin fibrils (Supplementary Fig. 2D, red arrowheads). These fibrils extend from splitting microtubules, seemingly to work as a 'guide rail' for the growth of branched microtubules (Fig. 2b; and Supplementary Fig. 2D, 'guide rail'). Computational averages of the cryo-EM images of microtubules allowed the visualization of CrSSNA1 directly attached to the surface of microtubules, revealing a ladder-like pattern (Fig. 5a, compare to 'microtubule-only control') with a periodicity of ~11 nm (Fig. 5b). We observed that CrSSNA1 facilitated preferential assembly of 13-protofilament microtubules similar to doublecortin[24] and EBs[25]. In contrast, 14-protofilament microtubules are predominantly polymerized in the absence of SSNA1 (Fig. 5c).

SSNA1 forms a head-to-tail fibril with 11-nm periodicity and covers the C-terminal tail of microtubules. SSNA1 is a protein with a relative molecular mass of 14,000 Da predicted to adopt a tropomyosin-like single parallel coiled-coil configuration[26,27] (Supplementary Fig. 3E). Fibril formation has previously been observed as a result of head-to-tail self-assembly[27,28]. Accordingly, we observed that CrSSNA1 readily forms short fibrillar appearances with occasional long fibril formations (Fig. 5g, 'FL'). Furthermore, the shorter fibrils of CrSSNA1 were converted into longer, organized bundles of fibrils after ~24 h incubation (Supplementary Fig. 3F). A closer look at these bundles revealed a striped, knob-like pattern, which leads to the formation of a sheet (Supplementary Fig. 3F, 24 h) with a 11-nm periodicity (Supplementary Fig. 3F, inset), and the inter-fibril distance of 3.5 nm. This pattern is comparable to that observed on the microtubule surface (Fig. 5a), indicating that the fibrils are covering microtubules along their long axis, giving a 11-nm spaced ladder-like pattern.

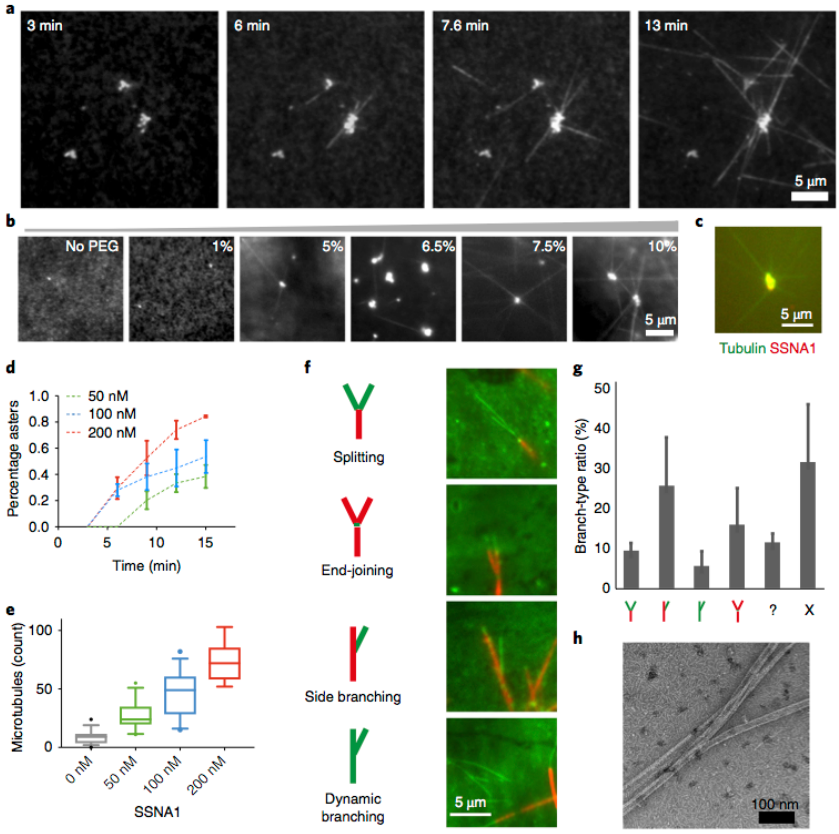

Fig. 4 | Nucleation and branching of microtubules mediated by CrSSNA1 under various conditions. a, Aster-like formation of microtubules (20% HiLyte488 tubulin) occurs within 3 min after mixing tubulin with a lower concentration (200 nM) of CrSSNA1 (upper) under conditions mimicking molecular crowding (7.5% PEG, typically used as a crowding agent), where tubulin alone does not form any polymers. Microtubules propagate out from tubulin concentrate, serving as a nucleation centre. These experiments were performed three independent times with similar results. **b**, 200 nM CrSSNA1 and 8 μM tubulin self-associate, forming clusters in the presence of PEG with concentration >~5%. **c**, SSNA1 antibody recognizes the microtubule nucleation centre. **d**, A plot of the percentage of the concentrates growing into asters with microtubules as a function of time (min) in the presence of 50, 100 and 200 nM CrSSNA1. The error bars are mean ± s.d. from $n = 3$ independent experiments. As little as 50 nM of CrSSNA1 is sufficient to observe aster formation in the presence of 7.5% PEG. **e**, Counts of microtubules observed per field of view, in the presence of different concentrations of CrSSNA1. The box plots cover 50% (boxes) and 90% (whiskers) of the entire population, with median values indicated as lines within the boxes. Sample size: 0 nM: $n = 42$ fields of view; 50 nM: $n = 29$; 100 nM: $n = 30$; 200 nM: $n = 25$. Data were pooled from three independent experiments except for the first point (0 nM) for which data were pooled from four independent experiments. **f**, Green coloured dynamic microtubules on red-microtubule GMPCPP seeds in the presence of a higher concentration of CrSSNA1 (30 μM) without molecular crowding agents to achieve globally concentrated conditions. 'branch-like' nucleation is observed. Branches were categorized as 'splitting', 'end-joining', 'side branching' or 'dynamic branching'. **g**, Ratios of different branch types ($n = 895$ branches, mean ± s.d. pooled from 3 independent experiments). '?' shows the bundled microtubules, which are difficult to categorize. 'X' shows microtubules without branching. Branch-like nucleation can be seen from the locally concentrated SSNA1 condition described in **a**–**e**; however observations of individual microtubules are challenging due to the high local protein concentrations. **h**, A negative-stain EM image of SSNA1-mediated branched microtubules in the presence of 200 nM CrSSNA1 and 7.5% PEG, representative of 3 independent experiments. See Supplementary Table 3 for source data.

To further characterize the interaction between SSNA1 and microtubules, we obtained a cryo-EM three-dimensional (3D) structure of CrSSNA1 in complex with microtubules (Fig. 5d–f and Supplementary Fig. 4A) with an overall resolution of 6.1 Å (Supplementary Fig. 4B). Due to the symmetry mismatch between microtubules (4- or 8-nm periodicity) and SSNA1 (11-nm periodicity), SSNA1 was averaged out, and the fibril appeared as a 'cloud' of protein density running parallel to the microtubule surface, with an apparent local resolution of ~11 Å (Supplementary Fig. 4C). However, it was possible to visualize thin lines of additional densities running parallel to the microtubule surface (Fig. 5e,f), which we interpreted as SSNA1 filaments. The SSNA1 filaments run between two protofilaments, proximal to the unstructured, highly acidic carboxy-terminal tails (E-hooks) of tubulin (Fig. 5f labelled 'C'). Removal of E-hooks resulted in weakening of SSNA1 crosslinking with microtubules as determined by EDC (~49% less crosslinked; Supplementary Fig. 4E). E-hooks create a negative electrostatic cloud by their periodical arrangement on the microtubule surface[29],

which could attract the SSNA1 fibrils. This could explain why SSNA1 interacts with microtubules despite the symmetry mismatch. It also suggests that the head-to-tail assembly of SSNA1 fibrils could guide protofilament assembly and microtubule polymerization by covering and neutralizing the E-hooks as shown previously[30].

The head-to-tail fibril formation of SSNA1 is essential for microtubule branching. On the basis of the observation that SSNA1 fibrils appear to guide the protofilaments of microtubules, we hypothesized that the microtubule branching activity is mediated by the formation of long SSNA1 fibrils that curve away and guide the protofilament out of the lattice (guide rail, Fig. 2b and Supplementary Fig. 2D). To test this, we created a series of truncated SSNA1 fragments that abolish fibril formation. On the basis of a PHYRE2 analysis[31] and previous reports[27], we found that SSNA1 contains a well-conserved α-helical region (residues 6–104) followed by an unstructured C-terminal tail (Supplementary Fig. 3E). A series of amino-terminal truncations showed that the first 19 residues were not necessary for fibril formation, as CrSSNA1(20–111) (20-C) formed cable-like bundled fibrils, which were less ordered compared to full-length protein (CrSSNA1 FL), but displayed an ~11-nm pattern (Fig. 5g,h, Supplementary Fig. 5A and Supplementary Table 1). In contrast, CrSSNA1(21-C), a truncation missing one more residue, Glu 20, was unable to form fibrils (Fig. 5g,h, Supplementary Fig. 5A and Supplementary Table 1). This observation correlates with the ability of CrSSNA1(20-C), but not CrSSNA1(21-C), to mediate microtubule branching (Supplementary Fig. 5A and Supplementary Table 1). The key role of the residue Glu 20 for fibril-formation and microtubule-branching activity of SSNA1 was further underpinned by point mutations E20A and E20A/D21A, which drastically reduced microtubule branch formation (Supplementary Fig. 5A and Supplementary Table 1). These mutants may form fibrils, but with much lower frequency and without a distinct higher-order organization.

In the C-terminal region of CrSSNA1, three distinctive lysine residues (Lys 105, Lys 106 and Lys 107) mark the beginning of the unstructured C terminus. CrSSNA1 truncations 1–104 and 1–105 (Fig. 5g,h, Supplementary Fig. 5A and Supplementary Table 1) showed that CrSSNA1(1–104) can no longer form fibrillar oligomers, or induce microtubule branching (Fig. 5g,h), while CrSSNA1(1–105) was purified as fibrils and showed microtubule branching activity (Supplementary Fig. 5A) at a similar efficiency to CrSSNA1-FL. These results indicate that the positive charge of the lysine residues is essential for the ability of CrSSNA1 to form fibrils. We confirmed this by generating a triple point mutant, K105A/K106A/K107A, which indeed abolished fibril formation and microtubule branching (Supplementary Fig. 5A and Supplementary Table 1) for both the full length and the 1–107 fragment. Altogether, our mutational analyses indicate that the key interaction for longitudinal fibril formation is mediated by Glu 20 of one unit and the C-terminal tail (Lys 105–107) of the adjacent interacting unit (Fig. 5i). To confirm this, we created mutants in which the charges of residues Glu 20/Asp 21 and Lys 105/Lys 106/Lys 107 were swapped. When two of the opposite charges were swapped (E20K/D21K/K105E/K106E or E20K/D21K/K106E/K107E), both cable-like formation and microtubule branching activity of SSNA1 were retained. In contrast, swapping of the two negative residues at the N terminus and the three positive residues at the C terminus (E20K/D21K/K105E/K106E/K107E), resulting in a change of net charge from +1 to −1, abolished microtubule branching (Supplementary Fig. 5B). However, this construct was still able to form SSNA1 fibrils and cable-like structures, indicating that the microtubule branching activity depended not only on fibril formation of SSNA1, but also on the presence of an extra negative charge at the unstructured SSNA1 C terminus. This was confirmed by the mutant E20A/D21A/K105A/K106A/K107A, termed 5A, showing a complete loss of microtubule branching activity (Fig. 5g).

Microtubule-branching-deficient SSNA1 mutants abolished the promotion of axon branches. Having gained insights into the molecular organization of SSNA1 and its effect on microtubule nucleation and branching, we hypothesized that the promotion of axon growth and branching observed in neurons overexpressing wild-type SSNA1 might be altered when microtubule-branching-deficient SSNA1 versions are expressed. Our results indeed showed that, in contrast to the SSNA1 wild type (Figs. 1 and 6a–c), SSNA1 with mutations abolishing microtubule branching in vitro also failed to promote the growth of axons or axon branches (Fig. 6a–c and Supplementary Fig. 6A–E) in primary neurons. Notably, a dominant-negative effect was also observed when the 5A mutant was overexpressed for the number of total neurite processes (Fig. 6c), showing a decreased number of major and minor branches. This dominant-negative effect was also found when the two negative residues at the N terminus and the three positive residues at the C terminus were swapped (swap-KK/EEE). Notably, swapping only two opposite charges and leaving the third C-terminal lysine intact (swap-KK/EE) could still promote axon growth (Supplementary Fig. 6D,E). Together these findings show that the ability of SSNA1 to induce fibril formation and microtubule branching at the molecular level correlates with its function of mediating axon branching and development, suggesting the intriguing possibility that it locally generates branched microtubules at axon branch sites.

Morphological change of microtubule networks in non-neuronal cells. To test whether the function of SSNA1 is conserved in different cell types, we used fibroblasts, which are structurally less specialized than neurons, and tested whether overexpression of SSNA1 has the capacity to change the microtubule organization (Fig. 6e–j). Super-resolution light microscopy with DNA-PAINT showed that individual microtubules are well resolved in the control cells with a wide-ranging network (Fig. 6e–g). In contrast, microtubules were rather short in SSNA1-overexpressing cells (Fig. 6h–j), suggesting that SSNA1 can promote nucleation, generating more but shorter microtubules. We also occasionally found microtubules forming three-way intersections, as if one microtubule emerged out of another in both control and SSNA1-overexpressing cells (Fig. 6g,j, arrowheads). These events occurred more often in SSNA1-overexpressing cells (2.8 ± 1.2 occurrences per 100 µm of microtubule) than control cells (1.0 ± 0.35 occurrences per 100 µm of microtubule). Although the limited resolution in light microscopy prevented us from discerning whether microtubules branched with a shared lattice or if two microtubules only attached to each other, the observations were consistent with our in vitro studies by electron microscopy.

Discussion

During cell polarization, the dynamics and distribution of the microtubule cytoskeleton is tightly regulated. Although the centrosome has a major role as a microtubule-organizing centre in less differentiated cells, the inactivation of centrosomes in neurons does not affect axon growth, a process strongly dependent on microtubule assembly[6]. Thus far, the molecular mechanisms regulating axonal microtubule nucleation, especially in the form of branching, have remained a mystery. Here, we show that SSNA1 accumulates at axon branches and promotes axon branching in primary neurons, and can nucleate microtubules in vitro. Mutations interfering with SSNA1 in vitro nucleation activity also affect the occurrence of axon branches in neurons. Together, these results suggest that SSNA1 could act as a microtubule nucleator at axon branch sites.

Strikingly, our work revealed that SSNA1 independently mediates microtubule branching by causing protofilaments to splay apart from the lattice. To our knowledge, no other microtubule-binding protein shows this activity. When tested, EB3 and ch-TOG, known regulators of microtubule dynamics, under the same conditions,

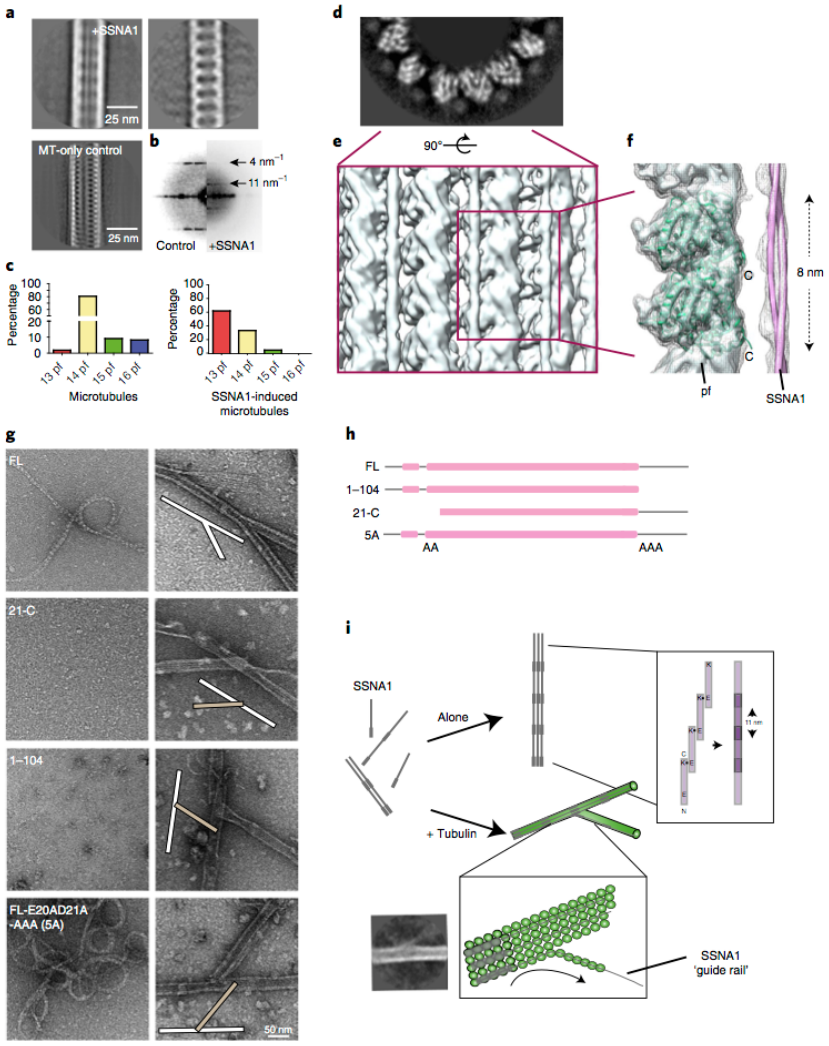

Fig. 5 | Molecular characterization of the branching action of SSNA1. a, Left: representative class average of the SSNA1-induced microtubules. Right: SSNA1 decoration emphasized by computationally subtracting microtubule densities[35]. Bottom left: average of microtubules without decoration for comparison. **b**, The power spectrum of microtubule class averages shows an additional 11 nm periodicity in the presence of SSNA1. **c**, Distribution of protofilament (pf) numbers of microtubules reconstituted from brain tubulin in the absence (left) and in the presence of SSNA1 (right) shifting the majority from 14- to 13-protofilament microtubules. **d**, Greyscale slice from the density map of the plus-end-on view of the SSNA1–microtubule 3D reconstruction. SSNA1 decoration and the secondary structures of tubulin density are well resolved. **e**, Rendering of the microtubule surface decorated with SSNA1. The resolution of the microtubule surface (~10 Å) is not as high as the core (< 8 Å) due to the SSNA1 decoration. **f**, Tubulin atomic model (PDB ID: 3jal) fitted to the map. The SSNA1 coiled-coil fibril is indicated as a tube representation. Note that the periodical feature of SSNA1 is averaged out because of the symmetrical mismatch between tubulin dimers (8 nm) and SSNA1 fibrils (11 nm). **g**, Morphological observation of SSNA1 and its branching activity. Left: observation of the purified protein at 0 h incubation (that is, immediately after purification). Right: a magnified view of the co-polymerized microtubules. Microtubule branching was observed with SSNA1-FL, while other protein fragments do not facilitate branching. For the proteins that do not cause the branching, examples of typical crossing of microtubules (white and beige bars at the scheme within the image), instead of branching, are shown. Detailed observations are available in Supplementary Fig. 5A. **h**, A graphical scheme of the SSNA1 constructs used in **g**. **i**, A scheme of the SSNA1 self-assembly and microtubule nucleation mediated by SSNA1. While SSNA1 oligomers alone can also undergo a slow self-assembly process, the SSNA1 oligomers interact with tubulin dimers to promote their co-polymerization. The polymerized SSNA1 may further act as a guide rail (bottom inset) for protofilament splitting, resulting in microtubule branch formation. A class average indicating the guide rail mechanism is shown. Other class averages are available in Supplementary Fig. 2E.

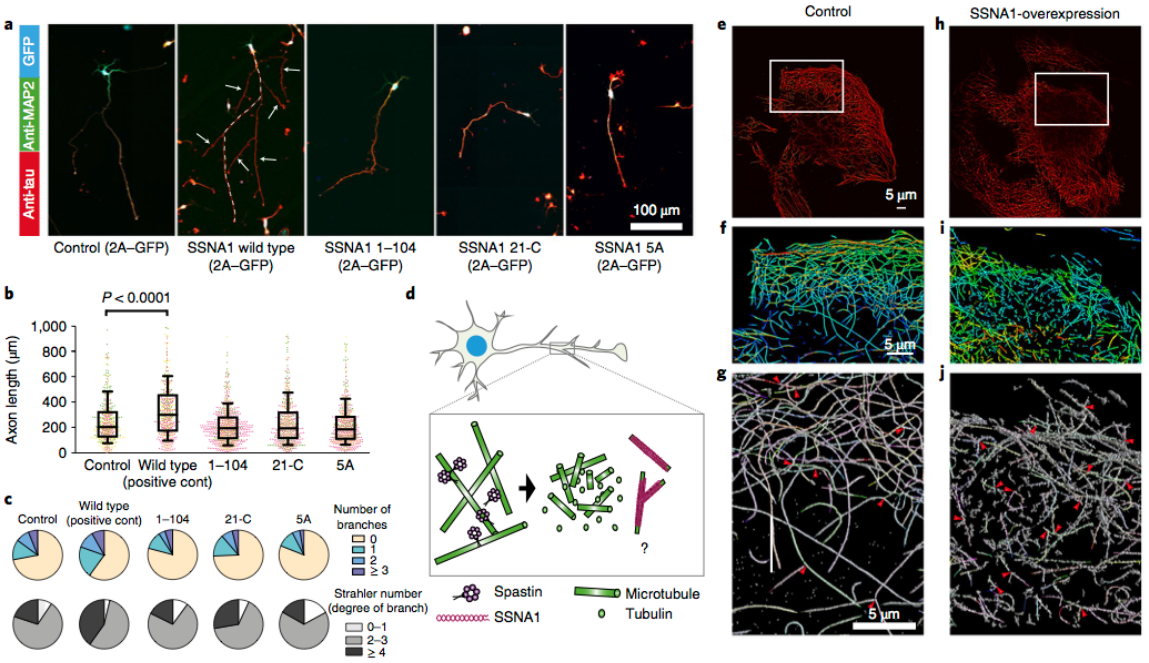

Fig. 6 | The effect of various SSNA1 constructs on primary hippocampal neurons and fibroblast cells a, Immunostaining of MAP2 (green), Tau (red) and GFP (blue, expression control) in SSNA1-overexpressing cells. For the SSNA1 wild type, the axon is indicated with a dashed line. **b**, Scatter dot plots of axon length under overexpression of various SSNA1 constructs. The control and wild-type profiles shown in Fig. 1 are placed as a negative and positive control, respectively. The promotion of axon development occurs only in overexpression of wild-type SSNA1, while no apparent effect was observed for the constructs that fail to mediate microtubule branching. Every cell is represented by a single point; control ($n = 496$ cells), wild type ($n = 490$), 1-104 ($n = 788$), 21-C ($n = 610$), 5A ($n = 642$) from 3 independent experiments, shown in magenta, green and yellow, and the overlaid box-and-whisker plots cover 50% (boxes) and 90% (whiskers) of the entire population, with median values indicated as lines within the boxes. **c**, Pie graphs showing the distribution of the number of branches and Strahler number under different overexpression conditions. The GFP-expression-control and SSNA1-wild-type-overexpression profiles in Fig. 1 are placed as controls. **d**, A schematic model describing how SSNA1-mediated microtubule nucleation could contribute to axon branch formation. Spastin has been shown to localize at axon branches[7] and to interact with SSNA1[36]. Taken together with our finding of SSNA1 localization at axon branches, it is possible that the two proteins work sequentially by spastin severing microtubules to provide tubulin oligomers, and SSNA1 nucleating microtubules at the branching site. **e**, A DNA-PAINT image of a 500-nm slice of the microtubule network in untreated cells (control). **f**, Zoomed-in view from **e**; the object is coloured in a rainbow code according to the depth. **g**, Individually recognized microtubules are highlighted in various colours. Three-way intersections are indicated with red arrowheads. **h–j**, Corresponding view of a 500-nm slice of the microtubule network in SSNA1 overexpressing cells. For analysis, 3 independent SSNA1-overexpressing and control cells were assessed each, containing the total microtubule lengths of 5,700 μm, 7,900 μm and 1,900 μm and 7,700 μm, 8,500 μm and 7,700 μm, respectively. See Supplementary Table 3 for source data.

did not induce branching (Supplementary Fig. 6F,G). In addition, we showed that microtubule branching requires co-polymerization of SSNA1 with microtubules, as well as specific amino-acid interactions. Taken together, these results indicate that the observed branching activity is highly specific to SSNA1.

Our work has uncovered a surprising example of how co-polymerization of a simple coiled-coil protein with tubulin can induce global remodelling of the microtubule network. Association of SSNA1 may reinforce longitudinal connections of tubulin oligomers, facilitate protofilament formation and act as a polymerization seed for microtubule formation. Concomitantly, the preference of SSNA1 for lateral connections may facilitate the lateral associations between microtubule protofilaments. Polymerized SSNA1 may precede microtubule protofilaments, guiding protofilaments out of the microtubule axis, thus providing a template for a new microtubule branch ('guide rail' mechanism). In a cellular context, however, the situation is more complex as SSNA1 activity is probably modulated by other factors. Further experiments are necessary to test this mode of action of SSNA1 for microtubule branching in cells.

Our in vitro reconstitutions showed that SSNA1 self-assembles into clusters together with tubulin at a high local concentration. As axons are densely packed with cytoskeletal components, this organization is a plausible prerequisite for the physiological function of SSNA1, allowing SSNA1 to concentrate locally, self-assemble and become a microtubule nucleation centre at designated locations. Alternatively, the requirement of a high local concentration of SSNA1 may be a means to limit the microtubule-remodelling activity of SSNA1 to specific subcellular areas such as axon branches, the midbody in dividing cells and the base of cilia.

As microtubules are much less dynamic in axons compared to less polarized cells[32–34], SSNA1-mediated branching may be restricted to locally destabilized sites of the microtubule cytoskeleton. Interestingly, SSNA1 interacts with spastin, a protein important for the initiation of axon branching and thought to increase the pool of soluble tubulin through microtubule fragmentation[7].

It is tempting to speculate that short, spastin-severed microtubules (that is, tubulin oligomers) provide the building blocks for SSNA1-mediated microtubule nucleation and branching. Thus, the synergistic action of spastin and SSNA1 could facilitate the formation of axonal branch points (Fig. 6d). Further investigation of SSNA1 activity in situ will provide valuable insights into the initiation and organization of axon branches. In particular, it will be interesting to explore whether SSNA1-mediated microtubule branching is a direct driving force for axon branching, or an intermediate state during early stages of neuronal morphogenesis. Considering the diverse sites at which SSNA1 is localized in various cell types[17,27], the microtubule-branching mechanism discovered here could have broad implications for understanding the regulation of various microtubule functions, providing new clues to previously unanswered questions about cytoskeleton and intracellular transport.

Online content

Any methods, additional references, Nature Research reporting summaries, source data, statements of data availability and associated accession codes are available at https://doi.org/10.1038/s41556-018-0199-8.

Received: 19 November 2017; Accepted: 20 August 2018;
Published online: 24 September 2018

References

1. Ishihara, K., Nguyen, P. A., Groen, A. C., Field, C. M. & Mitchison, T. J. Microtubule nucleation remote from centrosomes may explain how asters span large cells. *Proc. Natl Acad. Sci. USA* **111**, 17715–17722 (2014).
2. Meunier, S. & Vernos, I. Acentrosomal microtubule assembly in mitosis: the where, when, and how. *Trends. Cell Biol.* **26**, 80–87 (2016).
3. Petry, S. & Vale, R. D. Microtubule nucleation at the centrosome and beyond. *Nat. Cell Biol.* **17**, 1089–1093 (2015).
4. Kalil, K. & Dent, E. W. Branch management: mechanisms of axon branching in the developing vertebrate CNS. *Nat. Rev. Neurosci.* **15**, 7–18 (2014).
5. Lewis, T. L., Courchet, J. & Polleux, F. Cell biology in neuroscience: cellular and molecular mechanisms underlying axon formation, growth, and branching. *J. Cell Biol.* **202**, 837–848 (2013).
6. Stiess, M. et al. Axon extension occurs independently of centrosomal microtubule nucleation. *Science* **327**, 704–707 (2010).
7. Yu, W. et al. The microtubule-severing proteins spastin and katanin participate differently in the formation of axonal branches. *Mol. Biol. Cell* **19**, 1485–1498 (2008).
8. Petry, S., Groen, A. C., Ishihara, K., Mitchison, T. J. & Vale, R. D. Branching microtubule nucleation in *Xenopus* egg extracts mediated by augmin and TPX2. *Cell* **152**, 768–777 (2013).
9. Decker, F., Oriola, D., Dalton, B. & Brugués, J. Autocatalytic microtubule nucleation determines the size and mass of *Xenopus laevis* egg extract spindles. *eLife* **7**, e31149 (2018).
10. Murata, T. et al. Microtubule-dependent microtubule nucleation based on recruitment of gamma-tubulin in higher plants. *Nat. Cell Biol.* **7**, 961–968 (2005).
11. Janson, M. E., Setty, T. G., Paoletti, A. & Tran, P. T. Efficient formation of bipolar microtubule bundles requires microtubule-bound gamma-tubulin complexes. *J. Cell Biol.* **169**, 297–308 (2005).
12. Goshima, G., Mayer, M., Zhang, N., Stuurman, N. & Vale, R. D. Augmin: a protein complex required for centrosome-independent microtubule generation within the spindle. *J. Cell Biol.* **181**, 421–429 (2008).
13. Kamasaki, T. et al. Augmin-dependent microtubule nucleation at microtubule walls in the spindle. *J. Cell Biol.* **202**, 25–33 (2013).
14. Sánchez-Huertas, C. et al. Non-centrosomal nucleation mediated by augmin organizes microtubules in post-mitotic neurons and controls axonal microtubule polarity. *Nat. Commun.* **7**, 12187 (2016).
15. Pfannenschmid, F. et al. Chlamydomonas DIP13 and human NA14: a new class of proteins associated with microtubule structures is involved in cell division. *J. Cell Sci.* **116**, 1449–1462 (2003).
16. Lai, C. K. et al. Functional characterization of putative cilia genes by high-content analysis. *Mol. Biol. Cell* **22**, 1104–1119 (2011).
17. Goyal, U., Renvoisé, B., Chang, J. & Blackstone, C. Spastin-interacting protein NA14/SSNA1 functions in cytokinesis and axon development. *PLoS ONE* **9**, e112428 (2014).
18. Blanchoin, L. et al. Direct observation of dendritic actin filament networks nucleated by Arp2/3 complex and WASP/Scar proteins. *Nature* **404**, 1007–1011 (2000).
19. Volkmann, N. et al. Structure of Arp2/3 complex in its activated state and in actin filament branch junctions. *Science* **293**, 2456–2459 (2001).
20. Itzhak, D. N., Tyanova, S., Cox, J. & Borner, G. H. Global, quantitative and dynamic mapping of protein subcellular localization. *eLife* **5**, e16950 (2016).
21. Woodruff, J. B. et al. The centrosome is a selective condensate that nucleates microtubules by concentrating tubulin. *Cell* **169**, 1066–1077.e10 (2017).
22. Wilde, A. & Zheng, Y. Stimulation of microtubule aster formation and spindle assembly by the small GTPase Ran. *Science* **284**, 1359–1362 (1999).
23. Hyman, A. A., Salser, S., Drechsel, D. N., Unwin, N. & Mitchison, T. J. Role of GTP hydrolysis in microtubule dynamics: information from a slowly hydrolyzable analogue, GMPCPP. *Mol. Biol. Cell* **3**, 1155–1167 (1992).
24. Bechstedt, S. & Brouhard, G. J. Doublecortin recognizes the 13-protofilament microtubule cooperatively and tracks microtubule ends. *Dev. Cell* **23**, 181–192 (2012).
25. Des Georges, A. et al. Mal3, the *Schizosaccharomyces pombe* homolog of EB1, changes the microtubule lattice. *Nat. Struct. Mol. Biol.* **15**, 1102–1108 (2008).
26. Ramos-Morales, F., Infante, C., Fedriani, C., Bornens, M. & Rios, R. M. NA14 is a novel nuclear autoantigen with a coiled-coil domain. *J. Biol. Chem.* **273**, 1634–1639 (1998).
27. Price, H. P. et al. The orthologue of Sjögren's syndrome nuclear autoantigen 1 (SSNA1) in *Trypanosoma brucei* is an immunogenic self-assembling molecule. *PLoS ONE* **7**, e31842 (2012).
28. Rodríguez-Rodríguez, M. et al. Characterization of the structure and self-recognition of the human centrosomal protein NA14: implications for stability and function. *Protein Eng. Des. Sel.* **24**, 883–892 (2011).
29. Janke, C. The tubulin code: molecular components, readout mechanisms, and functions. *J. Cell Biol.* **206**, 461–472 (2014).
30. Wang, Q., Crevenna, A. H., Kunze, I. & Mizuno, N. Structural basis for the extended CAP-Gly domains of p150(glued) binding to microtubules and the implication for tubulin dynamics. *Proc. Natl Acad. Sci. USA* **111**, 11347–11352 (2014).
31. Kelley, L. A., Mezulis, S., Yates, C. M., Wass, M. N. & Sternberg, M. J. E. The Phyre2 web portal for protein modeling, prediction and analysis. *Nat. Protoc.* **10**, 845–858 (2015).
32. Witte, H. & Bradke, F. The role of the cytoskeleton during neuronal polarization. *Curr. Opin. Neurobiol.* **18**, 479–487 (2008).
33. Conde, C. & Cáceres, A. Microtubule assembly, organization and dynamics in axons and dendrites. *Nat. Rev. Neurosci.* **10**, 319–332 (2009).
34. Kapitein, L. C. & Hoogenraad, C. C. Building the neuronal microtubule cytoskeleton. *Neuron* **87**, 492–506 (2015).
35. Mizuno, N., Narita, A., Kon, T., Sutoh, K. & Kikkawa, M. Three-dimensional structure of cytoplasmic dynein bound to microtubules. *Proc. Natl Acad. Sci. USA* **104**, 20832–20837 (2007).
36. Errico, A., Claudiani, P., D'Addio, M. & Rugarli, E. I. Spastin interacts with the centrosomal protein NA14, and is enriched in the spindle pole, the midbody and the distal axon. *Hum. Mol. Genet.* **13**, 2121–2132 (2004).

Acknowledgements

We thank C. Grashoff, E. Lorentzen and J. von Blume for assistance at various stages of the project, E. Conti, W. Baumeister and the imaging, biochemistry and cryo-EM core facilities for resources and infrastructure (Max Planck Institute of Biochemistry). We thank A. Carter (University of Cambridge) and C. Kelley (Max Planck Institute of Biochemistry) for careful proofreading of the manuscript and helpful discussions. We thank PICT-IBiSA@Orsay and S. Leboucher (Institut Curie, Orsay) for technical assistance. We are grateful to G. Woehlke (Technical University Munich, Germany) for combined efforts of purification of tubulin, and to C. Gonzalez-Billault and C. Villablanca (University of Chile, Santiago) for help with the analysis of neurons. We also acknowledge C. Sindelar and R. Zhang for providing the software package for microtubule analysis and giving guidance on its use. The EM map of the SSNA1–microtubule complex is deposited with EMDB ID: EMD-4188. N.M., R.J. and C.B. acknowledge the Max Planck Society for the financial support. This study was supported by the DFG through grants within GRK1721, MI 1745/1, and the European Research Council (ERC-CoG-724209 to N.M., ERC-StG-680241 to R.J.). N.M. is a recipient of an EMBO Young Investigator award and a Boehringer Ingelheim Foundation Plus 3 Program grant. R.J. is supported by the DFG Emmy Noether Program (DFG JU 2957/1-1). C.J. is supported by the Institut Curie, the CNRS, the ANR-10-LBX-0038, ANR-10-IDEX-0001-02 PSL, ANR-12-BSV2-0007, INCA 2013-1-PLBIO-02-ICR-1 and 2014-PLBIO-11-ICR-1. A.H.C. acknowledges LISBOA-01-0145-FEDER-007660 and FCT.

Author contributions

N.B. and N.M. performed electron and light microscopy, designed mutant constructs and performed biochemistry experiments, analysed the data and prepared the figures. S.B. and M.M.M. performed experiments with neuron primary culture. N.B. and A.H.C. performed light microscopy experiments. N.B., C.B. and M.T. cloned and purified proteins. N.M., N.B., H.N., S.B., M.M.M. and C.J. analysed neuron data and G.C.

facilitated the automation of neuron analysis. N.M., N.B. and H.N. performed electron microscopic data collection and analysed the data. H.N. and T.S. performed super-resolution light microscopy experiments and N.M., H.N., G.C., C.B and R.J. analysed the data. Experiments were designed by N.M. and the manuscript was written by N.M. with contributions from the other authors.

Competing interests

The authors declare no competing interests.

Additional information

Supplementary information is available for this paper at https://doi.org/10.1038/s41556-018-0199-8.

Correspondence and requests for materials should be addressed to N.M.

Methods

Protein preparation and purification. The DNAs of CrSSNA1 and mouse SSNA1 were obtained by gene synthesis (GeneArt, ThermoFisher) and cloned into self-generated LIC (ligation-independent cloning) vectors. The SSNA1 fragments were prepared as hexahistidine (His) fusion proteins with a TEV-protease recognition site. The proteins were expressed in *Escherichia coli* BL21(DE3) (Merck) by induction with 0.4 mM IPTG (Carl Roth) overnight at 18 °C. Cells were sonicated in lysis buffer (50 mM Na-phosphate buffer pH 7.5, 150 mM NaCl, 10% (v/v) glycerol, 5 mM β-mercaptoethanol) supplemented with protease inhibitors (1 mM pepstatin A, 1 mM AEBSF and 1 mM leupeptin) and clarified. The soluble fraction was purified by Ni-NTA affinity chromatography. The His tag was either removed by TEV cleavage or left on the protein. Biochemical analysis did not show any differences with or without the tag. For CrSSNA1(1–104), an additional step of size-exclusion chromatography (Superdex 200, GE Healthcare) was applied. Circular dichroism spectra were obtained on a JASCO 715 CD spectrometer equipped with a Peltier thermostat, at 4 °C, 25 °C and 37 °C. Tubulin was purified from porcine brains (The Bayerische Landesanstalt für Landwirtschaft) according to a previously published protocol[37] or purchased from Cytoskeleton. The oligomerizations of SSNA1 variants were monitored for 0 h (immediately after purification), 24 h and 48 h.

The DNAs for mouse ch-TOG (amino acids 1–505) and human EB3 (amino acids 1–281) were obtained from the Mammalian Gene Collection (MGC, Source BioScience LifeSciences). mTOG protein was expressed in *E. coli* BL21(DE3)pLysS by induction with 0.5 mM IPTG and cells were grown overnight at 16 °C. Cells were sonicated in lysis buffer (50 mM Tris, pH 8.0, 300 mM NaCl, 10 mM imidazole,1 mM dithiothreitol) supplemented with protease inhibitors (1 mM pepstatin A, 1 mM leupeptin and 1 mM phenylmethylsulfonyl fluoride (PMSF)) and clarified. The protein was purified using Ni-affinity chromatography followed by ion exchange chromatography (Hi Trap S, GE Healthcare) and size-exclusion chromatography (Superdex 200, GE Healthcare). His tag was removed by 3C protease. EB3 was expressed in *E. coli* BL21(DE3). Cells were sonicated in lysis buffer (20 mM Pipes, 1 mM $MgCl_2$, 1 mM EGTA 500 mM NaCl, pH 6.8, 1 mM dithiothreitol) supplemented with protease inhibitors (1 mM pepstatin A, 1 mM leupeptin and 1 mM PMSF) and clarified. The protein was purified using Ni-affinity chromatography followed by size-exclusion chromatography (Superdex 200; GE Healthcare). His tag was removed by 3C protease.

Electron microscopy of SSNA1. SSNA1 constructs (0.05 mg ml^{-1}) of different time points of incubation (0, 24 and 48 h) were applied on manually prepared carbon-coated grids and stained with 1% (w/v) uranyl acetate. The specimens were observed using a CM200 (Thermo Fisher Scientific) at 160 kV at a nominal magnification of 50,000×, corresponding to 2.16 Å per pixel.

Electron microscopy of SSNA1–microtubule complex and image processing. For screening conditions that were also used for light microscopic observations, 8 or 15 μM of tubulin was mixed with 0.1 to 30 μM of SSNA1 in BRB80 buffer (80 mM Pipes-KOH pH 6.8, 1 mM $MgCl_2$, 1 mM EDTA) supplemented with 1 mM GTP or GMPCPP for 5 min, and directly applied on an EM grid for negative staining. The cluster of the microtubules observed in light microscopic environments was only partially preserved under the negative stain condition, due to the fixation process of the sample for negative-stain EM. The centre of the cluster is not visible due to high electron densities.

For cryo-EM, we used 15 μM of tubulin and two to five times excess of SSNA1 to maximize the decoration with the protein. Microtubules were stabilized using a non-hydrolysable GTP analogue mimicking GTP-bound conditions, GMPCPP. After 5 min, 5 μl of sample without dilution was applied to glow-discharged grids with holey carbon (Quantifoil, Cu, R1.2/1.3) and vitrification was carried out in liquid ethane using a home-made manual plunger. The cryo-EM specimens were observed on a Tecnai F20 (Thermo Fisher Scientific) at 200 kV with a magnification of 29,000×. Images were taken using a Falcon2 direct detector (Thermo Fisher Scientific), corresponding to 3.46 Å per pixel with a defocus of about −2.5 μm. The total 98 images with the dose of 50 electrons per square ångström were used for image analysis.

For counting the numbers of the protofilaments of the microtubules, we referred to a well-known specific interference pattern (moiré pattern) of the microtubules[38] observed under cryo-EM.

For the measurement of the branching angles, we used 99 branched microtubules. Using FIJI software, two-connector segments were drawn with each segment approximately 50 nm long, placing the junction of the segments at the centre of the branching points. Then the two segments were aligned along the direction of the two branched microtubules. Examples of branches with various angles are shown in Supplementary Fig. 2D.

For the initial analysis visualizing the 11-nm periodicity of SSNA1 on the microtubule surface, a data set acquired on the F20 (described above) was used. The EMAN2[39] e2helixboxer scheme was used to extract the segments of microtubules. The box size was set to 256 pixels corresponding to 886 Å with 90% overlap and 6,160 segments were extracted in total. For classification and averaging of the images, RELION2[40] software was used.

Data sets were collected using a Titan Arctica microscope (Thermo Fisher Scientific) working at 200 kV and equipped with a Falcon3 direct detector (Thermo Fisher Scientific), at a magnification of 92,000×, corresponding to 1.6 Å per pixel, and a Titan Krios microscope (Thermo Fisher Scientific) working at 300 kV and equipped with a K2 Summit direct electron detector, and controlled with SerialEM software, at a magnification of 105,000×, corresponding to 1.34 Å per pixel. The final reconstruction included in this report was carried out using the data set taken with the Titan Krios. For the data set that was included in the final reconstruction, 762 images were collected with defocus varying from −1.5 μm to −3.5 μm. The detector was operated in counting mode with a dose rate of 10.1 electrons per pixels per second. A total exposure time of 6 s, corresponding to an accumulative dose of 34.08 electrons per square ångström was fractionated into 24 video frames with 0.25 s exposure time and a dose of 1.42 electrons per square ångström for each frame. The video frames were aligned, and averaged using the UCSF Motioncorr2 program[41].

For the 2D classification of branched microtubules, RELION2 was used. Two hundred and twenty-six branched microtubules not overlapping with other microtubules were selected from the data set recorded with the Titan Krios and boxed out with a box size of 1,000 pixels, corresponding to 1,340 Å. The branch angles were variable, causing structural heterogeneity, limiting the resolution of averages.

For image analysis leading to the 3D reconstruction of the microtubule–SSNA1 complex, quality, defocus and astigmatism of each micrograph were assessed using CTFFIND4[42]. Out of 762 images, 478 images containing microtubules were selected for further processing. A total of 1,774 selected microtubules were segmented with a box size of 480 Å with 90% of overlap. As microtubules with 13 protofilaments were the majority, we chose to process 13-protofilament microtubules further. The 13-protofilament microtubules contain a seam that breaks the helical continuity of tubulin dimers, which is a building block. To circumvent this problem, a specially designed package described earlier[43] was used in combination with the method described previously[44–46]. Briefly, multi-reference alignment was performed using 20 Å low-pass-filtered, 2D projections of a microtubule with 13 protofilaments as a reference. The package uses a reference that was computationally synthesized using the atomic structure of tubulin decorated by kinesin. The alignment revealed the polarity and the position of the seam by following the segmented boxes that position along a single microtubule. After the determination of the seam, re-segmentation of the microtubules from the micrograph was performed using the alignment information and with the box size of 600 Å and every 80 Å as an interval. The FREALIGN[47] package was implemented in the package for refinement with options of helical analysis. For this, the known helical parameter of a microtubule with 13 protofilaments was used (helical_rise: −9.37308 Å, helical_twist: 27.692 degree, helical_subunit: 13). Afterwards, the method in refs [44–46] was implemented for refinement as this method follows the consistency of patterns within individual microtubules, independent of the kinesin-decorated pattern, as a reference of alignment. We however observed that the SSNA1 decoration on the microtubules affected the accuracy of the particle alignment as well as the seam detection as indicated in the local resolution estimation shown in Supplementary Fig. 4. While the reconstruction of the microtubules could be further improved by a more laborious strategy, SSNA1 on the contrary cannot be better resolved because of the existing symmetry mismatch with the microtubules. The resulting reconstruction is nevertheless informative, as it allows us to visualize a long SSNA1 fibril attached along a protofilament of microtubules. The global resolution was determined to be 6.1 Å by calculating the Fourier shell correlation of two independent reconstructions. However, we note that the alpha and beta tubulins are not sufficiently separated and the higher resolutions are only effective in the core of tubulin. The reconstruction was filtered based on local resolution estimation by the 'blocres' scheme[48] with a scan box size of 50 pixels.

Cryo-ET of SSNA1–microtubule complex and image processing. Ten-nanometre BSA-coated gold (Aurion) was used as a fiducial marker. A 4 μl volume of sample was mixed with 1 μl fiducial marker and then applied to glow-discharged grids (Quantifoil, Cu, R2/2). Plunge freezing immediately followed using Vitrobot (Thermo-Scientific). Tomographic tilt series were collected on a Titan Krios (Thermo-Scientific) operated at an acceleration voltage of 300 kV, equipped with a Gatan K2 Summit direct electron detector, with magnification of 64,000× corresponding to 2.23 Å per pixel. Images were collected in a sequential manner, starting at 0° and increasing to +59° with 1° increments. After acquiring +59°, the stage was returned to 0° and the tilt series was collected until −59° with 1° increments as well. Each tilt series was collected with the defocus value set between 3 and 7 μm. Images were acquired as videos in counting mode using a dose rate of 4.7 electrons per pixels per second. The total accumulative dose of the tilt series was 112.46 electrons per square ångström. The video frames were aligned using the UCSF Motioncorr2 program.

Tomogram reconstruction was performed using the IMOD package[49]. Tilt series were aligned using fiducial gold markers and further binned by a factor of 4 (final pixel size of 8.92 Å per pixel). Tomograms were reconstructed by back projection and a simultaneous iterative reconstruction technique with seven iterations in IMOD.

Subtilisin treatment of microtubules and crosslinking. Taxol-stabilized microtubules (20 μM) were mixed with 7.4 μM subtilisin (Sigma Aldrich) and incubated for 0–60 min at 37 °C. The reaction was stopped by adding 2.5 mM PMSF. In 10 min, subtilisin completes the cleavage of β-tubulin E-hooks and the cleavage of α-tubulin E-hooks follows. For the crosslinking assay, 5 μM microtubules were mixed with 25 μM of SSNA1, and 1-ethyl-3-[3-dimethylaminopropyl]carbodiimide hydrochloride (EDC) (Fisher) was added to a final concentration of 5 mM. Samples were incubated at room temperature for 1 h. The densities of SDS–PAGE were measured using Fiji.

Light microscopy of in vitro SSNA1-mediated microtubule nucleation. Flow cells were assembled with cover glass and passivated coverslips as described before[50]. The use of the GODCAT oxygen scavenging system, common for microtubule growth observation, blocked the effects of CrSSNA1 on microtubule polymerization in our assays. Therefore, instead we used the PCA/PCD/Trolox oxygen scavenging system[51], which contains 10 nM protocatechuate 3,4-dioxygenase from the *Pseudomonas* species, 2.5 mM 3,4-dihydroxybenzoic acid 'PCA' and 1 mM Trolox (Sigma). Total internal reflection fluorescence microscopy was performed on a DeltaVision Elite imaging system (GE Healthcare). For the formation of 'asters', the conditions used were: 8 μM tubulin (20% HiLyte488 Tubulin, Cytoskeleton), 50–200 nM CrSSNA1, 0–10 % PEG and 2 mM GTP. Further experiments containing PEG were performed in the presence of 7.5% PEG. For the detection of the localization of CrSSNA1, after 5 min of the incubation of the mixture of the samples, an anti-SSNA1 antibody was added, and then an anti-rabbit antibody labelled with Alexa Fluor 568 (Life Technology) was added for the visualization of the antibody. We observed that PEG causes formations of concentrate of SSNA1, which is detectable with >4% of PEG, and can mediate microtubule formation with >5% PEG, in good agreement with other proteins previously reported to nucleate microtubules[21]. With any of the above-mentioned conditions, it is confirmed that spontaneous formations of microtubules do not occur without SSNA1. As little as 50 nM CrSSNA1 was effective to mediate a microtubule formation in the presence of 7.5% PEG.

To mimic the nucleation event, seeds were used as a template. The seeds were formed by incubating 30 μM of tubulin with 15% of atto565-labelled tubulin in the presence of 0.5 mM GMPCPP at 37 °C for 30 min and then centrifuged at 15,800*g* for 8 min to remove excess GMPCPP. Pellets were dissolved in BRB80 buffer. Seeds (1 μM) were mixed with 15 μM tubulin containing 20% HiLyte488 tubulin, 2 mM GTP and 3–30 μM CrSSNA1, and then the microtubule growth was immediately observed. Snapshots were taken after 30 min of incubation. Videos were made by acquiring one frame every 15–20 s for 15–20 min. All experiments were performed at least three times independently. We observed branch formations both from templated GMPCPP-stabilized microtubules as well as dynamic microtubules. At 3 μM, branch-like microtubules started appearing (20%, 115 out of 559 microtubules) and at 30 μM, 50% (448 out of 895 microtubules) had branch-like protrusions of microtubules. To categorize the types of branch, the snapshots of microtubules in the presence of 30 μM SSNA1 were used, and all of the microtubules ($n = 895$) were selected out of 89 snapshots from 3 independent experiments ($n = 47, 21, 21$) and categorized into: 'splitting'—dynamic microtubules with GTP are growing out from the end of the preformed microtubules; 'end joining'—two pre-existing microtubules are annealed through dynamic tubulin oligomers; 'side branching'—dynamic microtubules are growing out of the wall of the pre-existing microtubules; 'dynamic branching'—newly formed dynamic microtubules branch out; 'indistinguishable'; and 'no branch'—microtubules without branching.

Mouse hippocampal primary neuron cultures. Animal care and use for this study were performed in accordance with the recommendations of the European Community (2010/63/UE). Experimental procedures were specifically approved by the ethics committee of the Institut Curie CEEA-IC no. 118 (authorization no. 04395.03 given by the National Authority) in compliance with the international guidelines. The study is compliant with all relevant ethical regulations regarding animal research.

Mouse hippocampal neurons were cultured as described previously[52]. Briefly, wild-type dams at 17.5 days of pregnancy were euthanized using cervical dislocation, the embryos were decapitated and their hippocampi were dissected. Hippocampi were digested with 0.25% trypsin–EDTA (ThermoFisher, 15090046) for 20 min at 37 °C, followed by mechanical dissociation with glass pipettes. Dissociated neurons were then plated in plating medium (MEM supplemented with 10% FBS and 0.6% w/v glucose (Sigma G-8769)) on coverslips coated with poly-D-lysine (no. 354210, Corning). Four hours after plating, media were replaced with neurobasal media containing 1% glutamate, 2% B27 and with/without lentivirus.

Overexpression of SSNA1 in cultured mouse hippocampal neurons. Mouse SSNA1(FL), SSNA1(1–104), SSNA1(21–119) (corresponding to 21-C), SSNA1(E20A/E21A/K105A/K112A/K117A) (corresponding to 5A), SSNA1 swap-KK/EE (E20K/E21K/K105E/K112E) and swap-KK/EEE (E20K/E21K/K105E/K112E/K117E) were cloned into modified lentiviral vector pTRIP using a one-step sequence and ligation-independent cloning method. The pTRIP vector contains a 2A peptide sequence between the EGFP and SSNA1 sequence so that the expression of protein constructs can be ensured with the expression of GFP signals without tagging. Lentiviral particles for the mouse SSNA1 constructs were produced as described previously[53]. Briefly, lentiviral vectors along with viral packaging vectors (psPAX2 and pCMV-VSV-G) were co-transfected in Lenti-X-293T cells using TransIT-293 transfection reagent (Mirus Bio LLC). The virus-containing medium was filtered and stored at −80 °C. The amount of virus to be used for experiments was determined by adding different volumes of virus to the neurons. Mouse hippocampal neurons were cultured as described in ref. [52]. On DIV0 (days in vitro 0), 4 h after plating, neurons were transduced with lentiviruses encoding different SSNA1 constructs. On DIV3, neurons were fixed as described in ref. [54].

Immunofluorescence analyses of primary neuron. Primary neurons fixed on DIV3 were stained with anti-MAP2 and Tau1 antibodies. Cells were then incubated with anti-mouse Alexa Fluor 647 and anti-rabbit Alexa Fluor 568. Nuclei were stained with DAPI (0.02 μg ml^{-1}, ThermoFisher Scientific). For immunostaining of SSNA1, anti-SSNA1 and anti-βIII tubulin were used. Antibody information is provided in Supplementary Table 2. Cells were mounted using ProLong Gold anti-fade (ThermoFisher Scientific). Cells were imaged on a Zeiss Axio Imager.M2 with 20× or 40× objectives. Acquired images were analysed using FIJI[55]. Cells with very short axons were included in the analysis so that underdeveloped neurons could be assessed as well. Note for the data set overexpressing swap-KK/EE and swap-KK/EEE, primary neurons were prepared at a different time, causing the change in general growth profiles of axons. Control (GFP transfected) was used as a standard for comparison of promotion or reduction of axon development of different mutants. Axons, defined as the longest protrusion from the soma, were selected using the Simple Neurite Tracer plugin[56]. The collateral branches longer than 15 μm were defined as major branches. The total number of collateral branches and the total length of all the branches for each axon was determined by tracing of the neuron morphology. In each image, the position of the cell bodies was determined by segmentation of the nuclei: after applying a Gaussian filter and subtracting the background, the image was thresholded using Otsu's method. In the overexpression experiments, the neurons were screened for transduction efficiency, as measured by EGFP expression. The branch network was obtained by segmenting and combining the intensity in the Tau1 and MAP2 fluorescence images: for each channel, the neurites were highlighted by mapping the curvature of the image (Compute Curvature plugin) and thresholding this quantity using Otsu's method. The resulting binary mask was then skeletonized to outline all of the neurites detected. By overlapping the traced axons with this image, only the neurites branching from the axons were kept and measured. The branching complexity of each neuron was summarized with the Strahler number[57,58] (Strahler Analysis plugin), using the location of its corresponding cell body to mark the root branch, which is the start point of the axon.

Immunostaining for DNA-PAINT. DNA-labelled antibodies were prepared as previously reported[59]. In brief, 300 μl of 1 mg ml^{-1} secondary donkey anti-rat antibody (Jackson ImmunoResearch, 711-005-152) was reacted with 10× mole excess maleimide–PEG2–succinimidyl ester crosslinker (Sigma-Aldrich, 746223), and then 10× mole excess of DNA was added to the antibody-crosslinker. Final usage concentration was 10 μg ml^{-1}.

Mouse embryonic fibroblast cells were transfected with pTRIP_2A_EGFP vector using Lipofectamine 2000 (Thermo Fisher Scientific). Cells were fixed and stained as described previously[59], and then were incubated at 4 °C overnight with primary rat α-tubulin (YL1/2) antibody. Antibody information is provided in Supplementary Table 2. DNA-labelled secondary antibody (10 μg ml^{-1}) was added and incubated for 1 h. Samples were then incubated for 5 min with 90-nm gold particles (Cytodiagnostics, G-90-100) at a 1:10 ratio in PBS, and then residual gold was washed away. Cells were kept at 4 °C until they were used for imaging within 48 h.

DNA-PAINT. Fluorescence imaging was carried out on an inverted Nikon Eclipse Ti microscope (Nikon Instruments) with the Perfect Focus System, applying an objective-type total internal reflection fluorescence (TIRF) configuration with an oil-immersion objective (Apo SR TIRF 100×, NA 1.49, oil). Two lasers were used for excitation: 561 nm (200 mW, Coherent Sapphire) or 488 nm (200 mW, Toptica iBeam smart). The laser beam was passed through a cleanup filter (ZET488/10× or ZET561/10×, Chroma Technology) and coupled into the microscope objective using a beamsplitter (ZT488rdc or ZT561rdc, Chroma Technology). Fluorescent light was spectrally filtered with two emission filters (ET525/50 m and ET500lp for 488 nm excitation and ET600/50 and ET575lp for 561 nm excitation, Chroma Technology) and imaged on a sCMOS camera (Andor Zyla 4.2) without further magnification, resulting in an effective pixel size of 130 nm after 2×2 binning. The camera readout sensitivity was set to 16-bit, and the readout bandwidth was set to 200 MHz.

Transfected cells were screened using 488 nm laser excitation at 0.01 kW cm^{-2}. The excitation was switched to 561 nm, the focal plane and TIRF angle were readjusted and imaging was subsequently performed using ~1.5 kW cm^{-2} 561 nm laser excitation. The imager strand concentration varied dependent on the

measurement from 2 nM to 5 nM Cy3b-P1 and was adjusted to minimize double-binding events. Imaging was performed in 1×PCA (Sigma-Aldrich, 37580-25G-F)/1×PCD (Sigma-Aldrich, P8279-25UN)/1×Trolox (Sigma-Aldrich, 238813-1G) in Buffer C (PBS + 500 mM NaCl) and imaged for 20,000–40,000 frames at 200 ms exposure time. 3D imaging was performed using a cylindrical lens in the detection path as previously reported[60].

Super-resolution data analysis. Raw data videos were reconstructed with the Picasso software[59]. Drift correction was performed with a redundant cross-correlation and/or gold particles as fiducials. Using Picasso, the localization information was converted to an image volume with isotropic pixel sampling of 10 nm. The volumes were denoised by applying a Gaussian filter with a standard deviation of 30 nm. The topology of the microtubules was derived using stretching open active contour modelling, as implemented in the SOAX software[61]. Three independent SSNA1-overexpressing fibroblasts and control cells were assessed each, containing the total tube lengths (that is, microtubule lengths) of 7,700 µm, 8,500 µm and 7,700 µm for control cells and 5,700 µm, 7,900 µm and 1,900 µm for SSNA1-overexpressing cells. In each cell, the occurrences of the three-way intersections were counted to be 0.96, 0.78 and 1.2 per 100 µm for control cells and 1.6, 3.2 and 4.2 per 100 µm for SSNA1-overexpressing cells. As the expression level of SSNA1 varies between individual cells, the transfected cells were selected on the basis of the signal of GFP, which was co-expressed with SSNA1. Three independent cells containing the strongest signals out of >500 cells have been selected.

Statistics and reproducibility. All microtubule nucleation assays and TIRF-based assays were performed independently at least three times unless otherwise stated. Similar results were observed in all of the replicates performed. Primary neuron preparation was performed from three independent mice.

The χ^2 two-sample test was performed to determine the significance of differences between two data sets. The Kruskal–Wallis test, followed by Dunn's multiple comparison post-hoc test, was performed to test the significance across multiple independent samples. Reproducibility was confirmed.

Reporting Summary. Further information on experimental design is available in the Nature Research Reporting Summary linked to this article.

Code availability. Morphology analysis of the neurons (total number of collateral branches and total length of all the branches for each axon) was performed using Fiji, with the help of scripts written ad hoc for the task. All scripts are available from the corresponding author upon request.

Data availability

The cryo-EM structure of the SSNA1–microtubule is available through EMDB with the accession code EMD-4188. The additional tomography images are available in Figshare (https://figshare.com/articles/Microtubule_branch_png/6809795). Source data for Figs. 1, 4, 6 have been provided as Supplementary Table 3. Other data supporting the findings of this study such as the cryo-tomography data are available from the corresponding author on reasonable request.

References

37. Shelanski, M. L., Gaskin, F. & Cantor, C. R. Microtubule assembly in the absence of added nucleotides. *Proc. Natl Acad. Sci. USA* **70**, 765–768 (1973).
38. Chrétien, D., Kenney, J. M., Fuller, S. D. & Wade, R. H. Determination of microtubule polarity by cryo-electron microscopy. *Structure* **4**, 1031–1040 (1996).
39. Tang, G. et al. EMAN2: an extensible image processing suite for electron microscopy. *J. Struct. Biol.* **157**, 38–46 (2007).
40. Scheres, S. H. W. RELION: implementation of a Bayesian approach to cryo-EM structure determination. *J. Struct. Biol.* **180**, 519–530 (2012).
41. Li, X. et al. Electron counting and beam-induced motion correction enable near-atomic-resolution single-particle cryo-EM. *Nat. Methods* **10**, 584–590 (2013).
42. Rohou, A. & Grigorieff, N. CTFFIND4: Fast and accurate defocus estimation from electron micrographs. *J. Struct. Biol.* **192**, 216–221 (2015).
43. Shang, Z. et al. High-resolution structures of kinesin on microtubules provide a basis for nucleotide-gated force-generation. *eLife* **3**, e04686 (2014).
44. Zhang, R. & Nogales, E. A new protocol to accurately determine microtubule lattice seam location. *J. Struct. Biol.* **192**, 245–254 (2015).
45. Zhang, R., Alushin, G. M., Brown, A. & Nogales, E. Mechanistic origin of microtubule dynamic instability and its modulation by EB proteins. *Cell* **162**, 849–859 (2015).
46. Alushin, G. M. et al. High-resolution microtubule structures reveal the structural transitions in αβ-tubulin upon GTP hydrolysis. *Cell* **157**, 1117–1129 (2014).
47. Grigorieff, N. Frealign: an exploratory tool for single-particle cryo-EM. *Methods Enzymol.* **579**, 191–226 (2016).
48. Cardone, G., Heymann, J. B. & Steven, A. C. One number does not fit all: mapping local variations in resolution in cryo-EM reconstructions. *J. Struct. Biol.* **184**, 226–236 (2013).
49. Kremer, J. R., Mastronarde, D. N. & McIntosh, J. R. Computer visualization of three-dimensional image data using IMOD. *J. Struct. Biol.* **116**, 71–76 (1996).
50. Crevenna, A. H. et al. Side-binding proteins modulate actin filament dynamics. *eLife* **4**, e04599 (2015).
51. Wieczorek, M., Bechstedt, S., Chaaban, S. & Brouhard, G. J. Microtubule-associated proteins control the kinetics of microtubule nucleation. *Nat. Cell Biol.* **17**, 907–916 (2015).
52. Kaech, S. & Banker, G. Culturing hippocampal neurons. *Nat. Protoc.* **1**, 2406–2415 (2006).
53. Lahaye, X. et al. The capsids of HIV-1 and HIV-2 determine immune detection of the viral cDNA by the innate sensor cGAS in dendritic cells. *Immunity* **39**, 1132–1142 (2013).
54. Magiera, M. M. & Janke, C. Investigating tubulin posttranslational modifications with specific antibodies. *Methods Cell Biol.* **115**, 247–267 (2013).
55. Schindelin, J. et al. Fiji: an open-source platform for biological-image analysis. *Nat. Methods* **9**, 676–682 (2012).
56. Longair, M. H., Baker, D. A. & Armstrong, J. D. Simple Neurite Tracer: open source software for reconstruction, visualization and analysis of neuronal processes. *Bioinformatics* **27**, 2453–2454 (2011).
57. Hollingworth, T. & Berry, M. Network analysis of dendritic fields of pyramidal cells in neocortex and Purkinje cells in the cerebellum of the rat. *Phil. Trans. R. Soc. Lond. B* **270**, 227–264 (1975).
58. Vormberg, A., Effenberger, F., Muellerleile, J. & Cuntz, H. Universal features of dendrites through centripetal branch ordering. *PLoS Comput. Biol.* **13**, e1005615 (2017).
59. Schnitzbauer, J., Strauss, M. T., Schlichthaerle, T., Schueder, F. & Jungmann, R. Super-resolution microscopy with DNA-PAINT. *Nat. Protoc.* **12**, 1198–1228 (2017).
60. Huang, B., Wang, W., Bates, M. & Zhuang, X. Three-dimensional super-resolution imaging by stochastic optical reconstruction microscopy. *Science* **319**, 810–813 (2008).
61. Xu, T. et al. SOAX: a software for quantification of 3D biopolymer networks. *Sci. Rep.* **5**, 9081 (2015).

nature cell biology

SUPPLEMENTARY INFORMATION

https://doi.org/10.1038/s41556-018-0199-8

In the format provided by the authors and unedited.

Direct induction of microtubule branching by microtubule nucleation factor SSNA1

Nirakar Basnet[1], Hana Nedozralova[1], Alvaro H. Crevenna[2], Satish Bodakuntla[3,4], Thomas Schlichthaerle[1,5,6], Michael Taschner[1,7], Giovanni Cardone[1], Carsten Janke[3,4], Ralf Jungmann[1,5], Maria M. Magiera[3,4], Christian Biertümpfel[1] and Naoko Mizuno[1]*

[1]Max Planck Institute of Biochemistry, Martinsried, Germany. [2]Biomolecular Self-Organization, Instituto de Tecnologia Química e Biológica António Xavier, Universidade Nova de Lisboa, Oeiras, Portugal. [3]Institut Curie, PSL Research University, CNRS, Orsay, France. [4]Universite Paris Sud, Universite Paris-Saclay, Orsay, France. [5]Department of Physics and Center for Nanoscience, Ludwig Maximilian University, Munich, Germany. [6]Graduate School of Quantitative Biosciences Munich (QBM), Ludwig Maximilian University, Munich, Germany. [7]Present address: Department of Fundamental Microbiology, University of Lausanne, Lausanne, Switzerland. *e-mail: mizuno@biochem.mpg.de

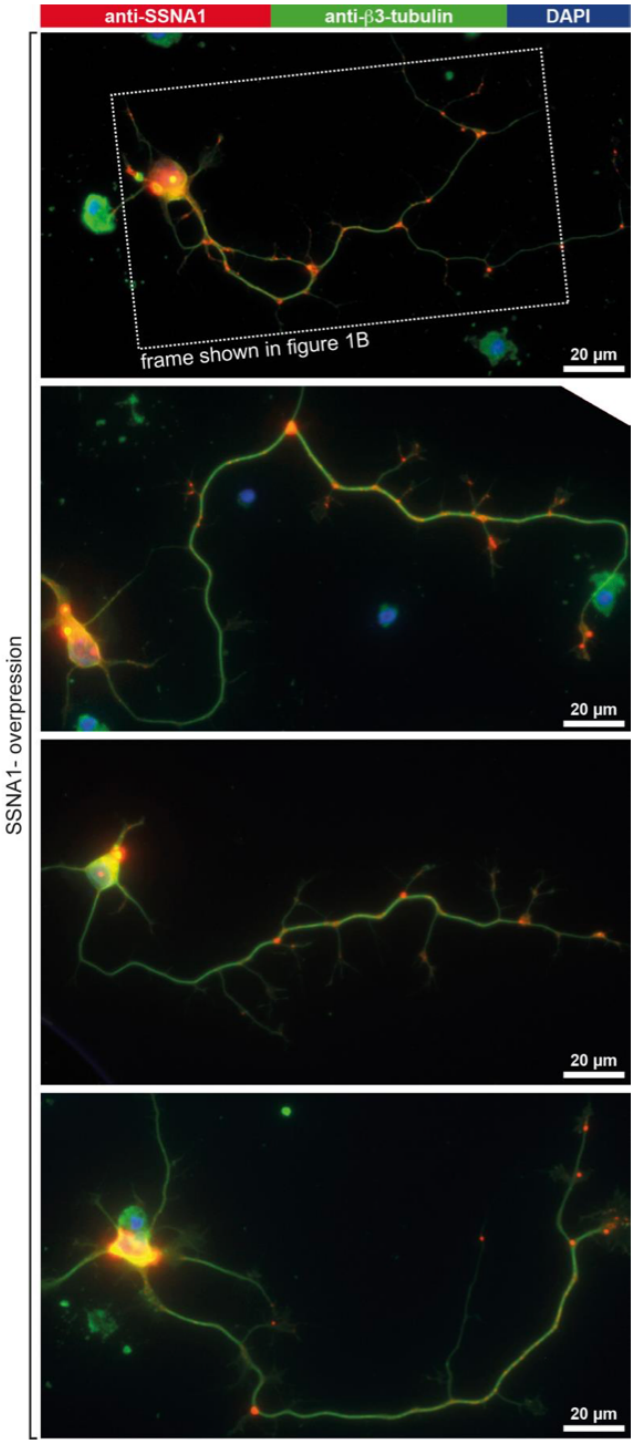
anti-SSNA1
anti-β3-tubulin
DAPI
frame shown in figure 1B
20 µm
20 µm
20 µm
20 µm
SSNA1- overpression

Supplementary Figure 1

Gallery of primary neurons (DIV3) showing the localization of SSNA1 (red) at the axon branching sites. β3-tubulin is shown in green. These images are representing three independent experiments.

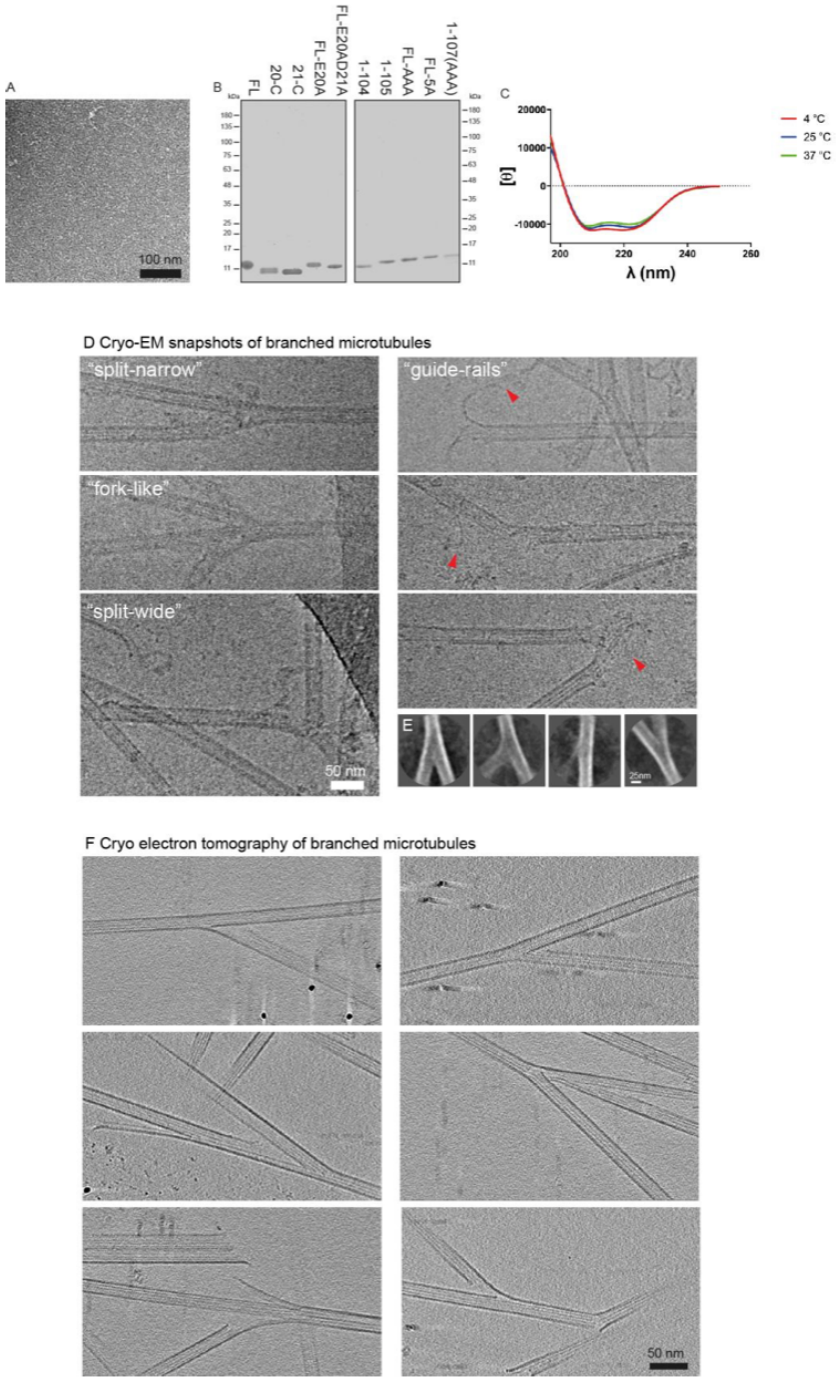

Supplementary Figure 2

(A) Purified CrSSNA1 FL observed under negative stain EM, showing no aggregation. Fibril formation can also occur concomitantly, which is shown in Fig. S5A. **(B)** SDS-PAGE of purified protein fragments reported in the study. **(C)** Circular dichroism spectra (Mean residue ellipticity (MRE: □) of the purified CrSSNA1 FL at different temperatures, showing well folded alpha-helical configurations. **(D)** Snapshots of microtubule branching during nucleation observed by cryo-EM in addition to the images shown in Fig. 2B. In addition to typically observed split of microtubules ("split", see Fig. 2B), widely or narrowly opened split ("split-wide" and "split-narrow"), microtubules branched into 3 splits ("fork-like") or a microtubule splitting both ways was observed. Red arrowheads indicate the split protofilaments or the cloud of molecules that are joining to the polymerizing microtubules. **(E)** Representative 2D class averages of microtubule branches (n = 226 branches) showing wide-range of branching formation. Due to the flexible junction points, 2D averages do not resolve details. **(F)** Gallery of cryo-electron tomographic slices of microtubule branches. At the branching points, the breakage of the protofilament lattice can be observed. These images represent 15 cryo-tomograms.

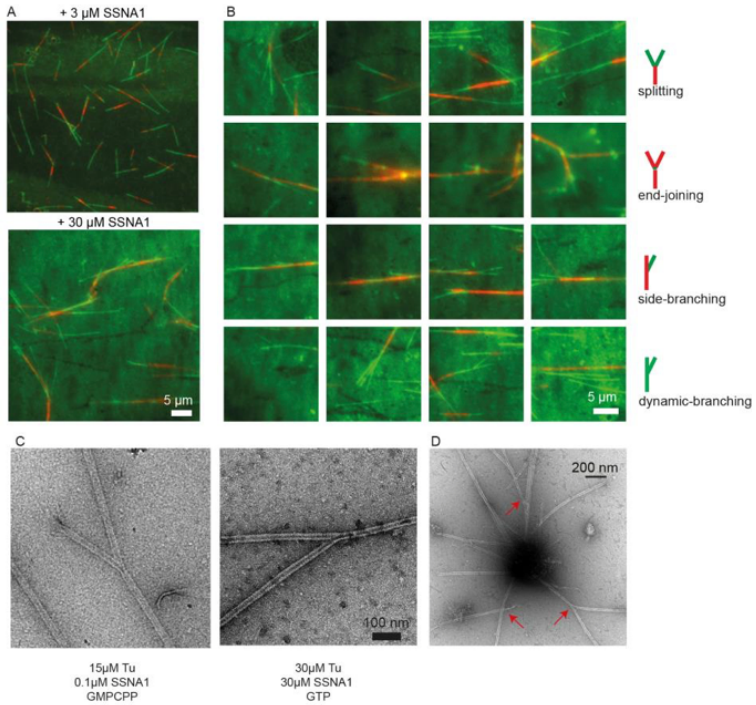
A
+ 3 μM SSNA1
+ 30 μM SSNA1
5 μm
B
splitting
end-joining
side-branching
dynamic-branching
5 μm
C
100 nm
15μM Tu
0.1μM SSNA1
GMPCPP
30μM Tu
30μM SSNA1
GTP
D
200 nm

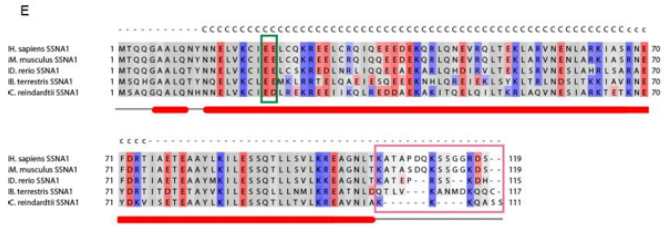
E
H. sapiens SSNA1
M. musculus SSNA1
D. rerio SSNA1
B. terrestris SSNA1
C. reindardtii SSNA1

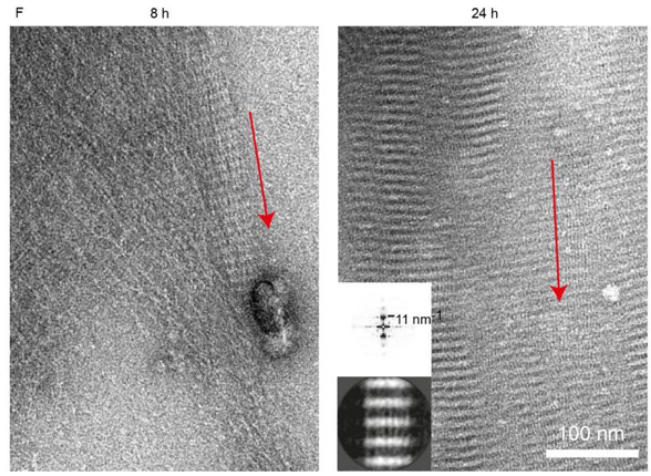
F
8 h
24 h
11 nm-1
100 nm

Supplementary Figure 3

(A) Dynamic microtubules (green) on microtubule seeds (red) in the presence of high concentration of SSNA1 (3 or 30 μM) without molecular crowding agent, to achieve globally concentrated conditions. At 3 μM, branch-like microtubules started appearing (20%, 115 out of 559 microtubules observed) and at 30 μM, 50% (448 out of 895 microtubules) had branch-like protrusion of microtubules. **(B)** Snapshots of microtubules showing 'branch-like' formations. Branches were categorized as 'splitting', 'end-joining', 'side-branching' or 'dynamic-branching'. **(C)** Negative-stain EM snapshots of branched microtubules with conditions tested in a fluorescence microscopy-based dynamic assay, showing branching happens under various conditions. **(D)** Snapshot of branched microtubules protruding out of a nucleation center in the presence of GMPCPP, used for cryo-EM ultrastructure observation. **(E)** The sequence based alignment of the SSNA1 proteins. Secondary structure elements, based on the prediction from PHYRE2 are depicted below the sequences with red bars for α-helices. Coiled-coil prediction from the Marcoil server is shown above the sequences. The charged amino acids are colored in blue for the positive, and red for the negative charge. The colors or grey-scale (for uncharged amino acids) are intensified based on the degree of conservation of the amino acids. The green box highlights residues E20/E(D)21, and the red box shows the unstructured tail region, which are both essential for microtubule branching. **(F)** A snapshot of SSNA1-FL fibrils forming sheet-like structure after 8 hours and 24 hours of incubation. The red arrows show the direction of a fibril. Fibrils laterally assemble together making an ordered sheet. This allows us to assess the basic arrangement of individual fibrils, showing 11-nm of repeat within a fibril as indicated in power spectrum of an average of fibril sheets. These images are representing three independent experiments.

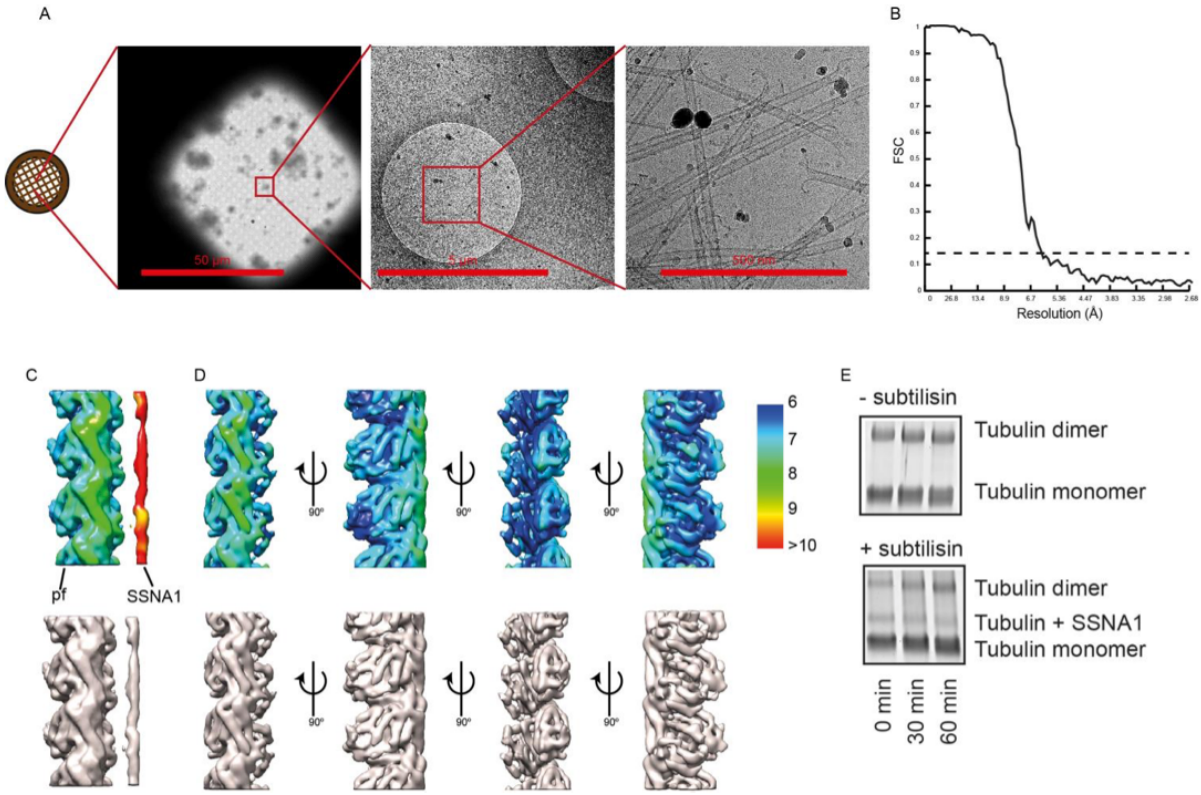

Supplementary Figure 4

(A) Snapshots showing 'cluster' formation embedded in vitreous ice for cryo-EM observation. The centers of microtubule nucleation clusters have high densities of microtubules. **(B)** Fourier Shell Correlation (FSC) of the 3D reconstruction of the SSNA1-microtubule complex. The global resolution of the 3D reconstruction is 6.1 Å according to the FSC=0.143 criteria, though it is only effective for the core of tubulin according to the local resolution mapping shown in D. **(C and D)** Local resolution representation of the 3D reconstruction according to the resolution-color code on the right color bar. **(C)** with a threshold that includes the SSNA1 decoration and **(D)** with the threshold that allows the visualization of the secondary structure elements in the tubulin core. While the tubulin core part shows a resolution ~6 Å, the decorated SSNA1 fibril is not resolved due to the symmetry mismatch between microtubules and SSNA1. The surface of the microtubules is not resolved either, presumably due to the coverage of SSNA1 knob-like pattern with 11 nm periodicity, blurring surrounding densities. Note the 11-nm knob-like pattern is averaged out due to the symmetry mismatch to the microtubule symmetry. **(E)** Chemical crosslinking of microtubules in the absence (top) and presence (bottom) of SSNA1. Subtilisin proteolyzes tubulin E-hooks, and subsequent crosslinking shows the loss of SSNA1-tubulin binding.

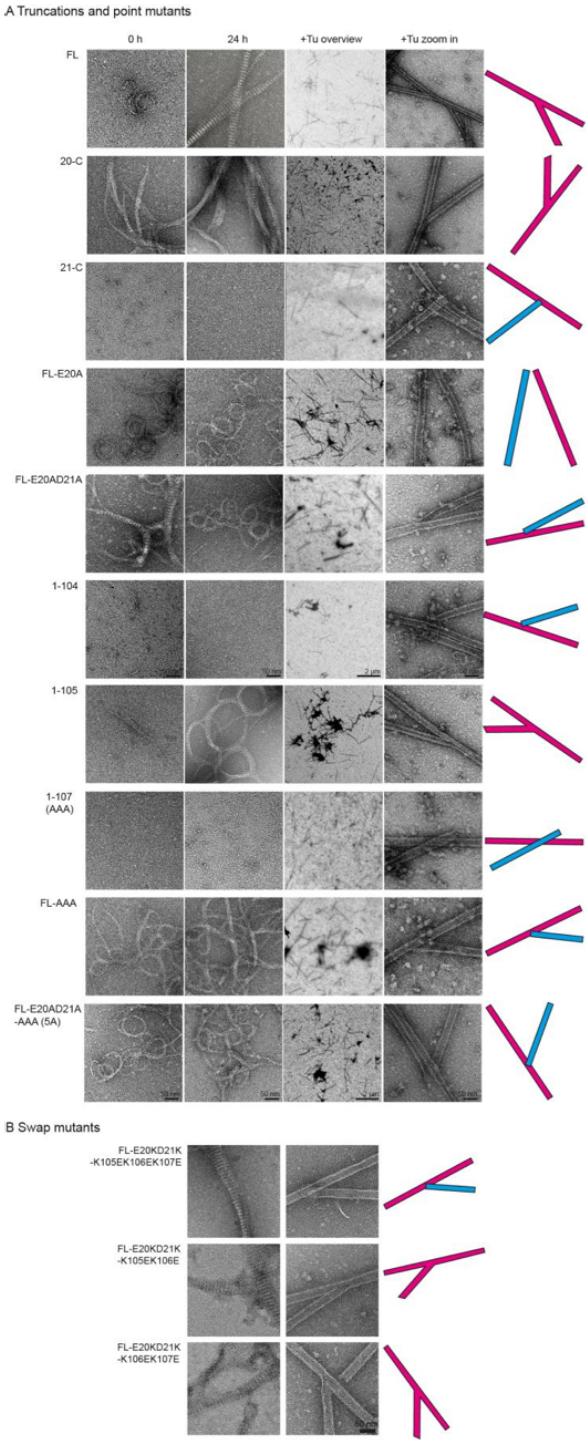
A Truncations and point mutants
0 h
24 h
+Tu overview
+Tu zoom in
FL
20-C
21-C
FL-E20A
FL-E20AD21A
1-104
1-105
1-107
(AAA)
FL-AAA
FL-E20AD21A
-AAA (5A)
B Swap mutants
FL-E20KD21K
-K105EK106EK107E
FL-E20KD21K
-K105EK106E
FL-E20KD21K
-K106EK107E

Supplementary Figure 5

(A) Gallery of electron micrographs of various CrSSNA1 truncation series tested for microtubule nucleation and branching. From left, observation of the purified protein at 0 h incubation (i.e. immediately after purification), 24h incubation at RT, an overview after the addition of tubulin resulting in co-polymerized microtubules, and a magnified view of the copolymerized microtubules. Microtubule branching is shown with FL, 20-C and 1-105, while other protein fragments do not facilitate branching. For the proteins that do not cause the branching, examples of typical crossing of microtubules (red and blue bars at the scheme at the right column), instead of branching are shown. **(B)** Gallery of electron micrographs of various CrSSNA1 swap mutants. Left – all the mutants form cable-like fibrils. Right - branch formation is not induced with the E20K/D21K/K105E/K106E/K107E mutant. These images are representing three independent experiments.

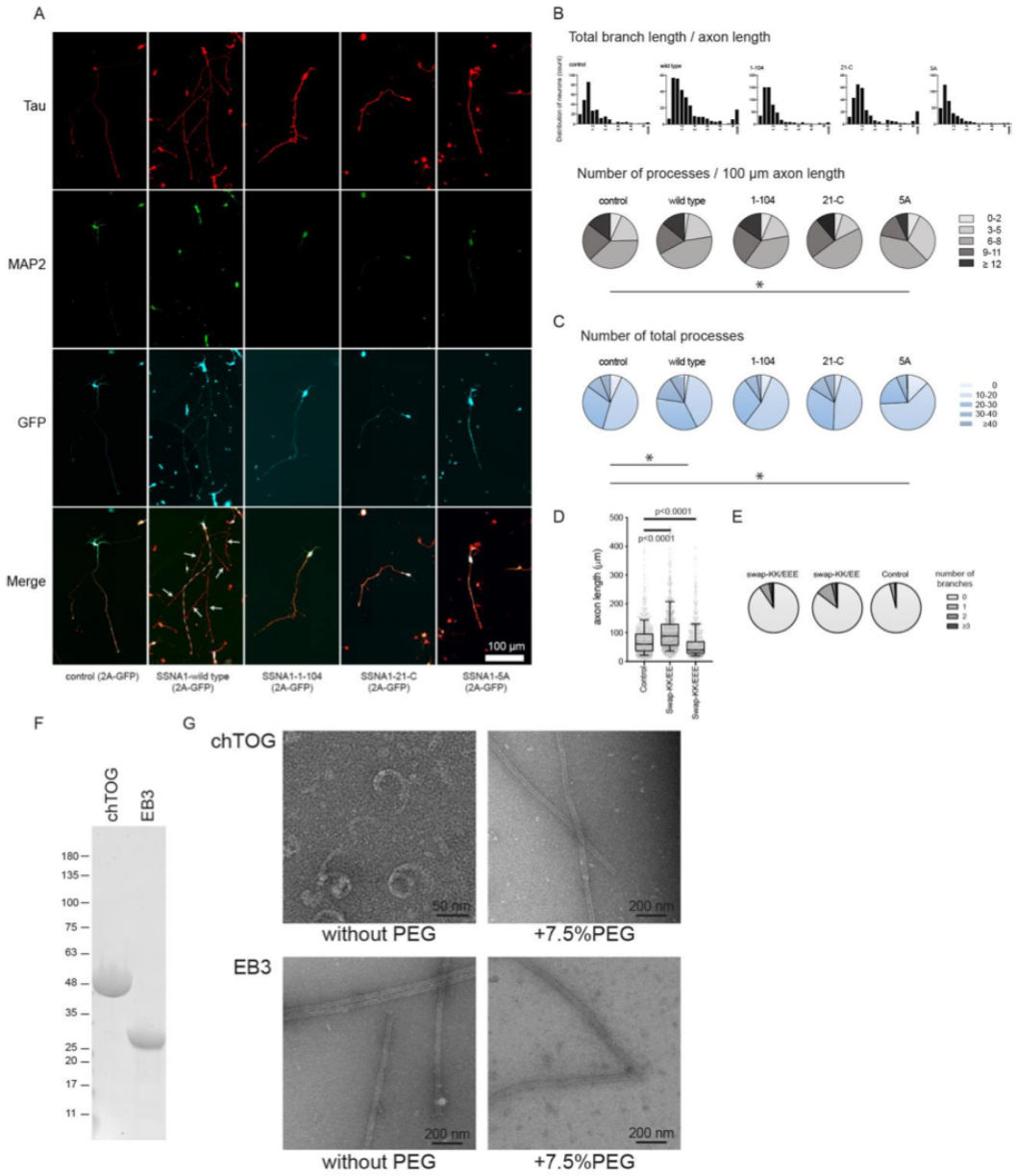

Supplementary Figure 6

(A) Unmerged images of primary neurons (DIV3) overexpressing various SSNA1 variants shown in Fig. 6. The axons are labeled in red by Tau1 antibody (first row, red), while the dendrites are marked with the MAP2 antibody (second row, green). The expression of the SSNA1 proteins was confirmed by concomitant GFP expression (third row, cyan). In the merged view of the SSNA1 WT, axon is guided with a dotted line. **(B-E)** Neuron morphology analysis of various overexpression conditions **B**) Distribution of neurons based on total branch length/axon length and pie graphs showing the distribution of the number of processes (major branches plus minor protrusions along axon). Sample size: Control (n=266 cells), wild type (n=289 cells), 1-104 (n=537 cells), 21-C (n=274 cells), 5A (n=358 cells)

pooled from 3 independent experiments and **(C)** Pie graphs showing the distribution of the total number of processes. Sample size: Control (n=266 cells), wild type (n=289 cells), 1-104 (n=537 cells), 21-C (n=274 cells), 5A (n=358 cells) pooled from 3 independent experiments. In **(B)** and **(C)**, statistics of 5A show significant difference ($\chi 2$ = 23.0, $p < 0.001$ and 36.3, $p < 0.001$ respectively) compared to control, indicating a negative effect of the 5A mutant overexpression to neurons. In **(C)**, wild type overexpressed neurons show the significant difference ($\chi 2$ = 12.83, $p < 0.01$). **(D)** Scatter dot plots of axon length under over-expression of various SSNA1 swap mutants. The promotion of axon development occurs in over-expression of swap-KK/EE, while slight dominant negative effect (shortening of axon) was observed in over-expression of swap-KK/EEE. Every cell is represented by a single point: Control (n=1348 cells), swap-KK/EE (n=789 cells), swap-KK/EEE (n=1129 cells) and the overlaid box-and-whisker plots cover 50% (boxes) and 90% (whiskers) of the entire population, with median values indicated as lines within the boxes. **(E)** Pie graphs showing the distribution of the number of branches. Distributions of the branches in swap-mutants expressed neurons differ significantly from control (GFP over-expression) according to χ^2 two-sample test (χ^2 = 14.4, $p < 0.005$ and 29.1, $p < 0.000005$, respectively). Sample size: Control (n=1348 cells), swap-KK/EE (n=789 cells), swap-KK/EEE (n=1127 cells). **(F)** Purification of chTOG and EB3. **(G)** Mixtures of tubulin with chTOG (upper) and EB3 (lower) were treated in the same way as SSNA1-tubulin mixture to test the induction of microtubule branches. No microtubule branching was observed in the tested conditions.

Supplementary Tables

Table 1: Series of truncations and mutations created and their microtubule branching activities

Table 2: Information of antibodies used in Immunoflourescence and DNA Paint experiments

Table 3: Statistics Source Data

Supplementary Videos

Supplementary video 1: Aster-like microtubule formation in the presence of SSNA1

TIRF microscopy showing aster-like microtubule formation in the presence of 200 nM SSNA1, 8 µM tubulin, 2 mM GTP and 7.5 % (w/v) PEG. The movie was recorded at 22 ºC for 15 min, 20 s each frame. The movie is played at 20 fps. Microtubules propagate out from the tubulin concentrate, which serves as nucleation center.

Supplementary video 2: Nucleation of microtubules from the side of a microtubule with 100 nM SSNA1

TIRF microscopy showing nucleation of microtubules from the side of a microtubule (pointed by the arrow) in the presence of 100 nM CrSSNA1, 8 µM tubulin, 2 mM GTP and 7.5% (w/v) PEG. The movie was recorded at 22 ºC for 15 min, 20 s each frame. The movie is played at 20 fps.

Supplementary video 3: Nucleation of microtubules from the side of a microtubule with 30 µM SSNA1

TIRF microscopy showing nucleation of microtubules from the side of a microtubule (pointed by the arrow) in the presence of 30 µM CrSSNA1 15 µM tubulin, 2 mM GTP and 7.5% (w/v) PEG. The movie was recorded at 22 ºC for 15 min, 15 s each frame. The movie is played at 20 fps.

Supplementary video 4: Nucleation of microtubules from the end of the microtubule seed

TIRF microscopy showing nucleation of microtubules (green) from the end of the red microtubule seed (pointed by the arrow) in the presence of 30 µM CrSSNA1, 15 µM tubulin, 2 mM GTP. The seed (red) was incubated with tubulin (green) and CrSSNA1 and the movie was recorded at 22 ºC for 15 min, 15 s each frame. The movie is played at 20 fps.

.

1.2. Structural insights into the cooperative remodeling of membranes by Amphiphysin/BIN1

Adam, J., Basnet, N., and Mizuno, N. (2015). Srep 5, 15452.

During my PhD study, I was able to contribute to a study about amphiphysin/BIN1 and how the self-assembly of these protein on a membrane results in its remodelling into a tubular structure. Amphiphysin/BIN1 is involved in forming deeply invaginated tubes in muscle T-tubules, however the mechanism how it is interacting with membrane, remodelling it and maintaining such a tubular structure was still not known. Using cryo-EM, this study shows that N-BAR domain self-assemble on the membrane surface on a cooperative manner in a helical arrangement. The biochemical assays and 3D reconstruction in this study shows that N-terminal amphiphatic helix H0 is essential for the initiation of the tube assembly and further organizes Bar-mediated polymerization. The regulatory SH3 domain of the Amphiphysin/BIN1 seems not to have any involvement in the self-assembly. For this study I performed light microscopy, negative-stain EM and the molecular fitting of the structure. Detailed author contributions are included in the attached article.

SCIENTIFIC REPORTS

OPEN

Structural insights into the cooperative remodeling of membranes by amphiphysin/BIN1

Received: 29 June 2015
Accepted: 24 September 2015
Published: 21 October 2015

Julia Adam, Nirakar Basnet & Naoko Mizuno

Amphiphysin2/BIN1 is a crescent-shaped N-BAR protein playing a key role in forming deeply invaginated tubes in muscle T-tubules. Amphiphysin2/BIN1 structurally stabilizes tubular formations in contrast to other N-BAR proteins involved in dynamic membrane scission processes; however, the molecular mechanism of the stabilizing effect is poorly understood. Using cryo-EM, we investigated the assembly of the amphiphysin/BIN1 on a membrane tube. We found that the N-BAR domains self-assemble on the membrane surface in a highly cooperative manner. Our biochemical assays and 3D reconstructions indicate that the N-terminal amphipathic helix Ho plays an important role in the initiation of the tube assembly and further in organizing BAR-mediated polymerization by locking adjacent N-BAR domains. Mutants that lack Ho or the tip portion, which is also involved in interactions of the neighboring BAR unit, lead to a disruption of the polymer organization, even though tubulation can still be observed. The regulatory region of amphiphysin/BIN1 including an SH3 domain does not have any apparent involvement in the polymer lattice. Our study indicates that the Ho helix and the BAR tip are necessary for efficient and organized self-assembly of amphiphysin/N-BAR.

Lipid bilayer membranes are essential components of a cell for the separation from the surrounding environment and for intracellular compartmentalization. Particular importance of the cellular membranes lies on their dynamic and flexible morphology, which is used for shaping diverse cellular components. This feature is essential for cellular trafficking such as vesicular transport or endocytosis. Specific membrane shapes are formed from flat surfaces by a coordinated deformation and remodeling[1].

For shaping membranes several regulator proteins are involved[2,3]. An important example of such membrane curving proteins is the BAR (Bin/Amphiphysin/Rvs) domain superfamily[4–6]. The highly conserved BAR domains form variably shaped dimers, which are used as a mold to shape membranes. The BAR domains recognize membrane curvatures via electrostatic interactions between the positive charges on its curved surface and the negative charges of the membrane headgroups. This causes a membrane to bend according to the intrinsic curvature of the BAR dimers - a mechanism called "scaffolding"[7–9]. A sub-class of the BAR superfamiliy, N-BAR proteins contain an N-terminal amphipathic helix termed H0, presumably located at the edge of the concave surface of a crescent-shaped BAR dimer. Previously, *in vitro* biophysical experiments showed that the H0 helices are only structured in the presence of lipids and the H0 helices are embedded on one leaflet of the membrane surface with its amphipathic feature[10–13], leading to the distortion of the membrane – a mechanism called "wedging"[14–17]. The crescent-shaped structure of N-BAR proteins has been well characterized by X-ray crystallography[4,7], cryo-EM 3D reconstructions of another N-BAR protein endophilin[18,19] and computational simulations[20,21]. These studies revealed that BAR proteins are polymerizing in a helical manner (lattice of spiraling rows) around the membrane tube, which is held together by BAR dimer-dimer interactions, however, the interaction with membranes including H0 is not well understood.

Cellular and Membrane Trafficking, Max Planck Institute of Biochemistry, Am Klopferspitz 18, D-82152 Martinsried, Germany. Correspondence and requests for materials should be addressed to N.M. (email: mizuno@biochem.mpg.de)

Amphiphysin is an N-BAR protein, involved in clathrin-mediated endocytosis (CME)[22]. It is thought to contribute to the dynamic curvature formation at the neck of budding vesicles during endocytosis by coordinating with other curvature forming proteins like clathrin, endophilin and dynamin[23,24]. While amphiphysin in CME is involved in the dynamic membrane deforming process, an isoform of amphiphysin, amphiphysin2/BIN1 is found as a component involved in the structural organization of muscle T-tubules[25,26]. T-tubules are deformed plasma membranes of muscle sarcolemma giving a platform for the excitation-contraction coupling machinery[27]. In Drosophila, amphiphysin is only implicated in T-tubule formation[28,29], and defects of amphiphysin show a phenotype of viable, flightless flies with a major disorganization of T-tubules[26]. Myoblastic C2C12 cell analysis showed the induction of T-tubule-like structures upon amphiphysin/BIN1 expression[25]. Together with the finding that vesicles are remodeled into a tubular shape in the presence of amphiphysin/BIN1 *in vitro*[10,30] and that the protein possesses a membrane curving BAR domain[10], amphiphysin/BIN1 is thought to be responsible for tubulogenesis of T-tubules.

Amphiphysin/BIN1 consists of a BAR domain followed by a region with unknown structure and a SH3 (Src Homology 3) domain. The SH3 domain is thought to recruit the downstream interaction partner dynamin. Mutations of the human amphiphysin/BIN1, K35N located in H0, D151N, R154Q in the BAR domains and Q434X and K436X in the SH3 domain lead to a neuromuscular disorder called centronuclear myopathy (CNM)[31–34] with various degrees of muscle weakness. CNM patients show a defect in the organization of the T-tubules, highlighting the importance of the formation of ordered T-tubules. *In vitro*, amphiphysin/BIN1 is able to transform liposome vesicles into narrow tubules[10,13] like other BAR domain proteins[18,19,35–37]. However, until now it is still not understood what the structural organization of amphiphysin/BIN1 is, how it remodels membranes and what its implication in T-tubules formation is.

In this work, we present the structural basis of the amphiphysin/BIN1 membrane remodeling activity using *in vitro* reconstitution and cryo-EM. To assess the effect on tube formation, a series of Drosophila amphiphysin/BIN1 truncations were produced and their membrane interactions were tested. Amphiphysin/BIN1 self-assembles on membrane surfaces in a cooperative manner to remodel a vesicle to a tube. The N-terminal H0 helix is not necessary for the membrane remodeling activity but it is required for fast and rigid tube formation. The regulatory domains were not incorporated into the tube but protruding outwards. The cryo-EM 3D reconstructions of amphiphysin/BIN1 tubes revealed a unique assembly of amphiphysin/BIN1 BAR domains wrapping around the membrane to form a membrane tube. Amphiphysin/BIN1 is tightly packed with its one tip immersed into the lipid bilayer, while the other tip protrudes out from the tube. A rod-like density connecting adjacent BARs, likely the H0 helix, stabilizes the BAR dimer-dimer interactions. The size of the tube, which is determined by the arrangement of the BAR domains was not as variable as for the case of other N-BAR mediated tubes[18] but local fluctuations were detected in which the rod-like density is no longer connecting the BAR units. Altogether, our analysis shows H0 is the key to efficiently arrange BAR dimers for an organized polymerization on a membrane surface.

Results

Ho helix facilitates efficient tube formation. Amphiphysin/BIN1 has been shown to remodel vesicles into tubes[10,13,30], resembling the formation of T-tubules in muscle cells[25]. To explore the roles of the H0 helix, the BAR domain and the regulatory regions of amphiphysin/BIN1 in the context of their membrane interactions, we created amphiphysin/BIN1 fragments including full length amphiphysin/BIN1 (FL, residues 1-602), full length amphiphysin/BIN1 without the H0 helix (deltaH0, 27-602), only N-BAR domain (N-BAR, 1-244) and N-BAR domain without H0 (N-BAR-deltaH0, 31-244 or 27-247) and followed membrane-remodeling by monitoring light-scattering at 400 nm (Fig. S1A). In all cases, an increase in scattering was observed as proteins and liposomes were mixed. This increase corresponded to the tube formation judging from the corresponding negative stain EM observation (Fig. S1B, S1C, Fig. 1A–C). While the N-BAR liposome mixture showed an immediate increase in scattering, the degree of scattering increase was lower in the presence of amphiphysin/BIN1 lacking H0 (deltaH0, N-BAR-deltaH0) (Fig. S1A, green and blue) or FL (Fig. S1A, orange). Moreover, a gradual decrease of the scattering signal was observed for N-BAR and FL (Fig. S1A, red and orange), while the scattering stayed constant for the case of deltaH0 and N-BAR-deltaH0 (Fig. S1A, green and blue). Negative-stain EM images of the mixture after 30 min of incubation showed that stable tubes are still retained when BAR fragments are added to liposomes (Fig. S1C, "+N-BAR-deltaH0"), while many of the tubes turned into small vesicles (~300 Å in size) in the presence of the proteins containing H0 helices (N-BAR) (Fig. S1C, "+N-BAR", red arrowhead). Occasionally we observed vesicles squeezed out from a tube (Fig. S1C, "+N-BAR", 30 min). By comparing these observations, the effects of H0 are pinpointed 1) to promote the initiation of membrane remodeling and 2) to finally squeeze the remodeled tubes into vesicles, presumably by a strong wedging effect.

Ho helix is necessary for the organization of the BAR assembly on a tube. To further assess the arrangement of the amphiphysin/BIN1 tube, remodeled tubes with amphiphysin/BIN1-FL, N-BAR and N-BAR-deltaH0 were observed using cryo-EM (Fig. 1D–1I). The majority of the tubes showed diameters of around 300 Å (Fig. 1J–L). Interestingly, when the N-BAR-deltaH0 is added, ~45% of tubes had a thicker morphology with a width of 650–850 Å (Fig. 1K). In these thick tubes, we did not identify

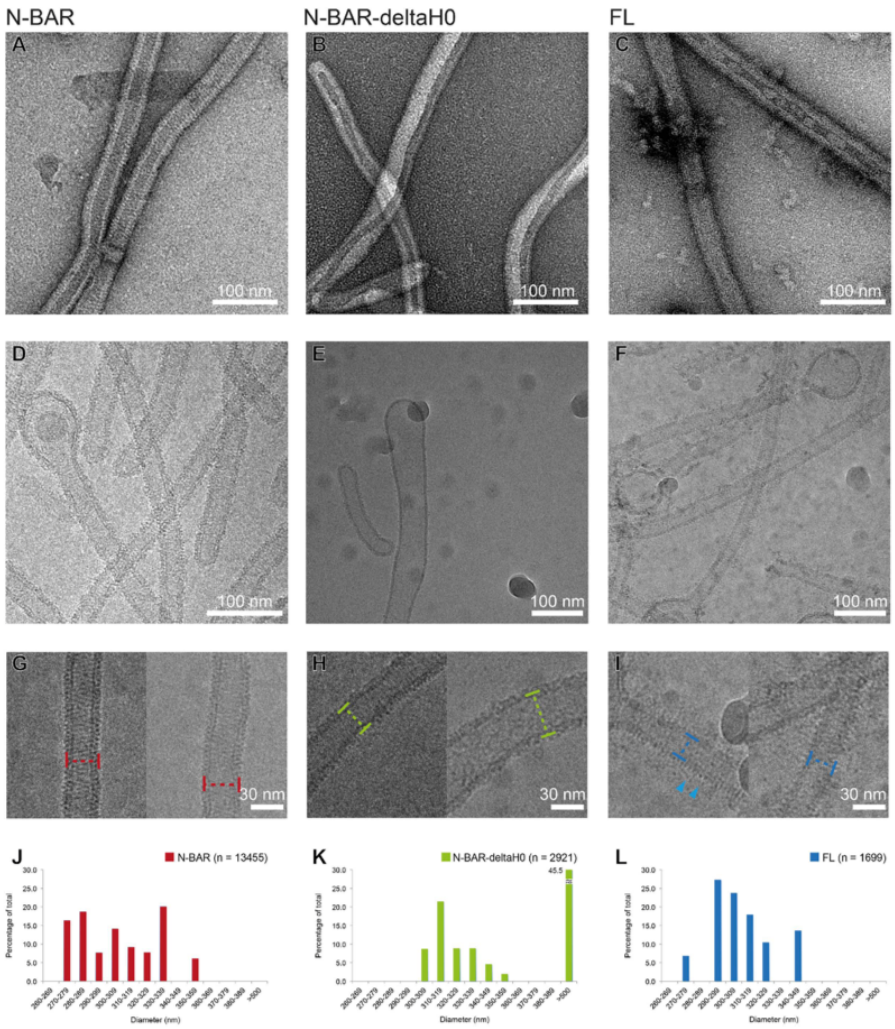

Figure 1. (**A**–**C**) Negative-stain EM images of tubes mediated by N-BAR (**A**), N-BAR-deltaH0 (**B**) and FL amphiphysin/BIN1(**C**). (**D**–**F**) Cryo-EM images of tubes mediated by N-BAR (**D**), N-BAR-deltaH0 (**E**) and FL (**F**). (**G**–**I**) Zoom-in views of N-BAR tubes (**G**), a thin N-BAR-deltaH0 tube (**H**, left) and a thick N-BAR-deltaH0 tube (**H**, right), and FL tubes (**I**). Markers show the definitions of the width at the outer membrane leaflet. In (**I**), needle-like densities around tubes are shown (arrowhead). (**J**–**L**) Histograms of the distributions of the width of the tubes mediated by N-BAR (**J**), N-BAR-deltaH0 (**K**) and FL (**L**).

any distinctive patterns (Fig. 1H, right) compared to the tubes with ~300 Å width (Fig. 1H, left). The 2D averages of the remodeled tubes generally exhibited striped patterns (Fig. 2), indicating proteins are making organized assemblies to some extent on a membrane surface. Particularly the 2D averages of the N-BAR-mediated tubes showed an interwoven pattern (Fig. 2, N-BAR "Averages"), which is an interfering moiré pattern of the overlapping the near and the far sides of the protein-coated tube as the cryo-EM image is a projection of a 3D object. The representative power spectrum revealed a typical diagonal pattern of periodical signals, indicative of a helical assembly of BAR proteins (Fig. 2, N-BAR, "PS"), agreeing with the assembly of other BAR protein-induced tubes[18,19,35,36]. The spacings of the protein assemblies derived from major layer lines are 44 and 55 Å (Fig. 2, N-BAR "PS").

N-BAR-deltaH0 mediated tubes have patterns of BAR domains somewhat periodically arranged. However, the spacing was detected to be ~36 Å according to the power spectrum (Fig. 2, N-BAR-deltaH0, "PS"), in contrast to 44 or 55 Å of spacing observed for N-BARs. In addition we did not observe the interwoven pattern revealed from the N-BAR mediated tube. This indicates that the assembly of the

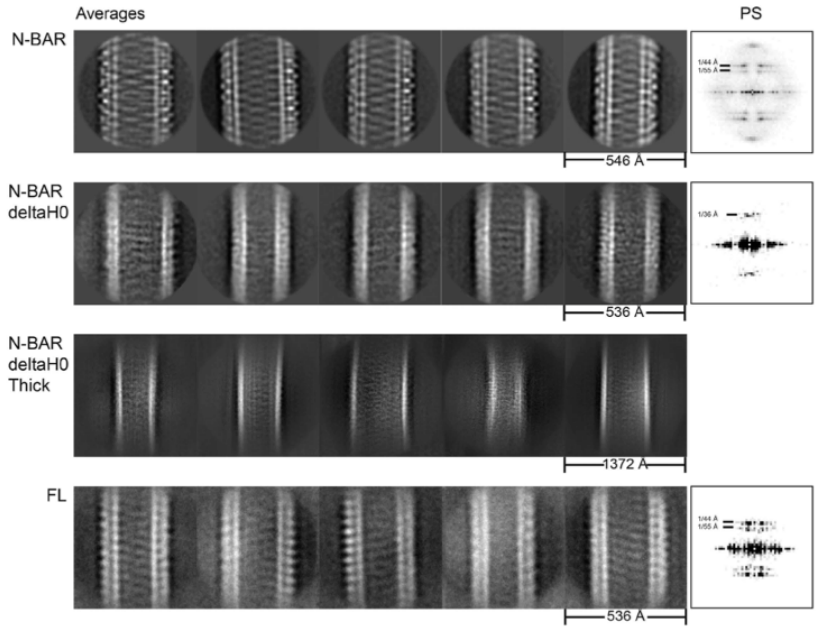

Figure 2. Left: Five representative 2D averages of tubes remodeled by N-BAR (first row), N-BAR-deltaH0 (second row), N-BAR-deltaH0 tubes with thicker size (third row), and FL (fourth row). For the N-BAR averages (first row, left to right), 1365, 1392, 1173, 692 and 1372 particles were used. The class averages of N-BAR-deltaH0 (second row, left to right) contain 234, 312, 165, 185 and 132 particles and 159, 403, 118, 282 and 447 particles for the thick class averages (third row, left to right). For FL (forth row, left to right) 398, 293, 284, 459 and 466 particles were used. Right: Power spectra of the most left 2D class averages. The 2D averages of N-BAR and FL reveal the organized protein assembly and the corresponding power spectra show periodical signal pattern of 44 and 55 Å corresponding to striped patterns within the tubes. N-BAR-deltaH0 reveals a spacing of ~36 Å and no interwoven pattern, indicating the protein assembly being not as rigid as in N-BAR mediated tubes and the change of the protein assembly.

N-BAR-deltaH0 is arranged enough to give a periodical pattern but it is not as rigid as the assembly of N-BAR. The change of the spacing indicates the H0 helix determines the arrangements of BAR assembly.

Together with the observation of tubular formation in a temporal manner, the role of amphiphysin H0 is likely to trigger the initial arrangement of the amphiphysin/BIN1, and to finally arrange an organized self-assembly of the BAR-units. However, H0 is not necessary for the amphiphysin/BIN1 mediated membrane tubulation itself.

Regulatory domain is protruding out of the tube. It has been suggested that the ~8 kDa dynamin binding SH3 domain of the N-BAR protein endophilin is incorporated in the tube packing[19]. In the case of Drosophila amphiphysin/BIN1, the regulatory domain consists of 350 a.a., including a stretch of unknown function and a dynamin-binding SH3 domain. To assess the involvement of the regulatory domain of amphiphysin/BIN1 in the membrane remodeling activity, cryo-EM images of FL were evaluated. The cryo-EM images of the FL-induced tubes showed a similar tube formation as N-BAR with comparable width distributions (Fig. 1L). In addition, we observed needle-like densities protruding from the tubes (Fig. 1F,I, arrowhead). The 2D classification revealed an average with an interwoven lattice pattern (Fig. 2, FL "Averages"), although the average is not as defined as for the case of N-BAR, likely due to the overlap coverage of needle-like densities on the tubes. The power spectrum of the FL average showed the essential two periodical signals shown in the N-BAR 2D average (layer line, 44 and 55 $Å^{-1}$), indicative of the same arrangement between FL and N-BAR mediated tubes. These observations indicate that the needle-like extra density is likely the regulatory domain and it is not incorporated in the tube lattice. It is rather likely that the N-BAR domain solely governs the tube formation.

Based on these morphological assessments, we have chosen to use the N-BAR protein fragment that contains BAR domains plus the N-terminal amphipathic helix (H0) as a minimal functional domain for observing further molecular interactions of amphiphysin/BIN1 in membrane remodeling.

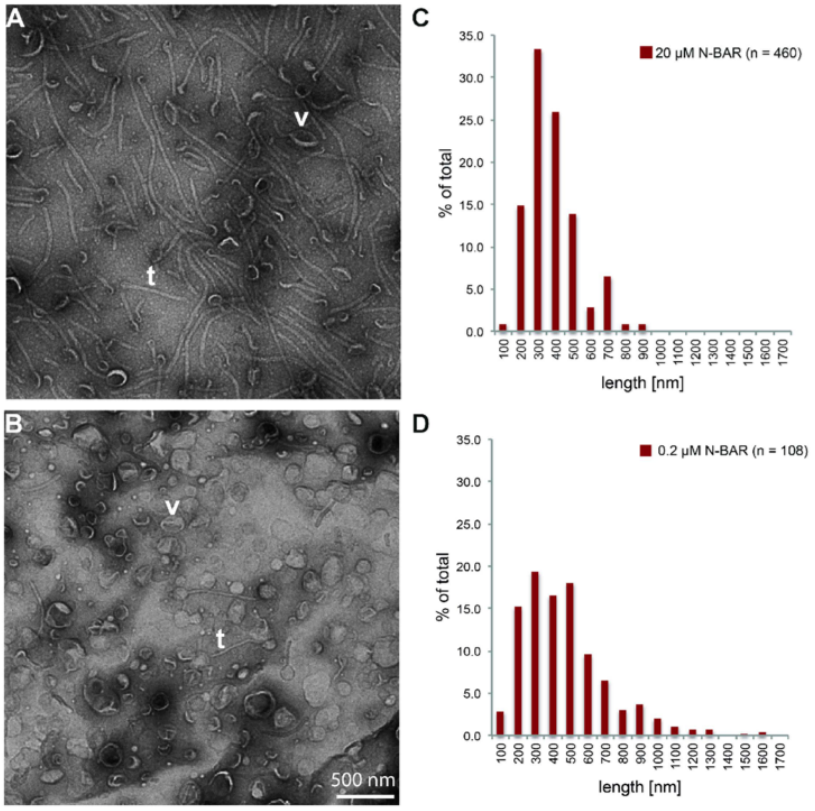

Figure 3. (**A**) Negative-stain EM observation of the N-BAR mediated tubes. 20 μM of N-BAR was added to 720 μM 200 nm-extruded liposome and after 10 min incubation, embedded on a grid without dilution. (**B**) 0.2 μM of N-BAR was added to the same liposome as (**A**). Most of the vesicles remained intact with this condition. v- examples of intact vesicles t: examples of tubes. (**C**) Histogram of the distribution of the lengths of the tubes shown in (**A**). (**D**) Histogram of the distribution of the lengths of the tubes shown in (**B**).

N-BAR makes a cooperative assembly on the membrane surface. In order to understand the effective protein concentration of amphiphysin/BIN1 for membrane remodeling, we tested the degree of tube formation as a function of protein concentration. Fluorescence light microscopy (Fig. S2A) as well as light-scattering measurements (Fig. S2B) showed that the critical concentration necessary for membrane remodeling in the presence of 720 μM liposomes is ~0.4 μM for the H0 containing protein fragments N-BAR and FL (Fig. S2B), while N-BAR-deltaH0 (Fig. S2) showed a critical concentration of ~1.6 μM. This indicates that H0 is needed for the efficient interaction of amphiphysin with membranes.

Further, negative-stain EM observations showed that most of the vesicles were remodeled into uniform tubes when 20 μM N-BAR was added to 720 μM 200 nm-extruded liposomes (Fig. 3A, t: an example of tube, v- an example of intact vesicle), and this condition was used for the cryo-EM based structural analysis (see below). As the protein concentration was lowered, a lesser degree of tubulation was observed and at around the critical concentration of 0.2 μM, vesicles are mostly intact with sparsely observed tubes (Fig. 3B). Strikingly, the tubes under these two conditions both have ~400 nm in length (see distributions of lengths, Fig. 3C,D). This means N-BAR assembly takes place in a cooperative fashion and suggests that the N-BAR has an ability of self-assembling on a lipid-membrane surface. If the protein assembly happens in a non-cooperative way, a larger number of shorter tube lengths or mild deformations of vesicles would be expected in the presence of the low concentration (0.2 μM) of N-BAR.

N-BAR tubes show a packed assembly. Cryo-EM images of the amphiphysin/BIN1 N-BAR-coated tubes revealed a relatively uniform morphology of the amphiphysin/BIN1 assembly. Image analysis and classification yielded tubes with several distinctive widths ranging between 250–360 Å (Fig. 2, N-BAR, "Averages", Fig. S3). Although the selected class averages showed distinctive features, we noted that the

tubes were often bend, or the width of the tubes was not rigidly defined (Fig. 1D,G), which is in contrast to helical polymers of the cytoskeleton, yielding a robust structural analysis such as microtubules[38] and actin[39,40].

Nevertheless, to gain insight into the density of the N-BAR on the membrane tube, mass-per-length (MPL) analysis was performed using scanning transmission electron microscopy (STEM) (Fig. S4). The analysis of relatively straight tubes showed an average MPL of 28 ± 3 kDa/Å. The distribution of the MPL profile is wider compared to the rigidly organized TMV control (13 ± 0.7 kDa/Å), reflecting that the tubes are not as uniformly packed. Considering that the measured density is a sum of lipids and proteins, we estimated the contribution of the protein mass as follows. Lipid density is generally estimated as ~50 Å^2/lipid[41], therefore it can be estimated that ~18 lipids locate on a 300 Å-width tube per Å. This corresponds to ~14 kDa of mass. Therefore we estimated that the contribution of the mass of protein is ~14 kDa/Å. This led to the density estimation of one 56 kDa amphiphysin/BIN1 dimer to occupy 4 Å of axial space (along the tube axis), which agrees well with our 3D reconstruction (see below).

3D reconstruction shows a packed arrangement of N-BAR domains. To see the N-BAR assembly on a tube, we chose 5 classes with distinctive features for further image analysis (Fig. 2, first row and S5, column "Averages"). The 3D reconstructions of particles from these classes revealed protomers of N-BAR dimers wrapping around the tubulated liposomes (Fig. 4A,B, Fig. S6). Reflecting its observed flexibility in packing, the resolution of the reconstruction appeared limited to a medium range resolution of ~11 Å (Fig. S5, column "FSC" and methods). The arrangement of the protomers showed a tightly packed organization of the BAR assembly. The helical rise was ~ 3.8 Å (see methods), well agreeing with 4 Å/BAR unit from the STEM measurement and corresponding to a translation of the BAR protomer of a 1-start helix towards the axis of the tube. The line-scan of the reprojection of the 3D reconstruction across the tube axis showed three peaks from the center of the tubes, corresponding to the inner leaflet, outer leaflet of the lipid bilayers and the attached protein density (Fig. S5, column "model radius"). The distance between inner and outer leaflets of the tube bilayer was measured to be ~33 Å.

The area occupied by one N-BAR unit (i.e. dimer) is 3000–4000 Å^2, varying depending on the diameter of the tubes, while the concave surface area of amphiphysin is calculated to be ~10,000 Å^2. This is in contrast to ~18,000 Å^2 calculated from the loosely packed version of endophilin BAR protein-remodeled tube[19]. The tightly packed arrangement is achieved by one tip of the BAR unit hidden underneath the membrane surface (Fig. 4C, tip1), while the other tip protrudes out from the surface of the tube (Fig. 4C, tip2). Due to this tight packing of the BAR units, the tip-to-tip arrangement observed for endophilin[18] or the CIP4 F-BAR domain[35] was not seen in the case of amphiphysin/BIN1. Rather, the interaction between neighboring BAR units was detected between the central portion of one BAR unit and a protruding tip of the neighboring BAR unit (Fig. 4C, marked as *). The BAR domain is attached on the outer membrane leaflet (Fig. 4B,D, Fig. S5, column "model radius"). The tip of the BAR domain protruding out from the surface of the membrane was responsible for the jaggy features on the side of the tubes seen in 2D averages (Fig. S5, column "Averages") and in the re-projection of the 3D reconstruction (Fig. S5, column "Reprojections").

We detected several classes of tubes with various diameters (Fig. S5, column "model radius", Fig. S6). The major class with the most distinctive features (1948 segments) has a diameter of 280 Å (Fig. 4). There was one class with a wider diameter (312 Å), identified discretely (Fig. S6A). In this class, a slightly less tight packing of the BAR units was revealed. In contrast, we detected populations of tubes whose diameters were smaller (240–260 Å), but appeared transiently fluctuating (Fig. S5, third to fifth row, and Fig. S6B–S6D).

Fitting of an atomic N-BAR model shows that multiple interfaces of the BAR domain can be involved in the tube assembly. The fitting of the crystal structure (PDB code 1uru) to the 3D reconstructions revealed the molecular organization of the BAR domains necessary to achieve the lattice packing of amphiphysin/BIN1-mediated tubes. The amphiphysin/BIN1 dimer consists of three alpha helices forming an anti-parallel coiled-coil in each monomer, resulting in a six-helix bundle (Fig. 5A).

The molecular fitting of the atomic model to the reconstruction from the major class with 280 Å diameter (Fig. 5B) showed that almost one fourth of the BAR dimer unit had a direct connection to the membrane surface (Fig. 5B, boxed area). This area includes approximately residues 130–190 in helix 2 and helix 3 (Fig. 5A,C) and a loop connecting these two helices. In particular, the tip area appeared immersed and surrounded by lipids possibly up to 9 Å in depth (Fig. 5C). This observation was in agreement with the recent EPR results showing residues 144, 147 and 151 to be deeply immersed into the acyl chain region of the lipids[13]. The tip region of the atomic model did not precisely fit to the tested EM map (Fig. 5D). This observation was consistent among all calculated reconstructions of various classes. This suggests that there could be a local geometrical rearrangement or fluctuation of the tip region upon membrane interaction and the lattice formation.

The inter-dimer connections between neighboring BAR units are visible (Figs 4C * and 5D, guided with pink bars). These densities are not occupied by the amphiphysin/BIN1 crystal structure. This is likely the H0 helix, which is not included in the crystal structure due to its unstructured nature without membrane. This connection is made around the junction between H1 and H2 (around residues 78–98) of a monomer and/or H1 (around residues 50–62) of the paired monomer within the dimer unit (Fig. 5E).

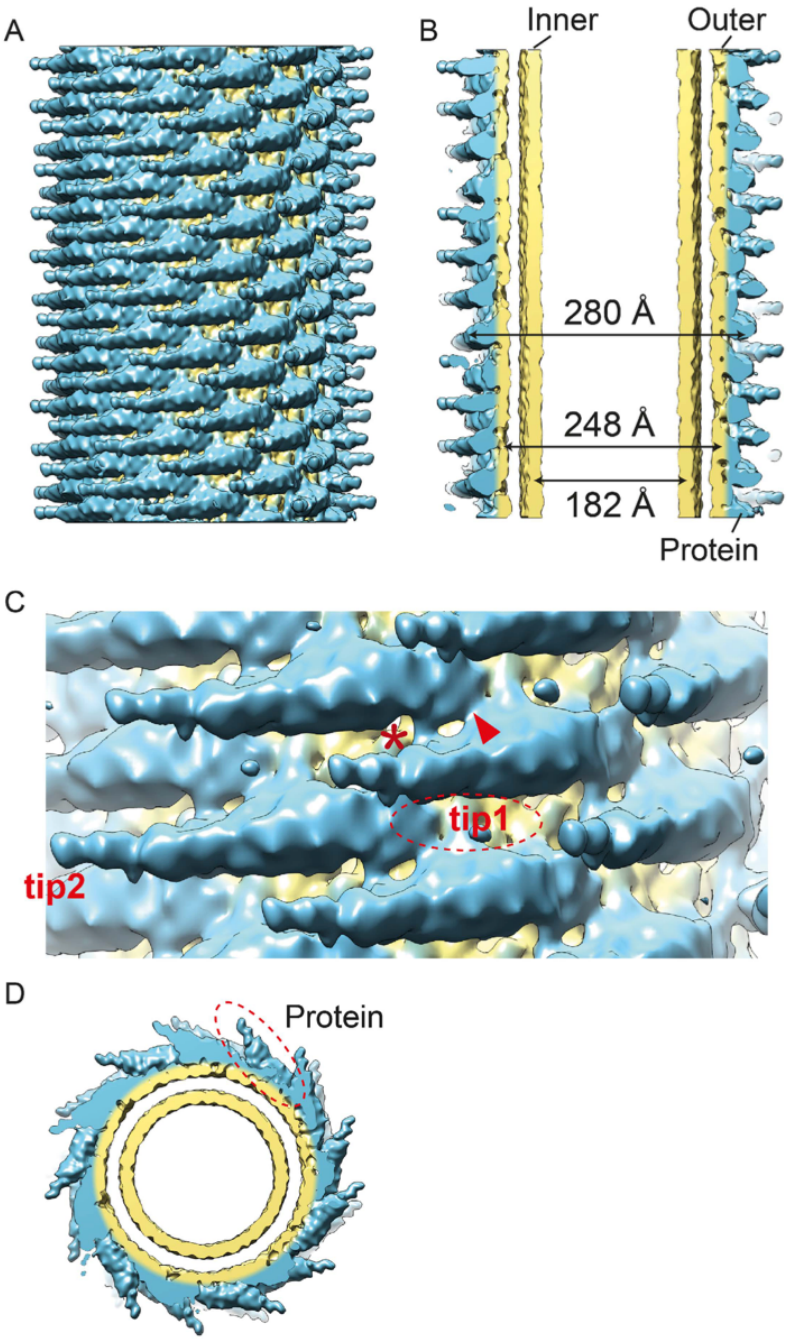

Figure 4. (**A**) 3D reconstruction of an amphiphysin/BIN1-mediated tube with a diameter of 280 Å. The density corresponding to the protein is colored in blue and the lipid corresponding parts are colored in in yellow. (**B**) The central portion of the 3D reconstruction is shown in (**A**). Inner leaflet (diameter of 182 Å) and outer leaflet (diameter of 248 Å) are colored in yellow. (**C**) Zoom in view of A. "*" indicates a rod-like density connecting adjacent BAR domains. The red arrowhead indicates an additional density connecting the adjacent BAR domains. "Tip1" shows a tip density hidden under the membrane. "Tip2" shows the second tip of the BAR unit. (**D**) End-on view of (**A**).

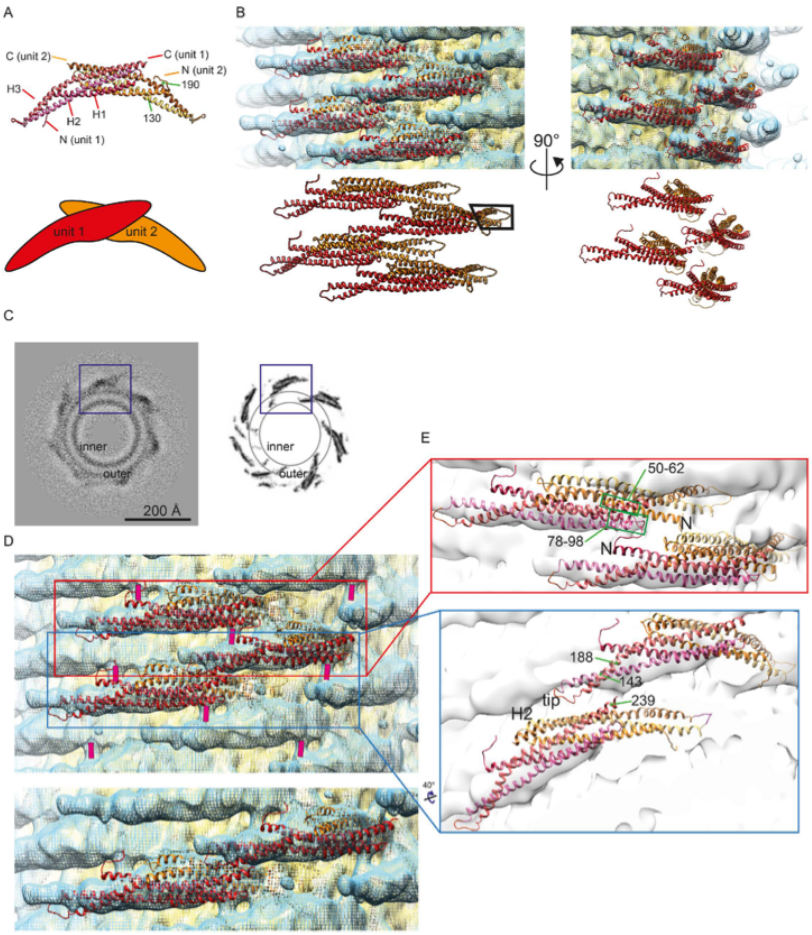

Figure 5. (**A**) Atomic model (PDB code 1URU) of Drosophila amphiphysin (top). The crescent BAR unit is achieved by dimerization (unit 1 and unit 2, bottom). The amphipathic H0 helix is not visualized, as it is unstructured in the crystallization condition. (**B**) Fitting of the atomic model shown in (**A**) to the amphiphysin mediated tube of 280 Å –diameter. The black box highlights the tip portion not visualized by the reconstruction. (**C**) The density of a section of the 3D reconstruction (left) in comparison to the densities of the amphiphysin atomic model fitted and symmetrized according to the arrangement calculated from the 3D reconstruction. Inner/outer: headgroup density of the inner or outer leaflet. One tip of the BAR is immersed into the acyl chain region according to the rigid body fitting. This part of the reconstruction was not resolved due to the surrounding lipids (boxed in (**B**)). (**D**) (Top) The rod-like density connecting the BAR units are marked with a pink bar. (Bottom) A cropped representation of (top) without the pink marker. (**E**) Representation of the atomic models showing the arrangement of the neighboring BAR units.

The second H0 helix in the BAR dimer unit was not resolved. The immersion of the tip density into the membrane portion has hampered the visualization of the H0 helix, although there is a small connection appearing to be a candidate (Fig. 4C, marked with red arrowhead).

The reconstruction with a wider diameter (312 Å, Fig. S6A) showed that the BAR domain was arranged slightly differently. The area occupied by one BAR unit increased to 3700 $Å^2$, compared to 3300 $Å^2$ in the class shown in Fig. 4. The interaction points are shifted by ~25 Å away from each other (Fig. S6A) compared to the reconstruction of 280 Å in diameter (Figs 4 and 5). In contrast, with narrower tubes, the crescent shaped BAR protein appeared to rotate along its long axis (Fig. S6, B–D). The dimer-dimer interaction surfaces were changed by the rotation of the BAR rather than a translation. We did not observe any obvious additional connections between adjacent BAR units in either of these reconstructions.

BAR tip is not necessary for tubulation but required for organized arrangement for the N-BAR lattice formation. All of the reconstructions showed that one tip of the BAR unit was protruding out from the tube, while the other tip was immersed into the membrane. To test the effect of the tips of the BAR units in tubulation, we made a mutant that lacks the tip portion (residues 147-176) (N-BAR-delta-tip) and an obligated amphiphysin/BIN1 N-BAR fusion heterodimer that contains an intact N-BAR domain of amphiphysin/BIN-1 and an N-BAR domain that lacks the tip portion (N-BAR-N-BAR-delta-tip) and assessed its membrane-remodeling ability. Interestingly, we observed that these protein fragments were also able to remodel a membrane surface to a tube (Fig. S7). The critical concentration of the N-BAR-delta-tip was measured to be 0.7 μM, slightly higher than the case for N-BAR (0.4 μM). The N-BAR-N-BAR-delta-tip showed a critical concentration of 0.2 μM, the lowest compared to all tested protein fragments. However, we observed a sporadic population of bundling of the tubes, possibly due to a re-arrangement of some of the BAR domains and the formation of inter-dimer, i.e. inter-tube crosslinks. This inter-dimer formation may increase the local protein concentration, thus, leading to a decrease in the critical concentration.

The negative-stain EM showed that these tubes are similar in size to the tubes mediated by wild-type fragments, but the internal order of the tubes was completely lost. This suggests that both tips are necessary for the organized membrane remodeling but not required for the membrane curving activity.

Discussion

Tight packing of amphiphysin/BIN1-mediated tube assembly and the structural scaffolding function. The 3D reconstructions of amphiphysin/BIN1-mediated tubes showed an intriguing difference from tubular formations facilitated by other BAR protein assemblies[18,19,36]. Particularly, endophilin and amphiphysin/BIN1 have very similar crystal structures[10,11,42,43] but we showed considerable differences in the packing in the presence of membranes. We showed that amphiphysin/BIN1-mediated tubes have a significantly higher degree of rigidity. This may be due to differences in the packing of the BAR units. The protein packing is much tighter in amphiphysin/BIN1 compared to endophilin-mediated tubes[18,19] and the neighboring BAR units of amphiphysin/BIN1 are well connected with each other. This may reflect the physiological role of amphiphysin/BIN1's function in giving a stable structure in muscle T-tubules, while endophilin is rather involved in a dynamic membrane curving process during endocytosis. The membrane squeezing process occurs through the inter-dimer connection. We have previously proposed a sliding mechanism for the case of endophilin, i.e. the interaction of the inter-dimer surface may not be based on specific electrostatic interactions but rather on shallow electrostatic surface potentials and therefore a continuous change of curvature is achieved (Fig. 6A, top). With amphiphysin/BIN1, we detected a population of a few tubes with relatively distinctive sizes, and the most rigidly arranged tube revealed a density linking a perpendicular connection between parallel arranged neighboring BAR domains. This connecting density is likely presenting the H0 helix, as this rod-like density is located proximal to the N-terminus of the BAR domain. Further, we did not detect such a rod-like density in the narrower tubes where BAR units appeared to be rotated along its long axis and which showed fluctuations in tube size. It appears that amphiphysin/BIN1 locks the interactions between the neighboring BAR domains in a discrete fashion and this locking is reinforced by H0 (Fig. 6A, bottom). When the interactions of H0 are lost and the fluctuation of the protein goes beyond a certain balance, the squeezing force may pinch off the tube to create small vesicles. The local fluctuation in the packing hampers a high-resolution structural analysis and it may be an intrinsic property of BAR protein-based assemblies on a flexible membrane platform.

Role of amphiphysin/BIN1 in T-tubule biogenesis. During the T-tubule development, it is thought that amphiphysin/BIN1 is responsible for the remodeling of the membrane into a tube[25]. Caveolin 3 is proposed to be involved in the early stage of T-tubule biogenesis[44] by forming caveolae at the plasma membrane and amphiphysin/BIN1 invaginates the plasma membrane deeper. Although co-localization of caveolin 3 and amphiphysin/BIN1 is observed[25], no direct interaction between both proteins has been reported so far and the recruitment process of amphiphysin/BIN1 is unclear. On the other hand, it is reported that amphiphysin/BIN1 preferably binds to PtdIIns(4,5)P2 through its BAR domain and clusters it. Subsequently, amphiphysin/BIN1 recruits the downstream player dynamin with its SH3 domain[45]. Therefore, it seems that PtdIns(4,5)P2 is key for the recruitment of all involved players. From this point of view, it is plausible that the local concentration of PtdIns(4,5)P2 may already take place during the caveolae formation for the efficient recruitment of amphiphysin/BIN1. The cooperative assembly of amphiphysin/BIN1 on a membrane surface may also play an important role for triggering the local clustering of necessary components and enrichment of PtdIns(4,5)P2. The biochemical and structural studies of these molecular interactions are important topics of further research.

Influence of the CNM causing mutation to the BAR-assembly. The mutations that cause the disease CNM are located at H0 (K35N, corresponding to K30 in Drosophila amphiphysin/BIN1), D151N (corresponding to D146) and R154Q (corresponding to R149) at the tip of the crescent BAR unit. This is consistent with our results that H0 and the tip areas are critical for the organized protein assembly. It also agrees well with previous *in vitro* studies[13,46]. Particularly, a recent report by Isas *et al.*[13] showed biophysically that the tip of the BAR unit including D151 is deeply immerged into the membrane, up to

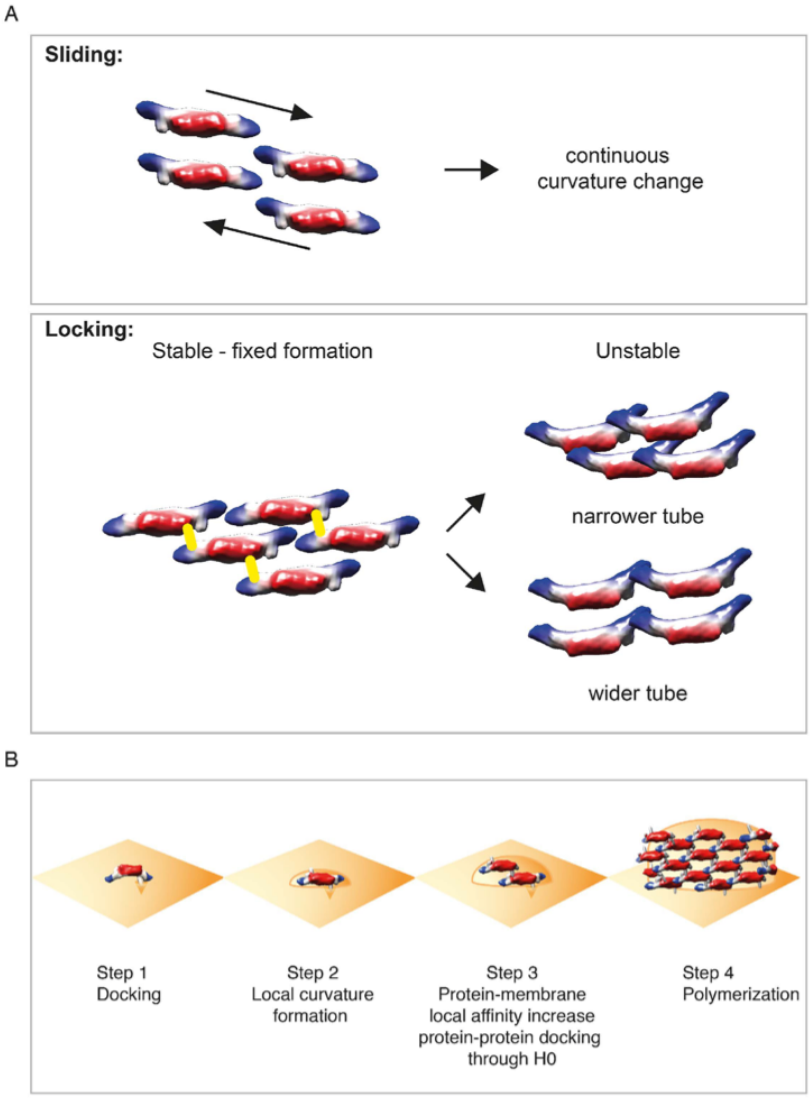

Figure 6. (**A**) A model how different BAR proteins are achieving membrane remodeling. (Top): Sliding mechanism, showing that neighboring BAR units have weak interactions with each other so that they may slide against each other to achieve a continuously changing curvature. This example is shown in endophilin-mediated tube formations[18]. (Bottom): Locking mechanism, showing that the BAR units have a preferred rigid formation with a help of H0, however, the BAR units can rotate along their long axis, therefore losing the connection point via the H0 helix and resulting in a variation of the diameter, i.e. curvature. When the balance of the tube arrangement is too disturbed, N-BAR proteins may even squeeze the tubes to produce small vesicles. (**B**) A model of the cooperative assembly of the N-BAR proteins depicting the wedging effect of the amphipathic H0 helix and the BAR scaffold. In this model, a change of the local curvature of the membrane caused by the landing of the first N-BAR unit is the driving force of the N-BAR cooperative assembly.

a hydrophobic lipid acyl chain region and the authors discussed the importance of this observation in the context of tubulation. This finding agrees well with our direct observation that the tip of one BAR unit is inserted in the lipid bilayer, although the other tip appears to be protruding out from the membrane surface. Interestingly, we noted that the deletion mutant that misses significant parts of the tip is still able

to remodel membranes. The negative-stain EM imaging of the resulting tubes did not reveal any representative pattern as seen in the N-BAR remodeled tubes, suggesting a lack of arranged organization of the BAR domains (Fig. S7). This was also true for the fusion protein fragments that have one tip missing. Likely, one tip of a crescent BAR domain is beneficial for membrane tubulation by directly interacting with lipids, while the other tip is important for the lattice formation and stabilization by interacting with the adjacent unit (Fig. 5). We observed a similar effect with the BAR fragment missing H0. Without H0, the organization of the BAR domain is partially lost likely by missing the density that connects adjacent BAR units (Fig. 5D, pink bar), even resulting in the shrinkage of the packing indicated by the power spectrum (Fig. 2). The defects of the tip mutation or deletion are subtle in terms of tubulation activity but they are disrupting the ultrastructure of the amphiphysin/BIN1 self-assembly, which likely connects to the disorganization of the T-tubules. We note that we have employed a specific lipid composition to facilitate structural analysis[13], but differences may be more pronounced under physiological lipid conditions.

Role of the Ho helix for the initiation of membrane remodeling. In our study, we hinted the role of the wedging by the H0 amphipathic helix and the scaffolding by the BAR crescent-like structure. For membrane remodeling itself to take place, H0 is not necessary. However, H0 is required to achieve an efficient and regular arrayed assembly of the BAR polymers. From these observations, we surmise that the amphipathic helices may be necessary for the initiation of curvature induction and the arrangement of BAR dimers in an organized fashion – poised to polymerize (Fig. 6B). The initial membrane induction from a flat to a curved membrane surface may occur through its wedging function of H0 (Fig. 6B, step1 and 2). When the membrane curvature fits to the crescent shape of the BAR domain, the BAR scaffold may efficiently attach and fix the membrane curvature. This process is more effective at the proximal vicinity to a membrane surface where the first BAR domain has already landed and pre-fixed the local membrane curvature (Fig. 6B, step3). The proteins may start arranging guided by this given membrane curvature and the final stabilization of the protein polymer may be held through the H0 connections (Fig. 6B, step4). This notion agrees with the previous observation that the local concentration of amphiphysin correlates with the curvature of membranes given[47]. Without H0, the initial protein binding to the membrane may be achieved by simply sensing the membrane curvature that is stochastically fluctuating. Hence, this process may be too slow for physiological requirements. On the other hand, the tip portion of the BAR may not be as important in terms of initial curvature formation as H0, as the critical concentration necessary for membrane remodeling for the N-BAR-delta-tip (0.7 μM) did not increase as much as the case for the N-BAR-deltaH0 fragments (1.6 μM).

Methods

Cloning and protein expression. The amphiphysin/BIN1 gene was obtained from the Drosophila cDNA library, the Berkeley Drosophila Genome Project (BDGP) Gold cDNA Collection (Drosophila Genomic Resource Center). The gene was amplified by PCR and cloned into self-generated pEC series vectors designed for Ligase Independent Cloning[48]. Recombinant amphiphysin/BIN1 N-BAR (aa 1-244 or aa 1-247), N-BAR-deltaH0 (aa 27-247 or 31-244), deltaH0 (aa 27-602 or 31-602) and FL (1-602) were cloned as 3C-protease cleavable hexahistidine (His) or SenP2-protease cleavable sumo-hexahistidine fusion proteins. For N-BAR-delta-tip protein fragments, residues 147-176, corresponding to the tip part of the BAR were deleted and the residue 146 and 176 were connected by (GS)5 linker by PCR. The N-BAR-single-tip-fusion dimer (N-BAR-N-BAR-delta-tip) was constructed by amplifying N-BAR and N-BAR-delta-tip with a (GS)7 or (GS)8 linker by PCR, respectively, and fusing them by ligation-independent cloning. In brief, T4 polymerase was used to generate complementary overhangs on both inserts that could be readily annealed with each other and the target vector. The fusion proteins were expressed in *E.coli* BL21 gold using auto-induction ZY media[49] supplemented with appropriate antibiotics. The bacterial cultures were grown at 37 °C until they reach an optical density of around 2. Afterwards the temperature was reduced to 18 °C and proteins were expressed over night. The cells were harvested by centrifugation (8000 × g, 10 min) and stored at −80 °C until further usage.

Protein purification. The harvested cells of recombinant amphiphysin/BIN1 fragments were lysed in 20 mM Hepes, pH 7.4, 500 mM NaCl, 1 mM DTT supplemented with 1 mM Pepstatin A, 1 mM AEBSF and 1 mM leupeptin. The soluble fraction was loaded on a His-Trap column (GE Healthcare). The column was washed with 20 mM Hepes pH 7.4, 500 mM NaCl, 250mM imidazole, 30 mM imidazole, 1 mM DTT. The protein was eluted with 20 mM Hepes pH 7.4, 300 mM NaCl and 1 mM DTT. The sumo-His-tag was cleaved by SenP2-protease over night at 4 °C. Afterwards for N-BAR and N-BAR-deltaH0, N-BAR-delta-tip, and N-BAR-N-BAR-delta-tip, a cation exchange chromatography and for deltaH0 and FL an anion exchange chromatography was carried out (gradient of Buffer A: 20 mM Hepes ph 7.4, 1 mM DTT and Buffer A2: 20 mM Hepes pH 7.4, 2 M NaCl, 1 mM DTT). For further protein purification, size exclusion chromatography (SEC) was followed using a Superdex 200 16/60 column (GE Healthcare) with 20 mM Hepes pH 7.4, 500 mM NaCl, 1 mM EDTA and 1mM DTT. The purified proteins were stored at −80 °C until further usage.

Liposome preparation and *in vitro* tubulation assay. The following synthetic lipids were used: POPG, POPE and POPC (Avanti Polar lipids). Additionally a bovine brain extract, Folch Fraction I (Sigma

Aldrich) was used. For tubulation experiments large uni-lamellar vesicles (LUVs) or multi-lamellar vesicles (MLVs) were prepared. The dried lipid film, containing 2POPG:1POPE (w/w) was hydrated with buffer (20 mM Hepes pH 7.4) to achieve MLVs. LUVs were obtained by extrusion with a filter membrane (200 nm) (Avanti Polar lipids). The lipid condition was determined based on the screenings done by Isas *et al.*[13]. All prepared lipids were either immediately used or stored at 4 °C for 2–3 days.

For the tubulation kinetics experiments various amphiphysin/BIN1 fragments (20 μM, 15 μM or 6 uM of N-BAR and N-BAR-deltaH0 or 6 μM of FL and deltaH0) were incubated with 180 μM of liposomes. The tubulation was measured by absorbance spectrometry at 400 nm and by negative-stain EM. For tubulation assays the absorbance was followed for 120 min. Additionally, aliquots of different proteins were taken at several time points up to 45 min and samples were assessed with negative-stain EM.

Tube length, diameter and critical tubulation concentration determination. 20 or 0.2 μM of N-BAR was added to 720 μM 200 nm-extruded LUVs and after 10 min incubation, embedded on a grid without dilution and stained with 1% (w/v) uranyl-acetate staining dye and screened by CM200 (FEI) operating at 160 kV. The images were recorded by CCD camera with the nominal magnification of 50,000× corresponding to 2.16 Å/pixel.. The N-BAR tube length was determined from negative-stain EM images with the "filament" option in bshow (bsoft package)[50]. Afterwards the measured values were evaluated by a histogram. The tube diameter was determined and calculated by plotting the class averages from cryo-EM dataset or from the reconstruction reprojections. The distributions of the tube diameters were analyzed by histogram. This was done for N-BAR, N-BAR-deltaH0 and FL. The critical tubulation concentration was determined by fluorescence light microscopy and light scattering measurement. For the fluorescence light microscopy 1% Atto488-DOPE was added to the liposomes (w/w 2POPG:1POPE) and after the preparation 720 μM of liposomes were used with various dilutions (6, 0.6, 0.06, 0.006 μM) of N-BAR, N-BAR-deltaH0, FL, N-BAR-delta-tip, N-BAR-N-BAR-delta-tip for observing the degree of tubulation. For the image recording a GE Deltavision Elite with a 60x/oil or 100x/oil objective and excitation 475 nm/emission 525 nm bandpass filter was used. Light scattering was measured to quantify the critical tubulation concentration. Various concentrations of of N-BAR, N-BAR-deltaH0, FL, N-BAR-delta-tip, N-BAR-N-BAR-delta-tip were mixed with 720 μM 2POPG:1POPE (w/w) and the absorbance change was observed. Due to the saturation of the signals at 400 nm, the measurements were performed at 490 nm wavelength.

STEM measurement. The N-BAR induced tubes were prepared in 20 mM Hepes, pH 7.4. For the STEM dark-field imaging, the samples were prepared in the standard procedure of the Brookhaven STEM facility. On the glow discharged carbon grids 3–5 μl of freshly mixed 20 μM of N-BAR and 720 μM of liposomes was added and incubated for 1 min. Then the specimen was washed for few times and afterwards plunged into liquid nitrogen for fast freezing. The grid was freeze-dried overnight and transferred under vacuum into the STEM. For the data analysis dark-field digital micrographs with a pixel size of 1 to 2 nm/pixel were used and analyzed by PCMass32 (available from the Brookhaven STEM resource, ftp.stem.bnl.gov). As an internal mass per length reference tobacco mosaic virus (TMV) (13.1 kDa/Å) was included in all samples. The N-BAR or TMV were boxed according to their size and through this the mass per length was measured. A histogram was plotted from these data.

EM grid preparation and image acquisition for negative stain and cryo-EM. EM observations were performed either with 20 μM proteins and 720 μM liposome, or 5 μM proteins and 180 μM liposome (4 times dilution). The negative staining samples were stained with 1% (w/v) uranyl-acetate staining dye and screened by CM200 (FEI) operating at 160 kV. The images were recorded by CCD camera with the nominal magnification of 50,000× corresponding to 2.16 Å/pixel.

The cryo-EM samples were applied to glow-discharged Quantifoil grids (Cu, R 2/1), incubated for 10 s, then manually blotted for 10 s with filter paper (Whatman No. 1) and vitrified with ethane by a manual plunger. The cryo-EM specimens were observed using a Tecnai F20 microscope (FEI) operating at 120 kV and 200 kV with a magnification of either 62,000× or 80,000×, resulting in a pixel size of 1.78 Å/pixel and 1.34 Å/pixel, respectively, and recorded with a CCD camera (FEI, Eagle) by using Serial EM software. The defocus range was 1–3 μm. Additionally, cryo-EM data sets were also taken with a Polara G2 F30 microscope (FEI) operating at 300 kV with a magnification of 62,000× and recorded with a Gatan K2 summit direct detector (3838 × 3710 pixel) and a GIF 2000 energy filter, corresponding to 1.82 Å/pixel using Serial EM software. In every grid hole only one position was imaged with a total exposure of 5s and a frame time of 0.1 s. For the image processing frame 10 to 40 was used with a total electron dose of 30 electrons per Å^2. The defocus range for of the data sets was 0.5–3.2 μm.

Image processing of cryo-EM data set. For the image processing the frames were aligned and the drifting of frames was corrected. The tubes were segmented by helixboxer of EMAN2[51]. 26754 segments were extracted with a box size of 300 pixels with an overlap of 90%. The defocus and astigmatism were determined by ctffind3[52] and afterwards the contrast transfer function was corrected by phase flipping by bctf from BSOFT software package[50]. All segments were 2D classified by Relion[53]. During this process 19423 segments were discarded due to bad quality. The result of the final round of the 2D classification is shown in Fig. S3.

We chose 5 classes for further assessment. These 5 classes have diameters of 280, 312, 262, 250, 242 Å and 1948, 1392, 692, 1173, 1372 segments respectively.

The reconstructions using particles from individual classes were performed by IHRSR[54] implemented into SPIDER software package[55]. As an initial model, a Gaussian noise filled cylinder with the same diameter as the test data was used. The first rounds of the reconstruction were performed using 2x binned images with an azimuthal increment of 4 degree, without the search for out-of-plane tilt, to accelerate the process. During the refinement, the azimuthal increment was set to 1 degree with an out-of-plane tilt of 1 degree increment up to +/− 10 degree, thus the references of 7200 reprjection images were created for projection matching. "hsearch" in IHRSR software package[54] was used to find a local conversing point, but this option was not used for initially determining the helical parameter. Instead, the initial helical parameters of individual class were calculated from the 2D class average and the corresponding Fourier Transform. Considering some heterogeneity, we calculated several possibilities and assessed the resulting 3D reconstruction by comparing the reprojections and the class averages and their power spectra. After the processing, the final helical parameters converged to a rise per subunit of 3.81 Å, an azimuthal rotation of 55.92° for the class shown in Fig. 4 and Fig. S5, first row. The other classes showed similar helical parameters (Δz, Δphi) as 3.83 Å, 55.96° (Fig. S5, second row, Fig. S6A), 3.84 Å, 56.01° (Fig. S5, third row, Fig. S6B), 3.82 Å, 55.93° (Fig. S5, fourth row, Fig. S6C) and 3.85 Å, 55.99° (Fig. S5, fifth row, Fig. S6D).

The resolution of all reconstructions was determined by the Fourier shell correlation (FSC) of the half data sets at the cut off 0.5. To calculate the resolution, we performed a few cycle of the IHRSR reconstructions to assure the independence of the reconstructions. The resolutions were calculated to be 10.3, 11.2, 10.9, 10.9, 12.1.

Fitting of the amphiphysin BAR crystal structure. The known crystal structure of Drosophila-amphiphysin BAR (PDB code 1URU) was manually fit into the reconstructed density of a BAR dimer. In order to perform amplitude correction of the 3D reconstructions, the fitted BAR dimer atomic model was converted to a density map using Chimera software and the helical symmetry of the reconstruction was imposed by bhelix (bsoft package). This helically symmetrized BAR map was used as a reference for the amplitude correction of the reconstruction. Bampweigh (bsoft package) was used for the amplitude correction. The final maps were low-pass filtered to 11–12 Å. BAR dimer interactions were analyzed using the program Chimera.

References

1. Zimmerberg, J. & Kozlov, M. M. How proteins produce cellular membrane curvature. *Nat Rev Mol Cell Biol* **7,** 9–19 (2006).
2. Suetsugu, S., Kurisu, S. & Takenawa, T. Dynamic shaping of cellular membranes by phospholipids and membrane-deforming proteins. *Physiol. Rev.* **94,** 1219–1248 (2014).
3. McMahon, H. T. & Boucrot, E. Membrane curvature at a glance. *J Cell Sci* **128,** 1065–1070 (2015).
4. Frost, A., Unger, V. M. & De Camilli, P. The BAR domain superfamily: membrane-molding macromolecules. *Cell* **137,** 191–196 (2009).
5. McMahon, H. T. & Gallop, J. L. Membrane curvature and mechanisms of dynamic cell membrane remodelling. *Nature* **438,** 590–596 (2005).
6. Bhatia, V. K. *et al.* Amphipathic motifs in BAR domains are essential for membrane curvature sensing. *EMBO J* **28,** 3303–3314 (2009).
7. Daumke, O., Roux, A. & Haucke, V. BAR Domain Scaffolds in Dynamin-Mediated Membrane Fission. *Cell* **156,** 882–892 (2014).
8. Qualmann, B., Koch, D. & Kessels, M. M. Let's go bananas: revisiting the endocytic BAR code. *EMBO J* **30,** 3501–3515 (2011).
9. Mim, C. & Unger, V. M. Membrane curvature and its generation by BAR proteins. *Trends Biochem Sci* **37,** 526–533 (2012).
10. Peter, B. J. *et al.* BAR domains as sensors of membrane curvature: the amphiphysin BAR structure. *Science* **303,** 495–499 (2004).
11. Gallop, J. L. *et al.* Mechanism of endophilin N-BAR domain-mediated membrane curvature. *EMBO J* **25,** 2898–2910 (2006).
12. Jao, C. C. *et al.* Roles of amphipathic helices and the bin/amphiphysin/rvs (BAR) domain of endophilin in membrane curvature generation. *J Biol Chem* **285,** 20164–20170 (2010).
13. Isas, J. M., Ambroso, M. R., Hegde, P. B., Langen, J. & Langen, R. Tubulation by Amphiphysin Requires Concentration-Dependent Switching from Wedging to Scaffolding. *Structure* **23,** 873–81 (2015).
14. Drin, G. & Antonny, B. Amphipathic helices and membrane curvature. *FEBS Lett.* **584,** 1840–1847 (2010).
15. Antonny, B. Mechanisms of membrane curvature sensing. *Annu. Rev. Biochem.* **80,** 101–123 (2011).
16. Mizuno, N. *et al.* Remodeling of lipid vesicles into cylindrical micelles by α-synuclein in an extended α-helical conformation. *J Biol Chem* **287,** 29301–29311 (2012).
17. Varkey, J. *et al.* Membrane curvature induction and tubulation are common features of synucleins and apolipoproteins. *J Biol Chem* **285,** 32486–32493 (2010).
18. Mizuno, N., Jao, C. C., Langen, R. & Steven, A. C. Multiple modes of endophilin-mediated conversion of lipid vesicles into coated tubes: implications for synaptic endocytosis. *J Biol Chem* **285,** 23351–23358 (2010).
19. Mim, C. *et al.* Structural Basis of Membrane Bending by the N-BAR Protein Endophilin. *Cell* **149,** 137–145 (2012).
20. Yin, Y., Arkhipov, A. & Schulten, K. Simulations of membrane tubulation by lattices of amphiphysin N-BAR domains. *Structure (London, England: 1993)* **17,** 882–892 (2009).
21. Cui, H. *et al.* Understanding the role of amphipathic helices in N-BAR domain driven membrane remodeling. *Biophys. J.* **104,** 404–411 (2013).
22. David, C., McPherson, P. S., Mundigl, O. & De Camilli, P. A role of amphiphysin in synaptic vesicle endocytosis suggested by its binding to dynamin in nerve terminals. *Proc Natl Acad Sci USA* **93,** 331–335 (1996).
23. Rao, Y. & Haucke, V. Membrane shaping by the Bin/amphiphysin/Rvs (BAR) domain protein superfamily. *Cell. Mol. Life Sci.* **68,** 3983–3993 (2011).
24. Taylor, M. J., Perrais, D. & Merrifield, C. J. A high precision survey of the molecular dynamics of mammalian clathrin-mediated endocytosis. *PLoS Biol* **9,** e1000604 (2011).
25. Lee, E. *et al.* Amphiphysin 2 (Bin1) and T-tubule biogenesis in muscle. *Science* **297,** 1193–1196 (2002).

26. Razzaq, A. Amphiphysin is necessary for organization of the excitation-contraction coupling machinery of muscles, but not for synaptic vesicle endocytosis in Drosophila. *Genes Dev* **15,** 2967–2979 (2001).
27. Al-Qusairi, L. & Laporte, J. T-tubule biogenesis and triad formation in skeletal muscle and implication in human diseases. *Skelet Muscle* **1,** 26 (2011).
28. Zelhof, A. C. *et al.* Drosophila Amphiphysin is implicated in protein localization and membrane morphogenesis but not in synaptic vesicle endocytosis. *Development* **128,** 5005–5015 (2001).
29. Leventis, P. A. *et al.* Drosophila Amphiphysin is a post-synaptic protein required for normal locomotion but not endocytosis. *Traffic* **2,** 839–850 (2001).
30. Takei, K., Slepnev, V. I., Haucke, V. & De Camilli, P. Functional partnership between amphiphysin and dynamin in clathrin-mediated endocytosis. *Nat Cell Biol* **1,** 33–39 (1999).
31. Nicot, A.-S. *et al.* Mutations in amphiphysin 2 (BIN1) disrupt interaction with dynamin 2 and cause autosomal recessive centronuclear myopathy. *Nat. Genet.* **39,** 1134–1139 (2007).
32. Böhm, J. *et al.* Adult-onset autosomal dominant centronuclear myopathy due to BIN1 mutations. *Brain* **137,** 3160–3170 (2014).
33. Mejaddam, A. Y., Nennesmo, I. & Sejersen, T. Severe phenotype of a patient with autosomal recessive centronuclear myopathy due to a BIN1 mutation. *Acta Myol* **28,** 91–93 (2009).
34. Toussaint, A. *et al.* Defects in amphiphysin 2 (BIN1) and triads in several forms of centronuclear myopathies. *Acta Neuropathol.* **121,** 253–266 (2011).
35. Frost, A. *et al.* Structural basis of membrane invagination by F-BAR domains. *Cell* **132,** 807–817 (2008).
36. Pang, X. *et al.* A PH domain in ACAP1 possesses key features of the BAR domain in promoting membrane curvature. *Dev Cell* **31,** 73–86 (2014).
37. van Weering, J. R. T. *et al.* Molecular basis for SNX-BAR-mediated assembly of distinct endosomal sorting tubules. *EMBO J* **31,** 4466–4480 (2012).
38. Alushin, G. M. *et al.* High-resolution microtubule structures reveal the structural transitions in αβ-tubulin upon GTP hydrolysis. *Cell* **157,** 1117–1129 (2014).
39. Ecken, von der, J. *et al.* Structure of the F-actin-tropomyosin complex. *Nature* **519,** 114–117 (2014)
40. Galkin, V. E., Orlova, A., Vos, M. R., Schröder, G. F. & Egelman, E. H. Near-atomic resolution for one state of f-actin. *Structure* **23,** 173–182 (2015).
41. Zemel, A., Fattal, D. R. & Ben-Shaul, A. Energetics and self-assembly of amphipathic peptide pores in lipid membranes. *Biophys. J.* **84,** 2242–2255 (2003).
42. Masuda, M. *et al.* Endophilin BAR domain drives membrane curvature by two newly identified structure-based mechanisms. *EMBO J* **25,** 2889–2897 (2006).
43. Weissenhorn, W. Crystal structure of the endophilin-A1 BAR domain. *J. Mol. Biol.* **351,** 653–661 (2005).
44. Parton, R. G., Way, M., Zorzi, N. & Stang, E. Caveolin-3 associates with developing T-tubules during muscle differentiation. *J Cell Biol* **136,** 137–154 (1997).
45. Picas, L. *et al.* BIN1/M-Amphiphysin2 induces clustering of phosphoinositides to recruit its downstream partner dynamin. *Nat Commun* **5,** 5647 (2014).
46. Wu, T., Shi, Z. & Baumgart, T. Mutations in BIN1 associated with centronuclear myopathy disrupt membrane remodeling by affecting protein density and oligomerization. *PLoS ONE* **9,** e93060 (2014).
47. Sorre, B. *et al.* Nature of curvature coupling of amphiphysin with membranes depends on its bound density. *Proc Natl Acad Sci USA* **109,** 173–178 (2012).
48. Li, M. Z. & Elledge, S. J. Harnessing homologous recombination *in vitro* to generate recombinant DNA via SLIC. *Nat. Methods* **4,** 251–256 (2007).
49. Studier, F. W. Protein production by auto-induction in high density shaking cultures. *Protein Expr. Purif.* **41,** 207–234 (2005).
50. Heymann, J. B. & Belnap, D. M. Bsoft: image processing and molecular modeling for electron microscopy. *J Struct Biol* **157,** 3–18 (2007).
51. Tang, G. *et al.* EMAN2: an extensible image processing suite for electron microscopy. *J Struct Biol* **157,** 38–46 (2007).
52. Mindell, J. A. & Grigorieff, N. Accurate determination of local defocus and specimen tilt in electron microscopy. *J Struct Biol* **142,** 334–347 (2003).
53. Scheres, S. H. W. RELION: implementation of a Bayesian approach to cryo-EM structure determination. *J Struct Biol* **180,** 519–530 (2012).
54. Egelman, E. H. The iterative helical real space reconstruction method: surmounting the problems posed by real polymers. *J Struct Biol* **157,** 83–94 (2007).
55. Frank, J. *et al.* SPIDER and WEB: processing and visualization of images in 3D electron microscopy and related fields. *J Struct Biol* **116,** 190–199 (1996).

Acknowledgements

We thank Elena Conti and Wolfgang Baumeister for resources and support, the Core Facility of the Max Planck Institute of Biochemistry for MS analysis, the Image Facility of the Max Planck Institute of Biochemistry for resources, Christian Biertümpfel for helpful discussions and careful readings of the manuscript. We thank Joseph Wall and Beth Lin (Brookhaven National Laboratory) for the STEM measurement and Ulrich Baxa for the instruction for the analysis of the STEM data and the interpretation. We acknowledge Ralf Langen for sharing the initial plasmids and for fruitful discussions. We also thank members of Mizuno lab for their help in protein purification and technical support and Michael Taschner and Eva Kowalinski for their kind help with cloning. This study was supported by the Max Planck Society and the Deutsche Forschungsgemeinschaft (DFG) through grants within the GRK1721 and MI 1745/1.

Author Contributions

J.A. and N.M. designed research. J.A., N.B. and N.M. performed research. J.A. and N.M. performed experiments including cloning, purification, EM data collection and the structural data analysis. J.A. and N.B. performed light microscopy, negative-stain EM and the molecular fitting. J.A. and N.M. wrote the manuscript. All authors reviewed the manuscript.

Additional Information

Accession codes: The reconstruction files are deposited in the Electron Microscopy Data Bank (EMDB) under the following accession number: 3192, 3193, 3194, 3195, 3196.

Supplementary information accompanies this paper at http://www.nature.com/srep

Competing financial interests: The authors declare no competing financial interests.

How to cite this article: Adam, J. *et al.* Structural insights into the cooperative remodeling of membranes by amphiphysin/BIN1. *Sci. Rep.* **5**, 15452; doi: 10.1038/srep15452 (2015).

Structural insights into the cooperative remodeling of membranes by amphiphysin/BIN1

Julia Adam, Nirakar Basnet and Naoko Mizuno*

Cellular and Membrane Trafficking,
Max Planck Institute of Biochemistry, Am Klopferspitz 18, D-82152 Martinsried, Germany

*Corresponding author
E-mail: mizuno@biochem.mpg.de
Phone: + 49 (89) 8578 – 3479
Fax: +49(89) 8578 – 3605

Supplementary Figure Legends

Figure S1

Tubulation of various amphiphysin fragments with vesicles observed by absorbance measurement and negative staining. (A) Absorbance measurement at 400 nm of 180 μM vesicles mixed with 5μM N-BAR, FL, N-BAR-deltaH0 and deltaH0. The increase in the absorbance at 400 nm corresponds to tube formation. The negative control shows the absorbance of vesicles without any protein. (B and C) Negative stain EM observation of (B) vesicles and (C) tube formations of NBAR-deltaH0 (left) and N-BAR (right). The tubes are observed immediately after mixing (22 sec) and at various time points (2 min, 10 min, 30 min and 45 min) up to 45 min. After ~30 min of incubation, N-BAR-mediated tubes visibly transform into small vesicles (right, bottom, red arrow heads).

Supplementary Fig. S1

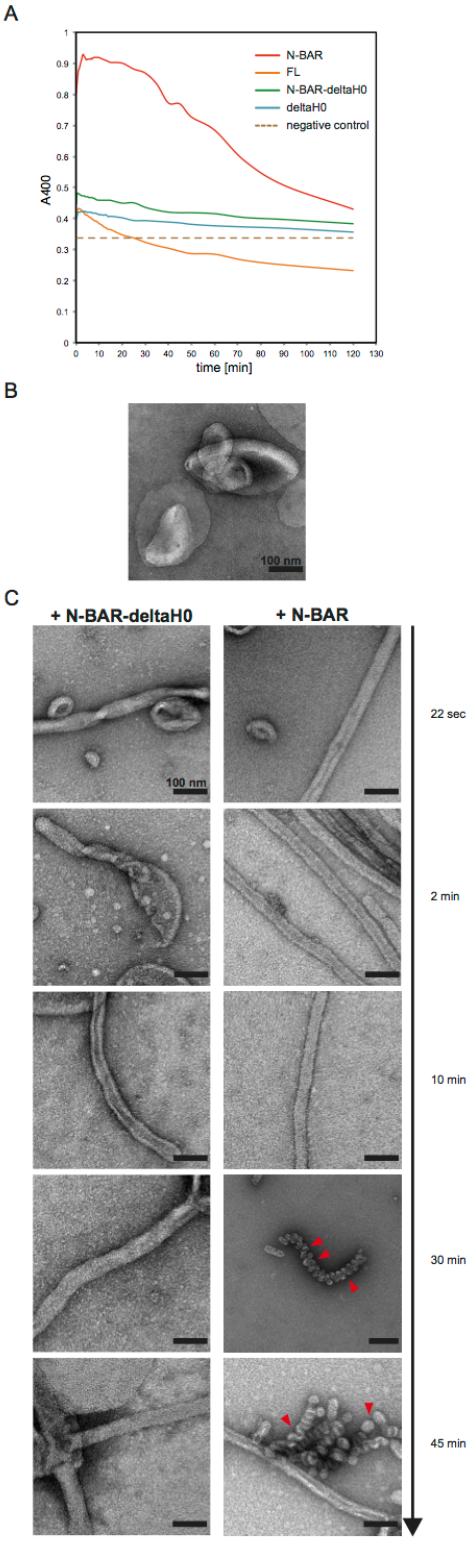

Figure S2

(A) Tubulation observed by fluorescence light microscopy. Various protein dilutions (6 µM, 0.6 µM, 0.06 µM, 0.006 µM) of N-BAR, N-BAR-deltaH0 and FL were incubated with 720 µM of fluorescently labeled vesicles. N-BAR and FL show distinct tubulation up to a concentration of 0.6 µM. In contrast N-BAR-deltaH0 mediated tabulation is only observed with 6 µM of protein. The degree of tubulation is described as ++ > + > +/- (tubulation very sparsely happening) > - (no tubulation). v: examples of vesicles and t: examples of tubes. (B) The light scattering of the mixture of 720 µM vesicles and various concentrations of N-BAR (left), N-BAR-deltaH0 (middle) and FL (right). The graphs show the critical concentrations where no tubulation occurs anymore (guided with flat lines) of 0.4 µM (N-BAR and FL) and 1.6 µM (N-BAR-deltaH0).

Supplementary Fig. S2

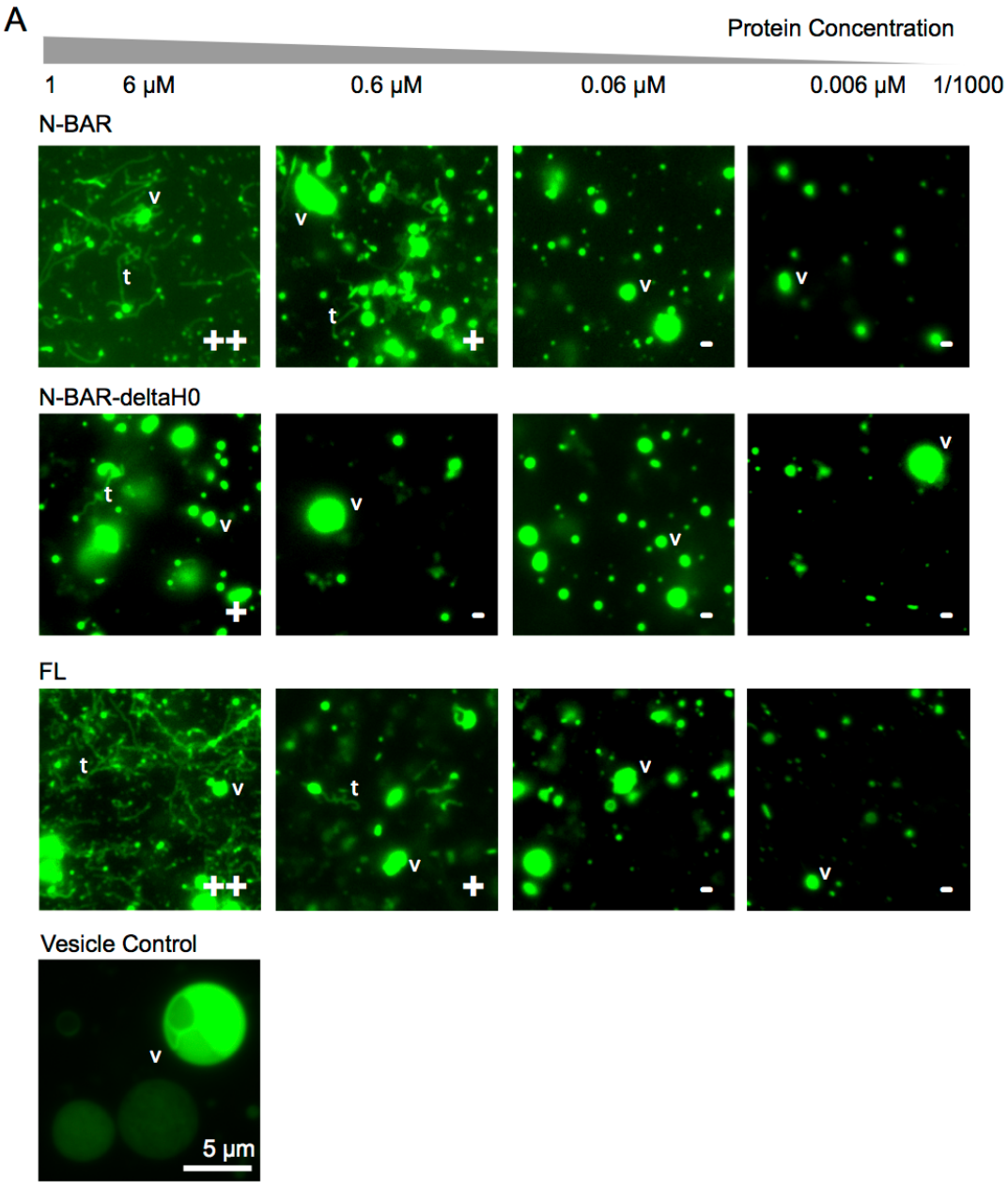

Figure S3

2D averages of N-BAR mediated tubes. After CTF correction (phase-flipping) of the collected micrographs, the N-BAR mediated tubes were boxed into 26754 segments (300x300 pixel, corresponding to 546 x 546 Å). The segmented tubes were classified with reference free classification scheme provided by Relion software. To achieve 2D averages with better features, bad segments were removed by several classification iterations. After removal of bad segments around 19423 boxed segments were used to obtain 50 final 2D class averages. The particles in the classes with the most distinctive features were used for further data analyses and 3D reconstructions as shown in Figure S5.

Supplementary Fig. S3

N-BAR tube class averages

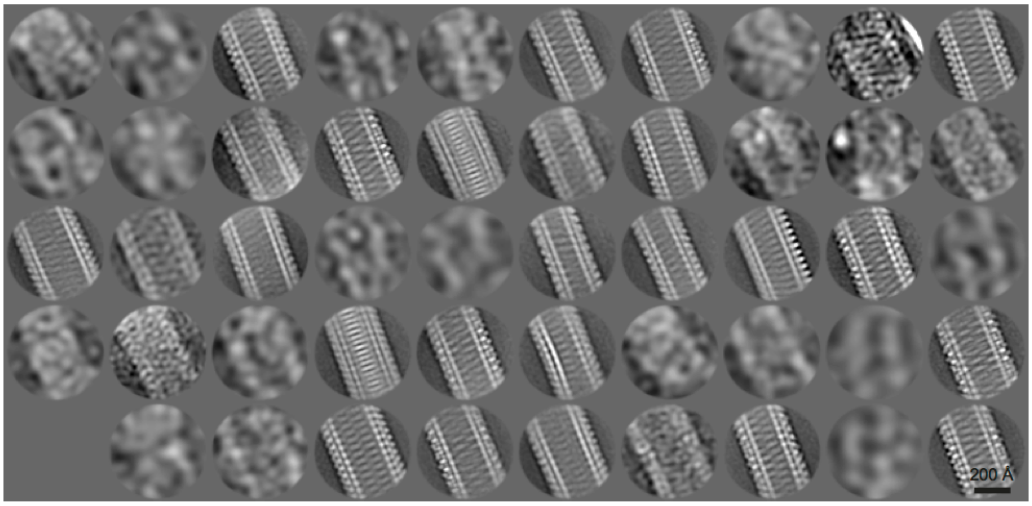

Figure S4

(A) STEM image of N-BAR tubes and TMV internal control. Boxes show examples of the MPL (mass per length) measurements (pink: N-BAR, blue: TMV). 20 μM of N-BAR were mixed with 720 μM of vesicles directly before the STEM sample preparation and measurement. (B) The distribution of N-BAR shows a MPL of 28±3 kDa/Å (N=148), while TMV shows 13±0.7 kDa/Å (N=66). The MPL was measured as described in Methods.

Supplementary Fig. S4

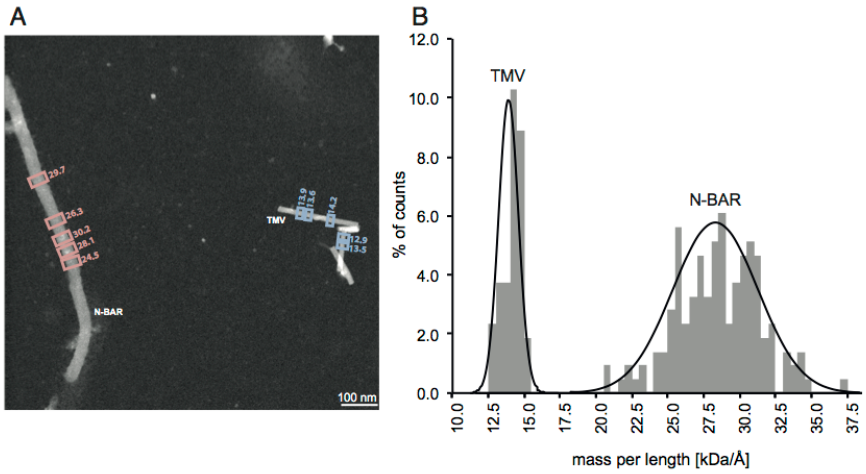

Figure S5

Quality control information of five selected classes of N-BAR mediated tubes. First column: Class averages. Second column: averaged power spectra of classified images (left) and the reprojections of the 3D reconstructions (right). Third column: Reprojections of 3D reconstructions. Fourth column: Density profile of the reprojection of the 3D reconstruction, revealing the tube radius. The profiles show three peaks from the tube center: inner leaflet, outer leaflet and the attached BAR protein densities. Fifth column: Fourier Shell Correlation profile. The resolutions were calculated to be 10.3, 11.2, 10.9, 10.9, 12.1 Å (top to bottom) at the FSC=0.5 cutoff criterion.

Supplementary Fig. S5

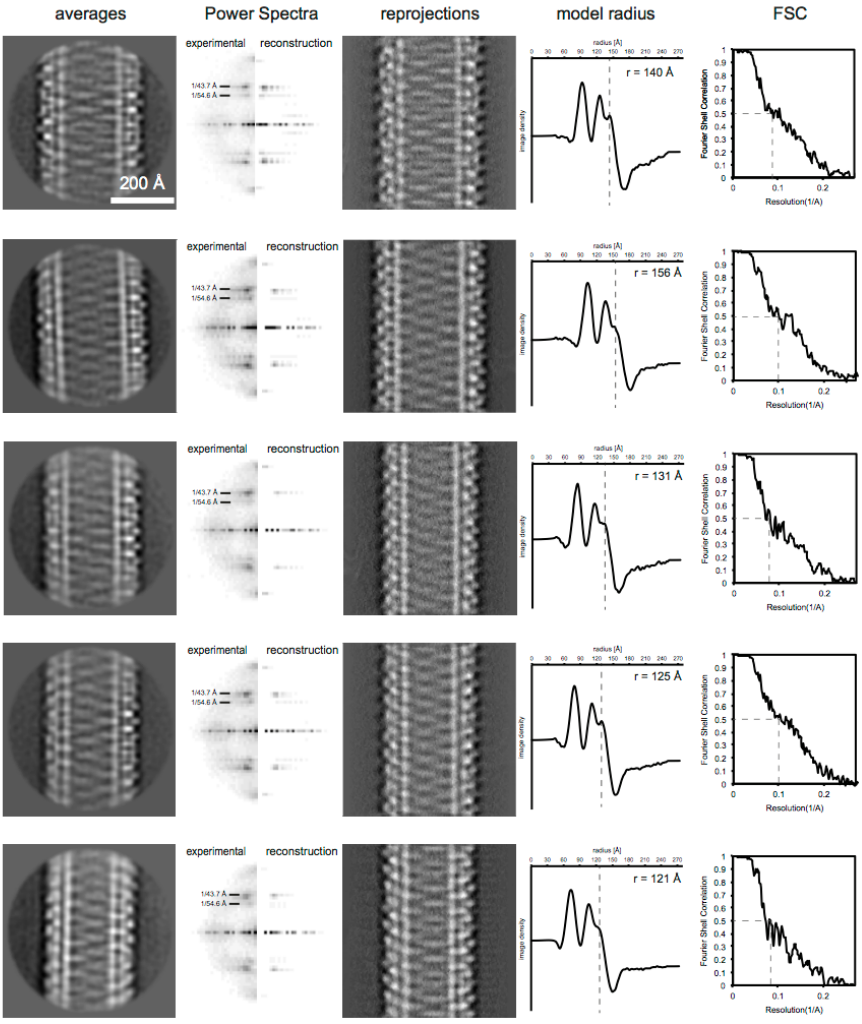

Figure S6

3D reconstructions of tubes with various sizes showing different arrangements of the BAR lattice packings. (A) The wider tube r = 156 Å reveals a slightly less tight BAR unit packing. The narrower tubes with (B) r = 131 Å, (C) r = 125 Å and (D) r = 121 Å show that the BAR units were rotated along the crescent dimer axis. For the fitting the amphiphysin BAR crystal structure (PDB: 1URU) was used.

Supplementary Fig. S6

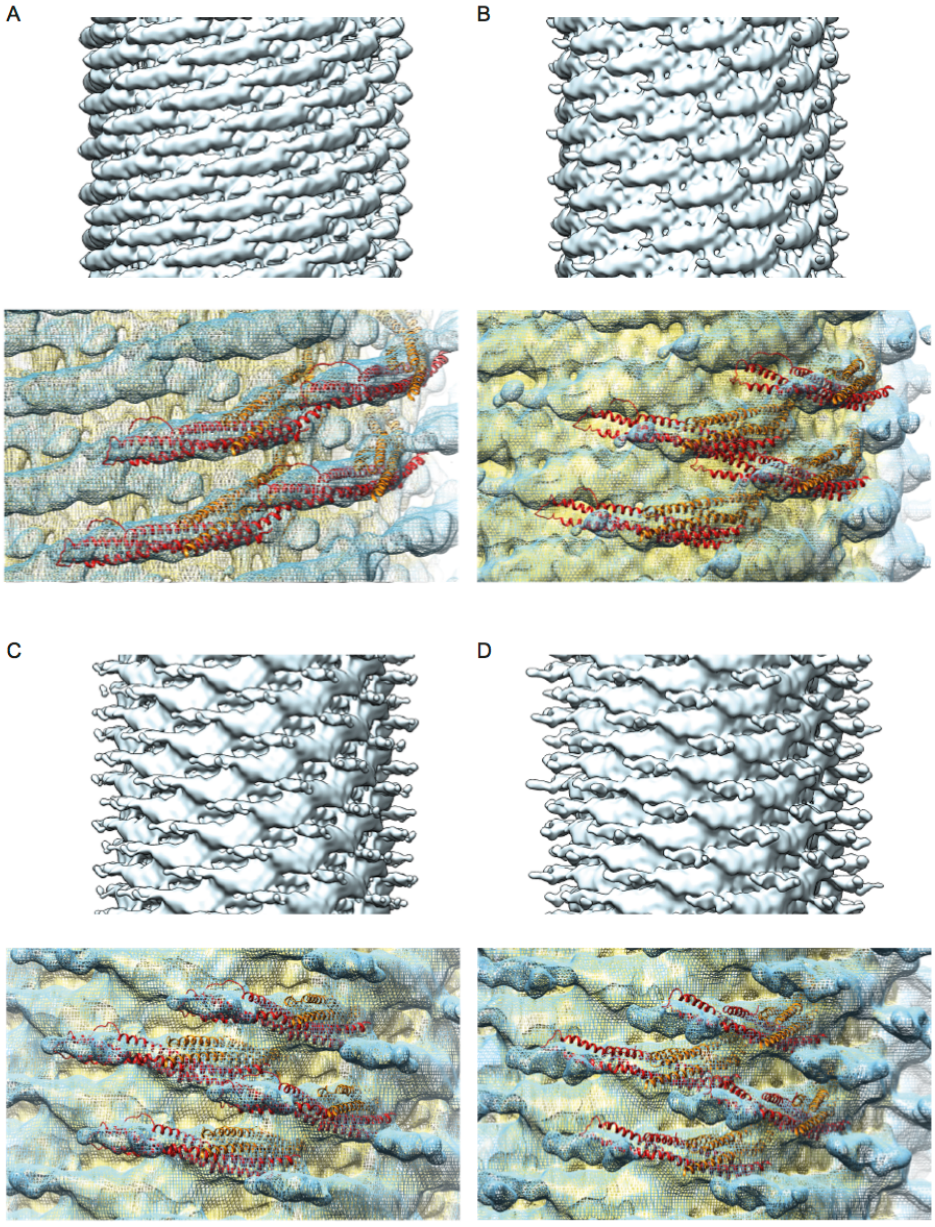

Figure S7

Membrane tubulation occurring by N-BAR-N-BAR-delta-tip heterodimer (left) and N-BAR-delta-tip homodimer (right). Tubulation of 720 μM fluorescently labeled vesicles mediated by 6 μM of the proteins observed by fluorescence light microscopy (top) and corresponding negative-stain EM observations (middle). v: examples of vesicles and t: examples of tubes. Bottom: Critical concentration measurements. Both protein fragments show tubulation of vesicles. The critical concentrations where no tubulation is happening anymore (guided with flat lines) were 0.2 μM for N-BAR-N-BAR-delta-tip and 0.7 μM for N-BAR-delta-tip. The measurement was done with the same mixture as in the fluorescence microscopy without labeled lipid.

Supplementary Fig. S7

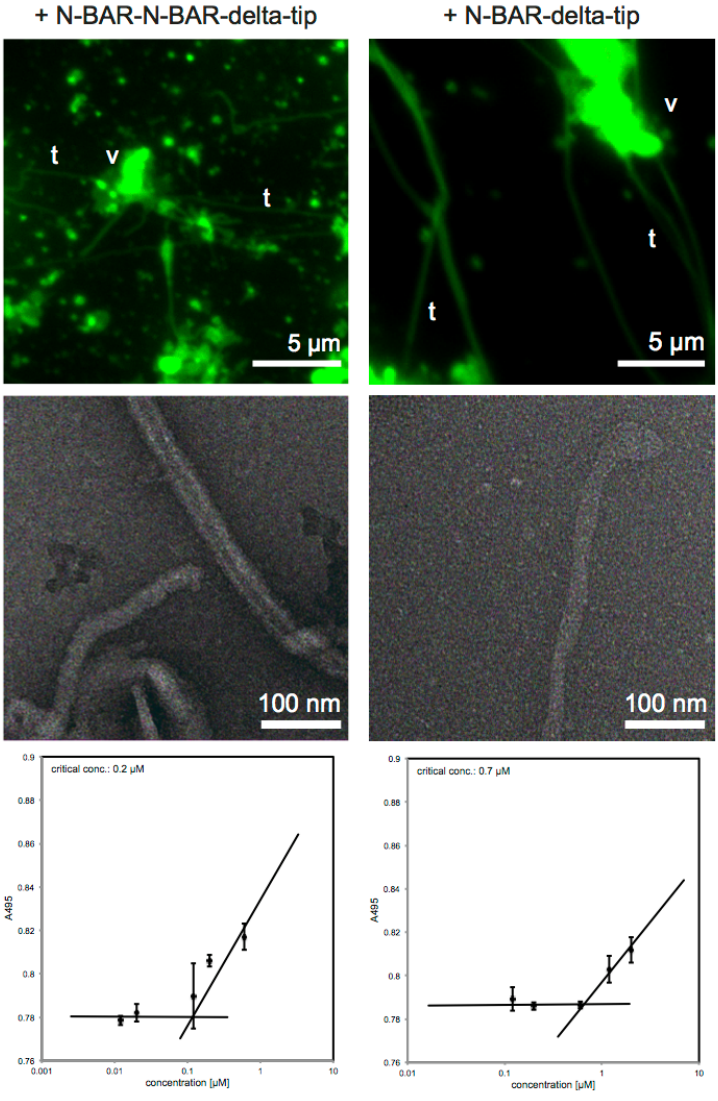

2. Discussion

Many if not all cell types are polarized and cell polarity is essential for migration, organization and development of the cells. Rod shaped cell of fission yeast *Schizosaccharomyces pombe* due to the polarized growth at the tip of the cell, polarized lamellopodium formation during fibroblast migration, formation of polarized axon and dendrites in neurons, generation of cell diversity due to asymmetric cell division of polarized embryonic and stem cells and apical cortical polarity in epithelial cells are some example of cell polarization in different cell types (Siegrist and Doe, 2007). It is known that actin and actin related proteins are important for cell polarity but studies have shown that microtubule can also induce as well as maintain cell polarity(Siegrist and Doe, 2007).

In complex and highly polarized cells like neurons, microtubule is central to the polarization processes such as axon initiation to axon differentiation and from axon elongation to axon branch formation. Not only in morphological changes but microtubule is also essential for intracellular transporting of various cargoes from and to soma. The importance of microtubule in neuron became more apparent when various mutation in microtubule related genes such as tau, spastin, dynein, kinesin, dynactin, doublecortin and lis1 were linked to various neurodevelopmental disease (Kapitein and Hoogenraad, 2015). Not only microtubule related genes but genetic studies have also linked various neurological disorders to mutations in various tubulin family members, which shows the importance of proper development and maintenance of complex microtubule arrays in the neurons (Tischfield et al., 2011).

Formation of collateral branches on axon body is essential to form complex neural network. Although we know about general cytoskeleton reorganization process during the branch formation, we still do not know the underlying exact molecular mechanism behind it. During branch formation, after initial membrane protrusion and deformation due to F-actin activity, the microtubule enters the branch sites and subsequently stabilizes the branch. This entry of microtubule to the branch site is crucial for the branch formation as time-lapse imaging have shown that only the branch sites which were invaded by the microtubules resulted into the branch formation (Kalil et al., 2000). Microtubules are parallelly bundled in the axons and in order to enter the branch sites it has to undergo certain degree of remodeling and reorganization. The first step is unbundling, then the microtubules are splayed and it enters to the branch site. But what kind of remodeling occurs, that the long, bundled array of microtubules enter the branch site?

It was shown that at the branch points splaying of the microtubules was accompanied by the fragmentation of the microtubules and then reorganization which ultimately leads to the entry and

stabilization of the branch points (Dent et al., 1999). The fragmentation observed at the branch sites is most likely caused by the microtubule severing protein spastin which is known to play important role in axon branch formation (Yu et al., 2008). But what happens after fragmentation? How the microtubule gets reorganized? We are still missing this piece of information.

In our study, we focus on a microtubule binding protein called SSNA1, which was reported to play a role in promoting axon elongation and branching but the mechanism through which it modulated microtubule dynamics was still not clear. We show that SSNA1 is a microtubule nucleating and branching factor which accumulates at the axon branches and promotes the branch formation in primary neurons. In-vitro reconstitution of SSNA1 and unpolymerized tubulin showed that SSNA1 forms small clusters along with the unpolymerized tubulin and nucleates microtubule from these clusters which are reminiscent of aster formation observed during microtubule nucleation (Ishihara et al., 2014; Wilde and Zheng, 1999).

SSNA1 not only promoted nucleation but also remodeled the microtubule into a branched structure. SSNA1 fibrils seems to guide protofilaments of a microtubule to split apart from the microtubule lattice and form daughter a microtubule. To our knowledge no other MTBPs can directly remodeled the microtubule nor there is any report mentioning the rigid, cylindrical microtubule has a plasticity to be remodeled in such a manner. We tested two other MTBPs, EB3 which regulates the microtubule dynamics at growing end and ch-TOG which is a known microtubule nucleator under the same experimental condition and both of these proteins did not induce microtubule branching. This property of remodeling microtubule seems to be unique to SSNA1 and it relies on its ability to self-assemble into fibrils in a head to tail fashion for the branching activity. SSNA1 mutants that abrogate the self-assembly of the protein did not show any branching activity and these mutants when expressed in primary neurons also failed to promote axon branching.

Microtubule nucleation and remodeling of microtubule add a new mode of microtubule organization inside the cell by forming a branched network. Local nucleation of microtubules forming a complex branched network, which is independent of centrosome plays an important role in various cellular processes (Petry and Vale, 2015). The current model for branched network of microtubules so far involves γ-tubulin mediated microtubule nucleation from the side of existing microtubule. This mode of branching is completely different from the SSNA1 where the new branched microtubule is formed by directly splitting the protofilament and it shares the lattice with the old microtubule. During co-polymerization of SSNA1 and tubulin, association of SSNA1 may reinforce longitudinal connection of tubulin oligomers and facilitates the protofilament formation which could then act as a seed for the

polymerization. Similarly, the preference of SSNA1 to form lateral connections may stabilize the lateral connections between the microtubule protofilaments. The protein is also self-assembling on the surface of microtubule lattice, during co-polymerization and this self-assembly could precede the formation of microtubule lattice. The preceding SSNA1 now could guide protofilaments outside the microtubule axis which then provides the template for a new microtubule branch ("guide-rail" mechanism)**.**

In a cellular context, the process of branching and microtubule remodeling mediated by the SSNA1 could be more complex with many factors involved simultaneously but SSNA1 could possibly be a missing link between microtubule fragmentation and reorganization observed during axon branch formation. Spastin is known to interact with SSNA1 and after severing of the microtubules by spastin, the pool of free tubulin generated could be then used by the SSNA1 for nucleation, remodeling and reorganization of microtubules at the branch points. Our in-vitro experiments show that SSNA1 not only remodels the microtubule during co-polymerization but has the ability to remodel pre-existing stable microtubules. Therefore, the at the branch point not only free tubulin or tubulin oligomers but also small fragments of microtubules could be remodeled by SSNA1.

During in-vitro reconstitutions, the SSNA1 makes cluster with unpolymerized tubulin at a high local concentration and this requirement of high concentration could actually act as a regulatory element in limiting the microtubule remodeling activity of SSNA1 to a specific sub-cellular localization in the cell like base of cilia, midbody of dividing cells and axon branch points in neurons. Axons are densely packed with microtubules and when spastin induces the fragmentation at the possible branch points, it could increase the local concentration of tubulin possibly creating a condition for SSNA1 to nucleate and reorganize the microtubules specifically at the branch points.

Our work shows how a small coil-coil protein SSNA1 could induce the microtubule nucleation while getting itself self-assembled on the surface of microtubule lattice and how this self-assembly and microtubule nucleation goes hand in hand and results into remodeling of the microtubule. This is the first time where the remodeling of microtubule lattice to such an extent in order to form a branched structure is observed and this gives us a new dimension to microtubule organization inside the cell.

3. Outlook and future perspectives

Since its discovery in 1950s the microtubule research has made a remarkable journey to understand the nature of one of the most important component of the eukaryotic cells (Brinkley, 1997). Microtubules due to its dynamic nature, can explore the space in cytoplasm, capture cargo, acts as a medium of transport of these cargoes, maintain the organization of the cell, act as a signaling hub and control cell shape and morphology in response to external signals and cues. When the cell enters the state of division, then the microtubule can disassemble and reassemble into an enigmatic structure called mitotic spindle which makes sure the proper segregation of genetic material to the daughter cells.

In specialized cells such as neurons it is essential for various processes such as neuronal migration, polarity, differentiation and signal transduction. For the proper functioning of nervous system and brain, individual neurons connect to multiple synaptic targets forming a complex neural circuitry and this is achieved through extensive branching of their axons. As any other polarizing and development event in neuron the microtubule is also central to the branch formation. In our study, we could show that the small coil-coil protein called SSNA1 localizes at the axon branches and promotes axon branch formation and elongation. We could co-relate its in-vitro activity of remodeling microtubule into branched structure to axon branching in neurons but we need further insights on its exact mechanism in-situ.

Various studies in the past have given us insights into the general mechanism of axon branching process. The cytoskeleton undergoes major reorganization during the branch formation with microtubule getting fragmented, reorganized followed by entry into branches and its subsequent stabilization. Then when does SSNA1 acts at the branch points? Since, SSNA1 remodels and nucleates microtubules and also interacts with microtubule severing enzyme spastin, one could imagine SSNA1 could be recruited at the branch sites through the interaction with spastin and act after the microtubules get fragmented but we cannot dismiss the possibility for SSNA1 to be the one to recruit spastin at the branch sites.

The axons were reported to form collateral branches through either bifurcation of growth cone or interstitial mode and it will be interesting to know if SSNA1 mediates the branching in both modes. The microtubules in neurons undergo various kind of post-translational modification and the protein itself could be the subject of post-translational modification and then how does these modifications

on protein or on microtubules regulate the dynamics? There are still lot of questions to be answered till we start getting the picture of what SSNA1 is exactly doing.

There are still a huge caveat of information missing regarding the axon branching itself. How the axon branch points are determined at axon? The presence of gradients of molecular cues were thought to play role in specificity of branching (Kalil and Dent, 2014) but how the signaling pathways induced by these external molecular cues converge into cytoskeleton and how it transforms the axonal cytoskeleton into dynamic actin and microtubule filaments that will initiate and stabilize the branch formation. It is very important to answer these questions in order to understand the remarkable ability of axons to branch and connect specific region of developing nervous system. The development of new genetic tools in combination with high-resolution imaging and more importantly development and application of cryo-electron tomography could shed some light in this complex but fascinating process.

4. List of figures

5. Abbreviation

APC	**Cancer associated protein**
ASPM	Abnormal spindle-like microcephaly-associated protein
APC	Adenomatous polyposis coil
BAR	Bin/Amphiphysin/Rvs
CAMSAP	Calmodulin-regulated spectrin-associated protein
CCP	Carboxypeptidases
DRG	Dorsal root ganglion neuron
EM	Electron microscopy
ENA/VASP	Enable/vasodilator-stimulated phosphoprotein
EB	End binding protein
GTP	Guanosine-5'-triphosphate
GMPCPP	Guanosine-5’-[(β,γ)-methyleno]triphosphate
MTBPs	Microtubule binding proteins
MCAF	Microtubule-actin crosslinking factor
MTOCs	Microtubule-Organizing Centers
MCAK	Mitotic centromere associated kinesin
MIPs	Microtubule inner proteins
+TIPs	Plus-end tracking proteins
PTMs	Post-translational modifications
PRC1	Protein regulator of cytokinesis 1
Pf	Protofilaments
SH3	Src Homology 3
TPX2	Targeting protein for Xklp2
TTL	Tubulin tyrosine Ligase
TTLL	TTL-like family
TAT	Tubulin acetyltransferase
TURC	Tubulin ring complex

6. References

Ahuja, R., Pinyol, R., Reichenbach, N., Custer, L., Klingensmith, J., Kessels, M.M., and Qualmann, B. (2007). Cordon-Bleu Is an Actin Nucleation Factor and Controls Neuronal Morphology. Cell *131*, 337–350.

Aillaud, C., Bosc, C., Peris, L., Bosson, A., Heemeryck, P., Van Dijk, J., Le Friec, J., Boulan, B., Vossier, F., Sanman, L.E., et al. (2017). Vasohibins/SVBP are tubulin carboxypeptidases (TCPs) that regulate neuron differentiation. Science *358*, 1448–1453.

Akella, J.S., Wloga, D., Kim, J., Starostina, N.G., Lyons-Abbott, S., Morrissette, N.S., Dougan, S.T., Kipreos, E.T., and Gaertig, J. (2010). MEC-17 is an α-tubulin acetyltransferase. Nature *467*, 218–222.

Akhmanova, A., and Hoogenraad, C.C. (2015). Microtubule Minus-End-Targeting Proteins Review. Current Biology *25*, R162–R171.

Akhmanova, A., and Steinmetz, M.O. (2008). Tracking the ends: a dynamic protein network controls the fate of microtubule tips. Nature Publishing Group *9*, 309–322.

Akhmanova, A., and Steinmetz, M.O. (2015). Control of microtubule organization and dynamics: two ends in the limelight. Nature Publishing Group *16*, 711–726.

Akhmanova, A., and Steinmetz, M.O. (2019). Microtubule minus-end regulation at a glance. J Cell Sci *132*, jcs227850.

Aki, T., Funakoshi, T., Kitayama, J.N., and Mizukami, Y. (2008). TPRA40/GPR175 regulates early mouse embryogenesis through functional membrane transport by Sjögren's syndrome-associated protein NA14. J. Cell. Physiol. *217*, 194–206.

Al-Bassam, J., and Chang, F. (2011). Regulation of microtubule dynamics by TOG-domain proteins XMAP215/Dis1 and CLASP. Trends in Cell Biology *21*, 604–614.

Al-Bassam, J., Larsen, N.A., Hyman, A.A., and Harrison, S.C. (2007). Crystal Structure of a TOG Domain: Conserved Features of XMAP215/Dis1-Family TOG Domains and Implications for Tubulin Binding. Structure *15*, 355–362.

Alushin, G.M., Lander, G.C., Kellogg, E.H., Zhang, R., Baker, D., and Nogales, E. (2014). High-Resolution Microtubule Structures Reveal the Structural Transitions in αβ-Tubulin upon GTP Hydrolysis. Cell *157*, 1117–1129.

Andersen, J.S., Wilkinson, C.J., Mayor, T., Mortensen, P., Nigg, E.A., and Mann, M. (2003). Proteomic characterization of the human centrosome by protein correlation profiling. Nature *426*, 570–574.

Arellano-Santoyo, H., Geyer, E.A., Stokasimov, E., Chen, G.-Y., Su, X., Hancock, W., Rice, L.M., and Pellman, D. (2017). A Tubulin Binding Switch Underlies Kip3/Kinesin-8 Depolymerase Activity. Developmental Cell *42*, 37–51.e38.

Baas, P.W., Ahmad, F.J., Pienkowski, T.P., Brown, A., and Black, M.M. (1993). Sites of microtubule stabilization for the axon. Journal of Neuroscience *13*, 2177–2185.

Baines, A.J., Bignone, P.A., biology, M.K.M., 2009 The CKK Domain (DUF1781) Binds Microtubules and Defines the CAMSAP/ssp4 Family of Animal Proteins. Academic.Oup.com

.

Barlan, K., Lu, W., and Gelfand, V.I. (2013). The Microtubule-Binding Protein Ensconsin Is an Essential Cofactor of Kinesin-1. Current Biology *23*, 317–322.

Bartolini, F., and Gundersen, G.G. (2006). Generation of noncentrosomal microtubule arrays. J Cell Sci *119*, 4155–4163.

Bartolini, F., Moseley, J.B., Schmoranzer, J., Cassimeris, L., Goode, B.L., and Gundersen, G.G. (2008). The formin mDia2 stabilizes microtubules independently of its actin nucleation activity. J Cell Biol *181*, 523–536.

Bastmeyer, M., and OLeary, D.D.M. (1996). Dynamics of Target Recognition by Interstitial Axon Branching along Developing Cortical Axons. Journal of Neuroscience 1450–1459.

Basto, R., Lau, J., Vinogradova, T., Gardiol, A., Woods, C.G., Khodjakov, A., and Raff, J.W. (2006). Flies without Centrioles. Cell *125*, 1375–1386.

Bhattacharyya, B., Sackett, D.L., and Wolff, J. (1985). Tubulin, hybrid dimers, and tubulin S. Stepwise charge reduction and polymerization. J. Biol. Chem. *260*, 10208–10216.

Brinkley, W.B.R. (1997). Microtubules: A Brief Historical Perspective. Journal of Structural Biology *118*, 84–86.

Brouhard, G.J., and Rice, L.M. (2018). Microtubule dynamics: an interplay of biochemistry and mechanics. Nature Publishing Group *19*, 451–463.

Brouhard, G.J., Stear, J.H., Noetzel, T.L., Al-Bassam, J., Kinoshita, K., Harrison, S.C., Howard, J., and Hyman, A.A. (2008). XMAP215 Is a Processive Microtubule Polymerase. Cell *132*, 79–88.

Brown, A. (1992). Newly assembled microtubules are concentrated in the proximal and distal regions of growing axons. J Cell Biol *119*, 867–882.

Carvalho-Santos, Z., Azimzadeh, J., Pereira-Leal, J.B., and Bettencourt-Dias, M. (2011). Tracing the origins of centrioles, cilia, and flagella. J Cell Biol *194*, 165–175.

Cassimeris, L. (2002). The oncoprotein 18/stathmin family of microtubule destabilizers. Current Opinion in Cell Biology *14*, 18–24.

Chabin-Brion, K., Marceiller, J., Perez, F., Settegrana, C., Drechou, A., Durand, G., and Poüs, C. (2001). The Golgi Complex Is a Microtubule-organizing Organelle. MBoC *12*, 2047–2060.

Chen, T.-J., Gehler, S., Shaw, A.E., Bamburg, J.R., and Letourneau, P.C. (2005). Cdc42 participates in the regulation of ADF/cofilin and retinal growth cone filopodia by brain derived neurotrophic factor. J. Neurobiol. *66*, 103–114.

Chrétien, D., and Wade, R.H. (1991). New data on the microtubule surface lattice. Biology of the Cell *71*, 161–174.

Conde, C., and Cáceres, A. (2009). Microtubule assembly, organization and dynamics in axons and dendrites. Nat Rev Neurosci *10*, 319–332.

Coue, M., Lombillo, V.A., and McIntosh, J.R. (1991). Microtubule depolymerization promotes particle and chromosome movement in vitro. J Cell Biol *112*, 1165–1175.

Cunha-Ferreira, I., Chazeau, A., Buijs, R.R., Stucchi, R., Will, L., Pan, X., Adolfs, Y., van der Meer, C., Wolthuis, J.C., Kahn, O.I., et al. (2018). The HAUS Complex Is a Key Regulator of Non-centrosomal Microtubule Organization during Neuronal Development. CellReports *24*, 791–800.

Daniels, M.P. (1973). Fine structural changes in neurons and nerve fibers associated with colchicine inhibition of nerve fiber formation in vitro. J Cell Biol *58*, 463–470.

De Groot, C.O., Jelesarov, I., Damberger, F.F., Bjelić, S., Schärer, M.A., Bhavesh, N.S., Grigoriev, I., Buey, R.M., Wüthrich, K., Capitani, G., et al. (2010). Molecular insights into mammalian end-binding protein heterodimerization. J. Biol. Chem. *285*, 5802–5814.

Dehmelt, L., and Halpain, S. (2004). The MAP2/Tau family of microtubule-associated proteins. Genome Biol. *6*, 204.

Dent, E.W., Callaway, J.L., Györgyi Szebenyi, Baas, P.W., and Kalil, K. (1999). Reorganization and Movement of Microtubules in Axonal Growth Cones and Developing Interstitial Branches. The Journal of Neuroscience 1–15.

Dent, E.W., Gupton, S.L., and Gertler, F.B. (2011). The Growth Cone Cytoskeleton in Axon Outgrowth and Guidance. Cold Spring Harb Perspect Biol *3*, a001800–a001800.

Dent, E.W., Kwiatkowski, A.V., Mebane, L.M., Philippar, U., Barzik, M., Rubinson, D.A., Gupton, S., Van Veen, J.E., Furman, C., Zhang, J., et al. (2007). Filopodia are required for cortical neurite initiation. Nature Cell Biology *9*, 1347–1359.

Dionne, L.K., Wang, X.-J., and Prekeris, R. (2015). Midbody: from cellular junk to regulator of cell polarity and cell fate. Current Opinion in Cell Biology *35*, 51–58.

Dixit, R., Jennifer L Ross, Goldman, E., and Holzbaur, L.F. (2003). Differential Regulation of Dynein and

Kinesin Motor Proteins by Tau. Science *112*, 467–480.

Dogterom, M., and Surrey, T. (2013). Microtubule organization in vitro. Current Opinion in Cell Biology *25*, 23–29.

Efimov, A., Kharitonov, A., Efimova, N., Loncarek, J., Miller, P.M., Andreyeva, N., Gleeson, P., Galjart, N., Maia, A.R.R., McLeod, I.X., et al. (2007). Asymmetric CLASP-Dependent Nucleation of Noncentrosomal Microtubules at the trans-Golgi Network. Developmental Cell *12*, 917–930.

Elliott, A., and Shaw, S.L. (2018). Update: Plant Cortical Microtubule Arrays. Plant Physiol. *176*, 94–105.

Ehrhardt, D.W., and Shaw, S.L. (2006). MICROTUBULE DYNAMICS AND ORGANIZATION IN THE PLANT CORTICAL ARRAY. Http://Dx.Doi.org/10.1146/Annurev.Arplant.57.032905.105329 *57*, 859–875.

Errico, A., Claudiani, P., molecular, M.D.H., 2004 Spastin interacts with the centrosomal protein NA14, and is enriched in the spindle pole, the midbody and the distal axon | Human Molecular Genetics | Oxford Academic. Academic.Oup.com

Etienne-Manneville, S. (2013). Microtubules in Cell Migration. Annu. Rev. Cell Dev. Biol. *29*, 471–499.

Findeisen, P., Mühlhausen, S., Dempewolf, S., Hertzog, J., Zietlow, A., Carlomagno, T., and Kollmar, M. (2014a). Six Subgroups and Extensive Recent Duplications Characterize the Evolution of the Eukaryotic Tubulin Protein Family. Genome Biology and Evolution *6*, 2274–2288.

Findeisen, P., Mühlhausen, S., Dempewolf, S., Hertzog, J., Zietlow, A., Carlomagno, T., and Kollmar, M.

(2014b). Six Subgroups and Extensive Recent Duplications Characterize the Evolution of the Eukaryotic Tubulin Protein Family. Genome Biology and Evolution *6*, 2274–2288.

Fiore, M., Goulas, C., and Pillois, X. (2017). A new mutation in TUBB1 associated with thrombocytopenia confirms that C-terminal part of β1-tubulin plays a role in microtubule assembly. Clinical Genetics *91*, 924–926.

Flynn, K.C., Hellal, F., Neukirchen, D., Jacob, S., Tahirovic, S., Dupraz, S., Stern, S., Garvalov, B.K., Gurniak, C., Shaw, A.E., et al. (2012). ADF/Cofilin-Mediated Actin Retrograde Flow Directs Neurite Formation in the Developing Brain. Neuron *76*, 1091–1107.

Fourest-Lieuvin, A., Peris, L., Gache, V., Garcia-Saez, I., Juillan-Binard, C., Lantez, V., and Job, D. (2006). Microtubule Regulation in Mitosis: Tubulin Phosphorylation by the Cyclin-dependent Kinase Cdk1. MBoC *17*, 1041–1050.

Fourniol, F.J., Sindelar, C.V., Amigues, B., Clare, D.K., Thomas, G., Perderiset, M., Francis, F., Houdusse, A., and Moores, C.A. (2010). Template-free 13-protofilament microtubule–MAP assembly visualized at 8 Å resolution. J Cell Biol *191*, 463–470.

Fourniol, F., Perderiset, M., Houdusse, A., and Moores, C. (2013). Structural Studies of the Doublecortin Family of MAPs. Methods in Cell Biology *115*, 27–48.

Franker, M.A.M., and Hoogenraad, C.C. (2013). Microtubule-based transport – basic mechanisms, traffic rules and role in neurological pathogenesis. J Cell Sci *126*, 2319–2329.

Frost, A., Unger, V.M., and De Camilli, P. (2009). The BAR Domain Superfamily: Membrane-Molding Macromolecules. Cell *137*, 191–196.

Gadadhar, S., Bodakuntla, S., Natarajan, K., and Janke, C. (2017). The tubulin code at a glance. J Cell Sci *130*, 1347–1353.

Gallo, G. (2007). Tau is actin up in Alzheimer's disease. Nature Cell Biology *9*, 133–134.

Ganguly, A., Yang, H., Sharma, R., Patel, K.D., and Cabral, F. (2012). The role of microtubules and their dynamics in cell migration. J. Biol. Chem. *287*, 43359–43369.

Garcin, C., and Straube, A. (2019). Microtubules in cell migration. Essays Biochem. *115*, EBC20190016–12.

Garvalov, B.K., Zuber, B., Bouchet-Marquis, C., Kudryashev, M., Gruska, M., Beck, M., Leis, A., Frischknecht, F., Bradke, F., Baumeister, W., et al. (2006). Luminal particles within cellular microtubules. J Cell Biol *174*, 759–765.

Geraldo, S., Khanzada, U.K., Parsons, M., Chilton, J.K., and Gordon-Weeks, P.R. (2008). Targeting of the F-actin-binding protein drebrin by the microtubule plus-tip protein EB3 is required for neuritogenesis. Nature Cell Biology *10*, 1181–1189.

Geyer, E.A., Burns, A., Lalonde, B.A., Ye, X., Elife, F.P., 2015 (2015). A mutation uncouples the tubulin conformational and GTPase cycles, revealing allosteric control of microtubule dynamics. Cdn.Elifesciences.org

.

Goodson, H.V., and Jonasson, E.M. (2018). Microtubules and Microtubule-Associated Proteins. Cold

Spring Harb Perspect Biol *10*, a022608.

Goyal, U., Renvoisé, B., Chang, J., and Blackstone, C. (2014). Spastin-Interacting Protein NA14/SSNA1 Functions in Cytokinesis and Axon Development. PLoS ONE *9*, e112428.

Gull, K. (2001). Protist tubulins: new arrivals, evolutionary relationships and insights to cytoskeletal function. Current Opinion in Microbiology *4*, 427–432.

Gupta, K.K., Li, C., Duan, A., Alberico, E.O., Kim, O.V., Alber, M.S., and Goodson, H.V. (2013). Mechanism for the catastrophe-promoting activity of the microtubule destabilizer Op18/stathmin. Pnas *110*, 20449–20454.

Gurel, P.S., Hatch, A.L., and Higgs, H.N. (2019). Connecting the Cytoskeleton to the Review Endoplasmic Reticulum and Golgi. 1–13.

Györgyi Szebenyi, Callaway, J.L., Dent, E.W., and Kalil, K. (1998). Interstitial Branches Develop from Active Regions of the Axon Demarcated by the Primary Growth Cone during Pausing Behaviors. The Journal of Neuroscience 1–11.

Hannak, E., Oegema, K., Kirkham, M., Gönczy, P., Habermann, B., and Hyman, A.A. (2002). The kinetically dominant assembly pathway for centrosomal asters in Caenorhabditis elegans is γ-tubulin dependent. J Cell Biol *157*, 591–602.

Hirokawa, N., Niwa, S., and Tanaka, Y. (2010). Molecular Motors in Neurons: Transport Mechanisms and Roles in Brain Function, Development, and Disease. Neuron *68*, 610–638.

Howes, S.C., Geyer, E.A., LaFrance, B., Zhang, R., Kellogg, E.H., Westermann, S., Rice, L.M., and Nogales, E. (2017). Structural differences between yeast and mammalian microtubules revealed by cryo-EM. J Cell Biol *216*, 2669–2677.

Hu, J., Bai, X., Bowen, J.R., Dolat, L., Korobova, F., Yu, W., Baas, P.W., Svitkina, T., Gallo, G., and Spiliotis, E.T. (2012). Septin-Driven Coordination of Actin and Microtubule Remodeling Regulates the Collateral Branching of Axons. Current Biology *22*, 1109–1115.

Hunyadi, V., Chrétien, D., Flyvbjerg, H., and Jánosi, I.M. (2007). Why is the microtubule lattice helical? Biology of the Cell *99*, 117–128.

Hyman, A.A., Salser, S., Drechsel, D.N., Unwin, N., and Mitchison, T.J. (1992). Role of GTP hydrolysis in microtubule dynamics: information from a slowly hydrolyzable analogue, GMPCPP. MBoC *3*, 1155–1167.

Ichikawa, M., Liu, D., Kastritis, P.L., Basu, K., Hsu, T.C., Yang, S., and Bui, K.H. (2017). Subnanometre-resolution structure of the doublet microtubule reveals new classes of microtubule-associated proteins. Nature Communications *8*, 1–12.

Ishihara, K., Nguyen, P.A., Groen, A.C., Field, C.M., and Mitchison, T.J. (2014). Microtubule nucleation remote from centrosomes may explain how asters span large cells. Pnas *111*, 17715–17722.

Jacobson, C., Schnapp, B., and Banker, G.A. (2006). A Change in the Selective Translocation of the Kinesin-1 Motor Domain Marks the Initial Specification of the Axon. Neuron *49*, 797–804.

Janke, C. (2014). The tubulin code: Molecular components, readout mechanisms, and functions. J Cell Biol *206*, 461–472.

Jenuwein, T., and Allis, C.D. (2001). Translating the Histone Code. Science *293*, 1074–1080.

Jiang, K., Hua, S., Mohan, R., Grigoriev, I., Yau, K.W., Liu, Q., Katrukha, E.A., Altelaar, A.F.M., Heck, A.J.R., Hoogenraad, C.C., et al. (2014). Microtubule Minus-End Stabilization by Polymerization-Driven CAMSAP Deposition. Developmental Cell *28*, 295–309.

Kader, M.A., Satake, T., Yoshida, M., Hayashi, I., and Suzuki, A. (2017). Molecular basis of the microtubule-regulating activity of microtubule crosslinking factor 1. PLoS ONE *12*, e0182641–18.

Kalil, K., Szebenyi, G., and Dent, E.W. (2000). Common mechanisms underlying growth cone guidance and axon branching. J. Neurobiol. *44*, 145–158.

Kalil, K., and Dent, E.W. (2014). Branch management: mechanisms of axon branching in the developing vertebrate CNS. Nat Rev Neurosci *15*, 7–18.

Kapitein, L.C., and Hoogenraad, C.C. (2011). Which way to go? Cytoskeletal organization and polarized transport in neurons. Molecular and Cellular Neuroscience *46*, 9–20.

Kapitein, L.C., and Hoogenraad, C.C. (2015). Building the Neuronal Microtubule Cytoskeleton. Neuron *87*, 492–506.

Kapitein, L.C., Schlager, M.A., Kuijpers, M., Wulf, P.S., van Spronsen, M., MacKintosh, F.C., and Hoogenraad, C.C. (2010). Mixed Microtubules Steer Dynein-Driven Cargo Transport into Dendrites. Current Biology *20*, 290–299.

Kaverina, I., and Straube, A. (2011). Regulation of cell migration by dynamic microtubules. Seminars in Cell and Developmental Biology *22*, 968–974.

Ketschek, A., and Gallo, G. (2010). Nerve Growth Factor Induces Axonal Filopodia through Localized Microdomains of Phosphoinositide 3-Kinase Activity That Drive the Formation of Cytoskeletal Precursors to Filopodia. Journal of Neuroscience *30*, 12185–12197.

Kollman, J.M., Merdes, A., Mourey, L., and Agard, D.A. (2011). Microtubule nucleation by γ-tubulin complexes. Nature Publishing Group *12*, 709–721.

Konishi, Y., and Setou, M. (2009). Tubulin tyrosination navigates the kinesin-1 motor domain to axons. Nat Neurosci *12*, 559–567.

Kuijpers, M., and Hoogenraad, C.C. (2011). Centrosomes, microtubules and neuronal development. Molecular and Cellular Neuroscience *48*, 349–358.

Kumar, P., and Wittmann, T. (2012). +TIPs: SxIPping along microtubule ends. Trends in Cell Biology *22*, 418–428.

L'Hernault, S.W., and Rosenbaum, J.L. (2002). Chlamydomonas .alpha.-tubulin is posttranslationally modified by acetylation on the .epsilon.-amino group of a lysine. Biochemistry *24*, 473–478.

Lai, C.K., Gupta, N., Wen, X., Rangell, L., Chih, B., Peterson, A.S., Bazan, J.F., Li, L., and Scales, S.J. (2011). Functional characterization of putative cilia genes by high-content analysis. MBoC *22*, 1104–1119.

Le Ma, and Tessier-Lavigne, M. (2007). Dual Branch-Promoting and Branch-Repelling Actions of Slit/Robo Signaling on Peripheral and Central Branches of Developing Sensory Axons. Journal of Neuroscience *27*, 6843–6851.

Leano, J.B., Rogers, S.L., and Slep, K.C. (2013). A Cryptic TOG Domain with a Distinct Architecture

Underlies CLASP-Dependent Bipolar Spindle Formation. Structure *21*, 939–950.

Lebrand, C., Dent, E.W., Strasser, G.A., Lanier, L.M., Krause, M., Svitkina, T.M., Borisy, G.G., and Gertler, F.B. (2004). Critical Role of Ena/VASP Proteins for Filopodia Formation in Neurons and in Function Downstream of Netrin-1. Neuron *42*, 37–49.

Lee, E., Marcucci, M., Daniell, L., Pypaert, M., Weisz, O.A., Ochoa, G.-C., Farsad, K., Wenk, M.R., and Pietro De Camilli (2002). Amphiphysin 2 (Bin1) and T-Tubule Biogenesis in Muscle. Science *297*, 1193–1196.

Lewis, T.L., Jr., Courchet, J., and Polleux, F. (2013). Cellular and molecular mechanisms underlying axon formation, growth, and branching. J Cell Biol *202*, 837–848.

Lindeboom, J.J., Nakamura, M., Hibbel, A., Shundyak, K., Gutierrez, R., Ketelaar, T., Emons, A.M.C., Mulder, B.M., Kirik, V., and Ehrhardt, D.W. (2013). A mechanism for reorientation of cortical microtubule arrays driven by microtubule severing. Science *342*, 1245533–1245533.

Löwe, J., Li, H., Downing, K.H., and Nogales, E. (2001). Refined structure of αβ-tubulin at 3.5 Å resolution 1 1Edited by I. A. Wilson. Journal of Molecular Biology *313*, 1045–1057.

Lu, M., Witke, W., Kwiatkowski, D.J., and Kosik, K.S. (1997). Delayed Retraction of Filopodia in Gelsolin Null Mice. J Cell Biol *138*, 1279–1287.

Lu, W., Fox, P., Lakonishok, M., Davidson, M.W., and Gelfand, V.I. (2013). Initial Neurite Outgrowth in Drosophila Neurons Is Driven by Kinesin-Powered Microtubule Sliding. Current Biology *23*, 1018–1023.

Maday, S., Twelvetrees, A.E., Moughamian, A.J., and Holzbaur, E.L.F. (2014). Axonal Transport: Cargo-Specific Mechanisms of Motility and Regulation. Neuron *84*, 292–309.

Maiato, H., Rieder, C.L., and Khodjakov, A. (2004). Kinetochore-driven formation of kinetochore fibers contributes to spindle assembly during animal mitosis. J Cell Biol *167*, 831–840.

Masoud, K., Herzog, E., Chabouté, M.E., and Schmit, A.C. (2013). Microtubule nucleation and establishment of the mitotic spindle in vascular plant cells. The Plant Journal *75*, 245–257.

Maurer, S.P., Fourniol, F.J., Bohner, G., Moores, C.A., and Surrey, T. (2012). EBs Recognize a Nucleotide-Dependent Structural Cap at Growing Microtubule Ends. Cell *149*, 371–382.

McIntosh, J.R. (2016). Mitosis. Cold Spring Harb Perspect Biol *8*, a023218–a023218.

McManus, J.J., Charbonneau, P., Zaccarelli, E., and Asherie, N. (2016). The physics of protein self-assembly. Current Opinion in Colloid & Interface Science *22*, 73–79.

Meunier, S., and Vernos, I. (2016). Acentrosomal Microtubule Assembly in Mitosis: The Where, When, and How. Trends in Cell Biology *26*, 80–87.

Meunier, S., Shvedunova, M., Van Nguyen, N., Avila, L., Vernos, I., and Akhtar, A. (2015). An epigenetic regulator emerges as microtubule minus-end binding and stabilizing factor in mitosis. Nature Communications *6*, 1–10.

Mitchison, T., and Kirschner, M. (1984). Dynamic instability of microtubule growth. Nature *312*, 237–242.

Mogensen, M.M., and Tucker, J.B. (1987). Evidence for microtubule nucleation at plasma membrane-associated sites in Drosophila. J Cell Sci *88 (Pt 1)*, 95–107.

Mulder, A.M., Glavis-Bloom, A., Moores, C.A., Wagenbach, M., Carragher, B., Wordeman, L., and Milligan, R.A. (2009). A new model for binding of kinesin 13 to curved microtubule protofilaments. J Cell Biol *185*, 51–57.

Murata, T., Sonobe, S., Baskin, T.I., Hyodo, S., Hasezawa, S., Nagata, T., Horio, T., and Hasebe, M. (2005). Microtubule-dependent microtubule nucleation based on recruitment of γ-tubulin in higher plants. Nature Cell Biology *7*, 961–968.

Nakata, T., and Hirokawa, N. (2003). Microtubules provide directional cues for polarized axonal transport through interaction with kinesin motor head. J Cell Biol *162*, 1045–1055.

Nakata, T., Niwa, S., Okada, Y., Perez, F., and Hirokawa, N. (2011). Preferential binding of a kinesin-1 motor to GTP-tubulin–rich microtubules underlies polarized vesicle transport. J Cell Biol *194*, 245–255.

Nawrotek, A., Knossow, M., and Gigant, B. (2011). The Determinants That Govern Microtubule Assembly from the Atomic Structure of GTP-Tubulin. Journal of Molecular Biology *412*, 35–42.

Nguyen, M.M., McCracken, C.J., Milner, E.S., Goetschius, D.J., Weiner, A.T., Long, M.K., Michael, N.L., Munro, S., and Rolls, M.M. (2014). γ-Tubulin controls neuronal microtubule polarity independently of Golgi outposts. MBoC *25*, 2039–2050.

Nguyen, M.M., Stone, M.C., and Rolls, M.M. (2011). Microtubules are organized independently of the centrosome in Drosophila neurons. Neural Dev *6*, 1–16.

Nicastro, D., Schwartz, C., Pierson, J., Gaudette, R., Porter, M.E., and McIntosh, J.R. (2006). The Molecular Architecture of Axonemes Revealed by Cryoelectron Tomography. Science *313*, 944–948.

Nieuwenhuis, J., Adamopoulos, A., Bleijerveld, O.B., Mazouzi, A., Stickel, E., Celie, P., Altelaar, M., Knipscheer, P., Perrakis, A., Blomen, V.A., et al. (2017). Vasohibins encode tubulin detyrosinating activity. Science *358*, 1453–1456.

Nogales, E., Downing, K.H., Amos, L.A., and Löwe, J. (1998a). Tubulin and FtsZ form a distinct family of GTPases. Nat Struct Mol Biol *5*, 451–458.

Nogales, E., Downing, K.H., Amos, L.A., and Löwe, J. (1998b). Tubulin and FtsZ form a distinct family of GTPases. Nat Struct Mol Biol *5*, 451–458.

Nogales, E., Wolf, S.G., and Downing, K.H. (1998c). Structure of the αβ tubulin dimer by electron crystallography. Nature *391*, 199–203.

Norris, C.R., and Kalil, K. (1991). Guidance of Callosal Axons by Radial Glia in the Developing Cerebral Cortex. The Journal of Neuroscience 3481–3492.

Ori-McKenney, K.M., Jan, L.Y., and Jan, Y.-N. (2012). Golgi Outposts Shape Dendrite Morphology by Functioning as Sites of Acentrosomal Microtubule Nucleation in Neurons. Neuron *76*, 921–930.

Park, I.Y., Powell, R.T., Tripathi, D.N., Dere, R., Ho, T.H., Blasius, T.L., Chiang, Y.-C., Davis, I.J., Fahey, C.C., Hacker, K.E., et al. (2016). Dual Chromatin and Cytoskeletal Remodeling by SETD2. Cell *166*, 950–962.

Peris, L., Thery, M., Fauré, J., Saoudi, Y., Lafanechère, L., Chilton, J.K., Gordon-Weeks, P., Galjart, N., Bornens, M., Wordeman, L., et al. (2006). Tubulin tyrosination is a major factor affecting the recruitment of CAP-Gly proteins at microtubule plus ends. J Cell Biol *174*, 839–849.

Peter, B.J., Kent, H.M., Mills, I.G., Vallis, Y., Butler, P.J.G., Evans, P.R., and McMahon, H.T. (2004). BAR Domains as Sensors of Membrane Curvature: The Amphiphysin BAR Structure. Science *303*, 495–499.

Petry, S., and Vale, R.D. (2015). Microtubule nucleation at the centrosome and beyond. Nature Cell Biology *17*, 1089–1093.

Petry, S., Groen, A.C., Ishihara, K., Mitchison, T.J., and Vale, R.D. (2013). Branching Microtubule Nucleation in Xenopus Egg Extracts Mediated by Augmin and TPX2. Cell *152*, 768–777.

Pfannenschmid, F., Wimmer, V.C., Rios, R.-M., Geimer, S., Kröckel, U., Leiherer, A., Haller, K., Nemcová, Y., and Mages, W. (2003). Chlamydomonas DIP13 and human NA14: a new class of proteins associated with microtubule structures is involved in cell division. J Cell Sci *116*, 1449–1462.

Pollard, T.D., and Goldman, R.D. (2018). Overview of the Cytoskeleton from an Evolutionary Perspective. Cold Spring Harb Perspect Biol *10*, a030288.

Portera-Cailliau, C., Weimer, R.M., De Paola, V., Caroni, P., and Svoboda, K. (2005). Diverse Modes of Axon Elaboration in the Developing Neocortex. PLoS Biol *3*, e272–15.

Price, H.P., Hodgkinson, M.R., Curwen, R.S., MacLean, L.M., Brannigan, J.A., Carrington, M., Smith, B.A., Ashford, D.A., Stark, M., and Smith, D.F. (2012). The Orthologue of Sjögren's Syndrome Nuclear Autoantigen 1 (SSNA1) in Trypanosoma brucei Is an Immunogenic Self-Assembling Molecule. PLoS ONE *7*, e31842.

Prokop, A., Beaven, R., Qu, Y., and Sanchez-Soriano, N. (2013). Using fly genetics to dissect the cytoskeletal machinery of neurons during axonal growth and maintenance. J Cell Sci *126*, 2331–2341.

Prosser, S.L., and Pelletier, L. (2017). Mitotic spindle assembly in animal cells: a fine balancing act. Nature Publishing Group *18*, 187–201.

Qiang, L. (2006). Tau Protects Microtubules in the Axon from Severing by Katanin. Journal of Neuroscience *26*, 3120–3129.

Qu, C., Dwyer, T., Shao, Q., Yang, T., Huang, H., and Liu, G. (2013). Direct binding of TUBB3 with DCC couples netrin-1 signaling to intracellular microtubule dynamics in axon outgrowth and guidance. J Cell Sci *126*, 3070–3081.

Rao, A.N., and Baas, P.W. (2018). Polarity Sorting of Microtubules in the Axon. Trends in Neurosciences *41*, 77–88.

Ravelli, R.B.G., Gigant, B., Curmi, P.A., Jourdain, I., Lachkar, S., Sobel, A., and Knossow, M. (2004). Insight into tubulin regulation from a complex with colchicine and a stathmin-like domain. Nature *428*, 198–202.

Razzaq, A., Robinson, I.M., McMahon, H.T., Skepper, J.N., Su, Y., Zelhof, A.C., Jackson, A.P., Gay, N.J., and O'Kane, C.J. (2001). Amphiphysin is necessary for organization of the excitation-contraction coupling machinery of muscles, but not for synaptic vesicle endocytosis in Drosophila. Genes Dev. *15*, 2967–2979.

Reed, N.A., Cai, D., Blasius, T.L., Jih, G.T., Meyhofer, E., Gaertig, J., and Verhey, K.J. (2006). Microtubule Acetylation Promotes Kinesin-1 Binding and Transport. Current Biology *16*, 2166–2172.

Reiner, O., and Sapir, T. (2013). LIS1 functions in normal development and disease. Current Opinion in Neurobiology *23*, 951–956.

Rice, L.M., Montabana, E.A., and Agard, D.A. (2008). The lattice as allosteric effector: Structural studies of αβ- and γ-tubulin clarify the role of GTP in microtubule assembly. Pnas *105*, 5378–5383.

Rodriguez, O.C., Schaefer, A.W., Mandato, C.A., Forscher, P., Bement, W.M., and Waterman-Storer, C.M. (2003). Conserved microtubule–actin interactions in cell movement and morphogenesis. Nature Cell Biology *5*, 599–609.

Rodríguez-Rodríguez, M., Trevino, M.A., Selection, D., 2011 Characterization of the structure and self-recognition of the human centrosomal protein NA14: implications for stability and function. Academic.Oup.com

.

Rogers, G.C., Rusan, N.M., Peifer, M., and Rogers, S.L. (2008). A Multicomponent Assembly Pathway Contributes to the Formation of Acentrosomal Microtubule Arrays in Interphase DrosophilaCells. MBoC *19*, 3163–3178.

Rogowski, K., Juge, F., Van Dijk, J., Wloga, D., Strub, J.-M., Levilliers, N., Thomas, D., Bré, M.-H., Van Dorsselaer, A., Gaertig, J., et al. (2009). Evolutionary Divergence of Enzymatic Mechanisms for Posttranslational Polyglycylation. Cell *137*, 1076–1087.

Rogowski, K., Van Dijk, J., Magiera, M.M., Bosc, C., Deloulme, J.-C., Bosson, A., Peris, L., Gold, N.D., Lacroix, B., Grau, M.B., et al. (2010). A Family of Protein-Deglutamylating Enzymes Associated with Neurodegeneration. Cell *143*, 564–578.

Roll-Mecak, A. (2015). Intrinsically disordered tubulin tails: complex tuners of microtubule functions? Seminars in Cell and Developmental Biology *37*, 11–19.

Roll-Mecak, A., and McNally, F.J. (2010). Microtubule-severing enzymes. Current Opinion in Cell Biology *22*, 96–103.

Rolls, M.M. (2011). Neuronal polarity in Drosophila: Sorting out axons and dendrites. Devel Neurobio *71*, 419–429.

Roossien, D.H., Lamoureux, P., and Miller, K.E. (2014). Cytoplasmic dynein pushes the cytoskeletal meshwork forward during axonal elongation. J Cell Sci *127*, 3593–3602.

Roostalu, J., Cade, N.I., and Surrey, T. (2015a). Complementary activities of TPX2 and chTOG constitute an efficient importin-regulated microtubule nucleation module. Nature Cell Biology *17*, 1422–1434.

Roostalu, J., Cade, N.I., and Surrey, T. (2015b). Complementary activities of TPX2 and chTOG constitute an efficient importin-regulated microtubule nucleation module. Nature Cell Biology *17*, 1422–1434.

Rubén M Buey, J Fernando Díaz, A., and Andreu, J.M. (2006). The Nucleotide Switch of Tubulin and Microtubule Assembly: A Polymerization-Driven Structural Change†. Biochemistry *45*, 5933–5938.

Sànchez-Huertas, C., Freixo, F., Viais, R., Lacasa, C., Soriano, E., and ders, J.L.U. (2019). Non-centrosomal nucleation mediated by augmin organizes microtubules in post-mitotic neurons and controls axonal microtubule polarity. Nature Communications 1–14.

Schaedel, L., Triclin, S., Chrétien, D., Abrieu, A., Aumeier, C., Gaillard, J., Blanchoin, L., Thery, M., and John, K. (2019). Lattice defects induce microtubule self-renewal. Nat. Phys. *15*, 830–838.

Schmidt, H., Stonkute, A., Jüttner, R., Schäffer, S., Buttgereit, J., Feil, R., Hofmann, F., and Rathjen, F.G.

(2007). The receptor guanylyl cyclase Npr2 is essential for sensory axon bifurcation within the spinal cord. J Cell Biol *179*, 331–340.

Sharp, D.J., and Ross, J.L. (2012). Microtubule-severing enzymes at the cutting edge. J Cell Sci *125*, 2561–2569.

Siegrist, S.E., and Doe, C.Q. (2007). Microtubule-induced cortical cell polarity. Genes Dev. *21*, 483–496.

SIMON, D.K., and OLeary, D.D.M. (1990). Limited Topographic Specificity in the Targeting and Branching of Mammalian Retinal Axons. Developmental Biology *137*, 125–134.

Sindelar, C.V., and Downing, K.H. (2007). The beginning of kinesin's force-generating cycle visualized at 9-A resolution. J Cell Biol *177*, 377–385.

Slep, K.C. (2009). The role of TOG domains in microtubule plus end dynamics.

Song, Y., Kirkpatrick, L.L., Schilling, A.B., Helseth, D.L., Chabot, N., Keillor, J.W., Johnson, G.V.W., and Brady, S.T. (2013). Transglutaminase and Polyamination of Tubulin: Posttranslational Modification for Stabilizing Axonal Microtubules. Neuron *78*, 109–123.

Spillane, M., Ketschek, A., Jones, S.L., Korobova, F., Marsick, B., Lanier, L., Svitkina, T., and Gallo, G. (2011). The actin nucleating Arp2/3 complex contributes to the formation of axonal filopodia and branches through the regulation of actin patch precursors to filopodia. Devel Neurobio *71*, 747–758.

Stiess, M., Maghelli, N., Kapitein, L.C., Gomis-Rüth, S., Wilsch-Bräuninger, M., Hoogenraad, C.C., Tolić-Nørrelykke, I.M., and Bradke, F. (2010). Axon Extension Occurs Independently of Centrosomal Microtubule Nucleation. Science *327*, 704–707.

Strome, S., Powers, J., Dunn, M., Reese, K., Malone, C.J., White, J., Seydoux, G., and Saxton, W. (2001). Spindle dynamics and the role of gamma-tubulin in early Caenorhabditis elegans embryos. MBoC *12*, 1751–1764.

Sui, H., and Downing, K.H. (2010). Structural basis of interprotofilament interaction and lateral deformation of microtubules. Structure *18*, 1022–1031.

Suozzi, K.C., Wu, X., and Fuchs, E. (2012). Spectraplakins: Master orchestrators of cytoskeletal dynamics. J Cell Biol *197*, 465–475.

Suter, D.M., and Miller, K.E. (2011). The emerging role of forces in axonal elongation. Progress in Neurobiology *94*, 91–101.

Sweeney, H.L., and Holzbaur, E.L.F. (2018). Motor Proteins. Cold Spring Harb Perspect Biol *10*, a021931–19.

Takei, K., Slepnev, V.I., Haucke, V., and Pietro De Camilli (1999). Functional partnership between amphiphysin and dynamin in clathrin-mediated endocytosis. Nature Cell Biology *1*, 33–39.

Tanaka, E. (1995). The role of microtubule dynamics in growth cone motility and axonal growth. J Cell Biol *128*, 139–155.

Tang, F. (2005). Netrin-1 Induces Axon Branching in Developing Cortical Neurons by Frequency-Dependent Calcium Signaling Pathways. Journal of Neuroscience *25*, 6702–6715.

Tassin, A.M., Maro, B., and Bornens, M. (1985). Fate of microtubule-organizing centers during myogenesis in vitro. J Cell Biol *100*, 35–46.

Tischfield, M.A., Cederquist, G.Y., Gupta, M.L., Jr, and Engle, E.C. (2011). Phenotypic spectrum of the tubulin-related disorders and functional implications of disease-causing mutations. Current Opinion in Genetics & Development *21*, 286–294.

Tolić-Nørrelykke, I.M., Sacconi, L., Thon, G., and Pavone, F.S. (2004). Positioning and Elongation of the Fission Yeast Spindle by Microtubule-Based Pushing. Current Biology *14*, 1181–1186.

Tran, P.T., Marsh, L., Doye, V., Inoué, S., and Chang, F. (2001). A Mechanism for Nuclear Positioning in Fission Yeast Based on Microtubule Pushing. J Cell Biol *153*, 397–412.

Uversky, V.N., and Eliezer, D. (2009). Biophysics of Parkinson's Disease: Structure and Aggregation of α- Synuclein. Cpps *10*, 483–499.

Valenstein, M.L., and Roll-Mecak, A. (2016). Graded Control of Microtubule Severing by Tubulin Glutamylation. Cell *164*, 911–921.

Verhey, K.J., and Gaertig, J. (2007). The Tubulin Code. Cell Cycle *6*, 2152–2160.

Vertii, A., Hehnly, H., and Doxsey, S. (2016). The Centrosome, a Multitalented Renaissance Organelle. Cold Spring Harb Perspect Biol *8*, a025049–15.

Viswanadha, R., Sale, W.S., and Porter, M.E. (2017). Ciliary Motility: Regulation of Axonemal Dynein Motors. Cold Spring Harb Perspect Biol *9*, a018325–24.

Voter, W.A., and Erickson, H.P. (1984). The kinetics of microtubule assembly. Evidence for a two-stage nucleation mechanism. J. Biol. Chem. *259*, 10430–10438.

Vulevic, B., and Correia, J.J. (1997). Thermodynamic and structural analysis of microtubule assembly: the role of GTP hydrolysis. Biophysical Journal *72*, 1357–1375.

Walczak, C.E., and Shaw, S.L. (2010). A MAP for Bundling Microtubules. Cell *142*, 364–367.

Wang, G., Jiang, Q., and Zhang, C. (2014a). The role of mitotic kinases in coupling the centrosome cycle with the assembly of the mitotic spindle. J Cell Sci *127*, 4111–4122.

Wang, Q., Crevenna, A.H., Kunze, I., and Mizuno, N. (2014b). Structural basis for the extended CAP-Gly domains of p150glued binding to microtubules and the implication for tubulin dynamics. Pnas *111*, 11347–11352.

Weber, K.L., Sokac, A.M., Berg, J.S., Cheney, R.E., and Bement, W.M. (2004). A microtubule-binding myosin required for nuclear anchoring and spindle assembly. Nature *431*, 325–329.

Wehenkel, A., and Janke, C. (2014). Towards elucidating the tubulin code. Nature Cell Biology *16*, 303–305.

Weisbrich, A., Honnappa, S., Jaussi, R., Okhrimenko, O., Frey, D., Jelesarov, I., Akhmanova, A., and Steinmetz, M.O. (2007). Structure-function relationship of CAP-Gly domains. Nat Struct Mol Biol *14*, 959–967.

Wiese, C., and Zheng, Y. (2000). A new function for the γ -tubulin ring complex as a microtubule minus-end cap. Nature Cell Biology *2*, 358–364.

Wilde, A., and Zheng, Y. (1999). Stimulation of Microtubule Aster Formation and Spindle Assembly by the Small GTPase Ran. Science *284*, 1359–1362.

Witte, H., Neukirchen, D., and Bradke, F. (2008). Microtubule stabilization specifies initial neuronal polarization. J Cell Biol *180*, 619–632.

Wu, J., and Akhmanova, A. (2017a). Microtubule-Organizing Centers. Annu. Rev. Cell Dev. Biol. *33*, 51–75.

Yamada, K.M., Spooner, B.S., and Wessells, N.K. (1970). AXON GROWTH: ROLES OF MICROFILAMENTS AND MICROTUBULES. Pnas *66*, 1206–1212.

Yang, L., Liu, A., Cao, S., Putri, R.M., Jonkheijm, P., and Cornelissen, J.J.L.M. (2016). Self-Assembly of Proteins: Towards Supramolecular Materials. Chemistry – a European Journal *22*, 15570–15582.

Yu, W., Qiang, L., Solowska, J.M., Karabay, A., Korulu, S., and Baas, P.W. (2008). The Microtubule-severing Proteins Spastin and Katanin Participate Differently in the Formation of Axonal Branches. MBoC *19*, 1485–1498.

Zanic, M., Stear, J.H., Hyman, A.A., and Howard, J. (2009). EB1 Recognizes the Nucleotide State of Tubulin in the Microtubule Lattice. PLoS ONE *4*, e7585.

Zhang, R., and Nogales, E. (2015). A new protocol to accurately determine microtubule lattice seam location. Journal of Structural Biology *192*, 245–254.

Zhang, R., Alushin, G.M., Brown, A., and Nogales, E. (2015). Mechanistic Origin of Microtubule Dynamic Instability and Its Modulation by EB Proteins. Cell *162*, 849–859.

Zhou, F.-Q., Zhou, J., Dedhar, S., Wu, Y.-H., and Snider, W.D. (2004). NGF-Induced Axon Growth Is Mediated by Localized Inactivation of GSK-3β and Functions of the Microtubule Plus End Binding Protein APC. Neuron *42*, 897–912.

7. Acknowledgement

First, I want to thank and express my deep gratitude to my PhD supervisor Naoko Mizuno for taking me as a PhD student, providing me a great environment to work and giving me freedom and opportunity to reach my scientific goals. It was really nice working with her and I really appreciate all the support she gave me, saw some positives in my chaos and mess and guided me till the end. I would also like to thank Christian Biertümpfel, for all the help, support and guidance he gave me during my PhD and made sure we have enough resources to go through the hard time.

I would like to thank my thesis advisor Elena Conti for providing excellent research environment to work in the department. It was really fun to work here. I also want to express my extended thanks to my thesis advisory committee.

I want to thank all the people in the " Light Microscopy Core facility " for all the technical help and especially Giovani Cardone for helping me through the analysis of both light and electron microscope images. I also want to thank " Biochemistry core facility " and "Crystallization facility" at the Max Planck Institute for the excellent technical support. I would like to thank and really appreciate all the past and present members of EM facility, Mike Strauss, Daniel Bollschweiler and Tillman Schäfer for all the support and technical help I got without considering time and day. I would like to thank Rajan Prabu for all the software support and technical discussion. I would like to thank Wolfgang Baumeister for giving us opportunity to access his microscopy infrastructure and Jürgen Plitzko and Günter Pfeiffer for their technical support.

I want to thank all my collaborators who helped me during different stages of PhD thesis. I would like to thank Carsten Janke, Magda Magiera and Satish Bodakuntla from Institute Curie, Orsay,Paris. I would also like to thank Alavaro H. Ceravanna for helping me setting up and analyze TIRF assasys. I also want to thank Rui Zhang Washington University in St. Louis for helping me during the analysis of microtubules cryo-EM data. I also want to thank Taschi for all the help and scientific discussions during my PhD.

I want to thank all my past and present lab members Steffi, Dirk, Chris, Charlotte, Hana, Iosune, Sven, Xinag, Qianmin, Wolfgang and Julia. Thanks for the amazing time here and for all the support, discussions and suggestions. I also want to thank Guilia, Iulia, Shun and Karina from Biertümpfel group. You guys really made this place fun and I was always happy to come to the lab. Thank you for everything and a memorable time. I want to extend my thanks to all the people form Conti department for great

working atmosphere and all the scientific discussions over the year.

I want to especially thank Meera for all the scientific discussions, support, care and love.

Finally, I want to thank my parents and my brother. Without their continuous love, support, encouragement and sacrifices, it would not have been possible for me to reach here. Thank you for everything.